

University of Groningen

MIF-CD74 interaction as a promising target in drug discovery

Go, Tjie Kok

IMPORTANT NOTE: You are advised to consult the publisher's version (publisher's PDF) if you wish to cite from it. Please check the document version below.

Document Version

Publisher's PDF, also known as Version of record

Publication date:

2019

[Link to publication in University of Groningen/UMCG research database](#)

Citation for published version (APA):

Go, T. K. (2019). *MIF-CD74 interaction as a promising target in drug discovery*. [Thesis fully internal (DIV), University of Groningen]. University of Groningen.

Copyright

Other than for strictly personal use, it is not permitted to download or to forward/distribute the text or part of it without the consent of the author(s) and/or copyright holder(s), unless the work is under an open content license (like Creative Commons).

The publication may also be distributed here under the terms of Article 25fa of the Dutch Copyright Act, indicated by the "Taverne" license. More information can be found on the University of Groningen website: <https://www.rug.nl/library/open-access/self-archiving-pure/taverne-amendment>.

Take-down policy

If you believe that this document breaches copyright please contact us providing details, and we will remove access to the work immediately and investigate your claim.

Downloaded from the University of Groningen/UMCG research database (Pure): <http://www.rug.nl/research/portal>. For technical reasons the number of authors shown on this cover page is limited to 10 maximum.

MIF-CD74 interaction as a promising target in drug discovery

Tjie Kok
2018



university of
 groningen



The research described in this thesis was conducted in the Department of Chemical and Pharmaceutical Biology at the University of Groningen and supported financially by Directorate General of Higher Education Indonesia (DIKTI) in collaboration with the University of Surabaya (Ubaya), Indonesia and the University of Groningen (RuG), The Netherlands.

Printing of this thesis was funded by the University Library and the Graduate School of Science and Engineering, University of Groningen (RuG), The Netherlands.

ISBN (printed version): 978-94-034-1227-6

ISBN (electronic version): 978-94-034-1226-9

Layout and cover: Tjie Kok

Printing: Ipskamp printing

Copyright © 2018 Tjie Kok



university of
 groningen

MIF-CD74 interaction as a promising target in drug discovery

PhD thesis

to obtain the degree of PhD
 at the University of Groningen
 on the authority of the
 Rector Magnificus Prof. E. Sterken
 and in accordance with
 the decision by the College of Deans.

This thesis will be defended in public on

Friday 25 January 2019 at 16.15 hours

by

Tjie Kok

born on 20 August 1969
 in Surabaya, Indonesië

Supervisors

Prof. dr. F.J. Dekker

Prof. dr. G.J. Poelarends

Assessment Committee

Prof. dr. Martina Schmidt

Prof. dr. Roland Pieters

Prof. dr. Peter Olinga

Paranymphs:

Joko P. Wibowo

Lieuwe Biewenga

Uw woord is een lamp voor mijn voet, een licht voor mijn pad

Psalmen 119:105 (Statenvertaling)

Table of Contents

- Chapter 1.** Introduction and scope of the thesis
- Chapter 2.** Small-molecule inhibitors of MIF as a potential class of therapeutics for inflammatory diseases and cancer
- Chapter 3.** High yield production of human CD74 as fusion proteins
- Chapter 4.** Development of chromenes as MIF inhibitors
- Chapter 5.** Synthesis of a focused compound collection of isoxazole, benzoxazole and triazole-phenol scaffolds to explore the structure-activity relationship for MIF tautomerase activity inhibition
- Chapter 6.** Summary and future perspectives

Appendices

Acknowledgements

List of publications

About the author

Chapter 1

Introduction and scope of the thesis

Protein-protein interactions (PPIs) underlie a great number of biological processes found in signal transduction cascades, and play crucial roles in disease progression [1]. PPIs have the potential to provide a vast number of both intracellular and extracellular therapeutic targets. The potential of modulation of PPIs for drug discovery triggered great interest in development of inhibitors over the past decade [2]. However, there is a number of challenges inherent in developing PPI inhibitors that prevented this effort from reaching its full fruits. Expression of the interacting proteins for *in vitro* experiments proves often to be difficult, in particular when the interaction partners include membrane bound receptors. Another challenge is the development of convenient assay formats to screen for novel hit and lead compounds. Finally, it is challenging to translate PPI inhibition to cell-based studies, animal models and ultimately clinical applications. In this thesis, we focus on the PPI interactions of macrophage migration inhibitory factor (MIF) and its binding partners such as the Cluster of Differentiation 74 (CD74) receptor. We aim to improve the production of the purified CD74 protein in bacteria in order to provide a suitable MIF-CD74 binding assay. Furthermore, we aim to identify novel MIF binders. Ultimately, this will contribute to drug discovery that employs MIF as a molecular target.

Initially, MIF was described as a T cell-derived mediator that prevents random movement of macrophages. Its activity was associated with delayed-type hypersensitivity reactions, which is a feature of some human chronic diseases [3]. Moreover, it is released at infection sites, causing macrophages to localize and perform antigen processing and phagocytosis [4]. Currently, MIF is identified as a cytokine with a key role in innate and adaptive immune responses that is associated with the progression of multiple diseases [5][6]. Consequently, an increasing number of roles in the pathogenesis of various inflammatory diseases and cancer have been described for MIF [7].

MIF is produced in many organs and tissues by various cells [8]. *In vivo*, MIF exerts its action by binding to membrane receptors, such as the CD74 receptor. Although MIF-CD74 binding is the best-characterized interaction, also binding to other receptors has been reported. It has been elucidated that MIF binding to the chemokine receptors CXCR2, CXCR4 and CXCR7 also plays an important role in MIF actions [9]. Apart from its cytokine activity, MIF possesses

tautomerase enzyme activity and is a member of the tautomerase superfamily [10]. The tautomerase enzyme activity is a property that is extensively employed in the screening for small molecule MIF binders (see Chapter 2). MIF has also a close relative as identified from the human genome. D-dopachrome tautomerase (D-DT) has been identified as a gene with marked homology to MIF. Because of its similarity, D-DT is also called as MIF2. An overlapping functional spectrum of MIF and D-DT has been suggested [6][11][12]. Therefore, the close homology of MIF with D-DT should be taken into account in the evaluation of MIF cytokine activities and the development of small molecule MIF modulators.

The CD74 receptor is also referred to as HLA class II histocompatibility antigen gamma chain or HLA-DR antigen-associated invariant chain Ii. This is a non-polymorphic type II transmembrane glycoprotein that has been described to be involved in many biological processes in the cell, such as antigen loading and transport of MHC class II molecules from the endoplasmic reticulum to the Golgi complex [13]. This receptor is also recognized as part of a complex to which MIF binds and that enables initiation of MIF induced signaling in inflammation [9]. Thus this receptor complex participates in the progression of MIF cytokine-related diseases. The extracellular domain of CD74 is involved in direct interaction with MIF. It has been reported that CD74 undergoes progressive proteolytic degradation in the endosomal/lysosomal system, eventually leaving the small class-II-associated invariant chain peptide (CLIP) as a fragment that binds MIF [14].

Production of relatively large amounts of the functional extracellular moiety of CD74 is indispensable for further exploration of MIF-CD74 interaction and discovery of novel inhibitors to disrupt this interaction. Our previous findings showed that the production of extracellular moiety of CD74 in bacterial cells gave very low yields. To overcome this problem, we aim for the production of the extracellular domain of CD74 as fusion protein for enhancing the solubility and stability (see Chapter 3). Towards this aim we applied two different fusion partners: MBP (maltose-binding protein) and Fh8 (a small protein secreted by the parasite *Fasciola hepatica*). Both fusion partners are also intended to facilitate purification of the fusion proteins: MBP fusion proteins bind to immobilized amylose resins and can be eluted using maltose, and Fh8 fusion proteins make calcium-dependent interaction with hydrophobic resins and can be eluted using a calcium chelating agent, such as EDTA [15]. We put factor Xa and 3C cleavage sites on MBP-CD74 and Fh8-CD74 proteins, respectively. Following the production and purification of the fusion proteins, the MBP and Fh8 can be removed by cleaving them with factor Xa and 3C protease, respectively. All the fusion proteins and the cleaved products are characterized by SDS-PAGE and mass spectrometry, and their functionality in PPI are evaluated by ELISA and ITC.

Numerous studies describe the involvement of the MIF-CD74 interaction in the progression of inflammatory diseases and cancer. In this perspective, it is not surprising that over the past few years many efforts have been taken to develop small-molecule inhibitors targeting the MIF-CD74 interaction as potential therapeutics. Small-molecule inhibitors offer certain advantages compared to biologicals, such as antibodies. Advantages of small-molecule inhibitors are their low manufacturing cost, their low immunogenicity on repeated administration and their flexible delivery options, including oral administration. Development of MIF binding inhibitors often starts from screening for inhibition of the MIF tautomerase activity, which does not necessarily imply interference with the MIF-CD74 interaction. Nevertheless, MIF tautomerase inhibitors have potential to interfere with the MIF-CD74 interaction. For instance, allosteric inhibitors of MIF tautomerase activity may be capable to induce conformational changes that result in disruption of the MIF-CD74 interaction. While purposeful design of this type of compounds could be tricky, due to not-easy-to predict induced conformational modifications, targeting MIF tautomerase activity remains a convenient and efficient approach to develop MIF inhibitors [16]. Moreover, recent findings indicating that the interaction of MIF-CD74 take places in the area surrounding MIF tautomerase enzyme active site [17], support the idea that structure-based designed MIF tautomerase inhibitors holds promises to interfere with the MIF-CD74 interaction.

Several methods can be applied to develop small inhibitors in drug discovery. These methods range from random screening of large libraries of compounds to screening of focused compound collections and structure-based design methods. Random screening of large libraries usually covers a broad chemical space and enables the identification of unique hit and lead compounds. [1]. MIF inhibitors identified by Orita [19] and Cournia [20] are examples of this. Screening of focused compound collections enables a more comprehensive exploration of a predefined chemical space in which MIF binding has been identified or is to be expected. Several selection methods for screening of focused compound collections have been described. A method defined in our groups is the substitution-oriented screening (SOS) [1][18] in which scaffolds of inhibitors with known interactions with the target are employed for library design. This enables the screening of a large variety in substitution around scaffolds with known activity. Thus, SOS covers a smaller chemical space but enables a more profound exploration of the chemical space around a known scaffold [18]. The disadvantage of this method is it does not enable the identification of inhibitors with unique scaffolds. MIF inhibitors identified by Alam *et al.* with the isoxazoline scaffold [21], Jorgensen *et al.* with the triazole scaffold [22] are examples of MIF inhibitors

developed using this method. We apply this method to identify chromene-based MIF inhibitors in Chapter 4.

In contrast to screening methods, structure-based design provides the possibility for a directed exploration of the structure-activity relationship. Structure-based design requires a known inhibitor scaffold that has been crystallized with the target to provide an experimental structural basis for inhibitor design. Using systematic variations at specific positions in the inhibitor, the binding space in relation to the structure of the target can be explored systematically. The aim is to optimize the inhibitor potency and selectivity [18]. This method is often applied in combination with screening methods for generation of hit compounds that are subsequently optimized using structure-based design. This method has been used to explore and optimize the binding properties of MIF inhibitor with the isoxazoline scaffold [21][23], the triazole scaffold [22], or the biaryltriazole scaffold [24]. In this thesis we employ the structure-based design to explore structure-activity relationship for inhibitors of the triazole-phenol type in Chapter 5.

In **Chapter 2**, we provide a review of the role of MIF in the pathogenesis of inflammatory diseases and cancer. In addition, we provide an overview of small-molecule inhibitors of MIF tautomerase activity and we give future perspective on the development of such inhibitors [7].

In **Chapter 3**, we report the production and purification of the extracellular part of the CD74 receptor. This protein was expressed as fusion protein to solubility enhancing domains such as MBP and Fh8. We characterized the purified MBP-CD74 and Fh8-CD74 fusion proteins, as well as the CD74 cleavage products. Binding of the CD74 domain to MIF was identified using an ELISA assay. The successful production of functional CD74 in high quantities is the first important step for further characterization of its structural features and for identification of its binding characteristics to MIF. Hence, it will foster further development of the relevant small-molecule inhibitors for MIF-CD74 interaction [15].

In **Chapter 4**, we describe the development of chromenes as MIF inhibitors. Inspired by the known MIF inhibitor Orita-13, a SOS for MIF inhibitors was done with a diversely-substituted collection of compounds with a chromene scaffold. The chromene compounds were synthesized using versatile cyanoacetamide chemistry. The SOS provided several hit compounds for which the IC_{50} 's were determined. In addition, we evaluated the reversibility of binding and also analysed the enzyme kinetic of the most potent inhibitor. The newly identified

inhibitors will support further development of novel inhibitors as potential therapeutic agents against immune diseases in which MIF is involved [25].

In **Chapter 5**, we report structure-based design of compounds with isoxazole, benzoxazole and triazole-phenol scaffolds. Compounds with various substitutions were synthesized and their inhibition of MIF tautomerase activity was evaluated to explore the structure-activity relationship. This provided several substituted triazole-phenol compounds as MIF tautomerase inhibitors. It is expected that by making use of MIF enzymatic pocket to anchor small-molecule inhibitors, we can assemble substituents on the triazole ring that protrude the solvent interface of the pocket (“caps”) to target the inhibition on MIF-CD74 interaction.

In **Chapter 6**, we provide a summary of our work and we describe the challenges. Finally we give suggestions and perspectives for future work.

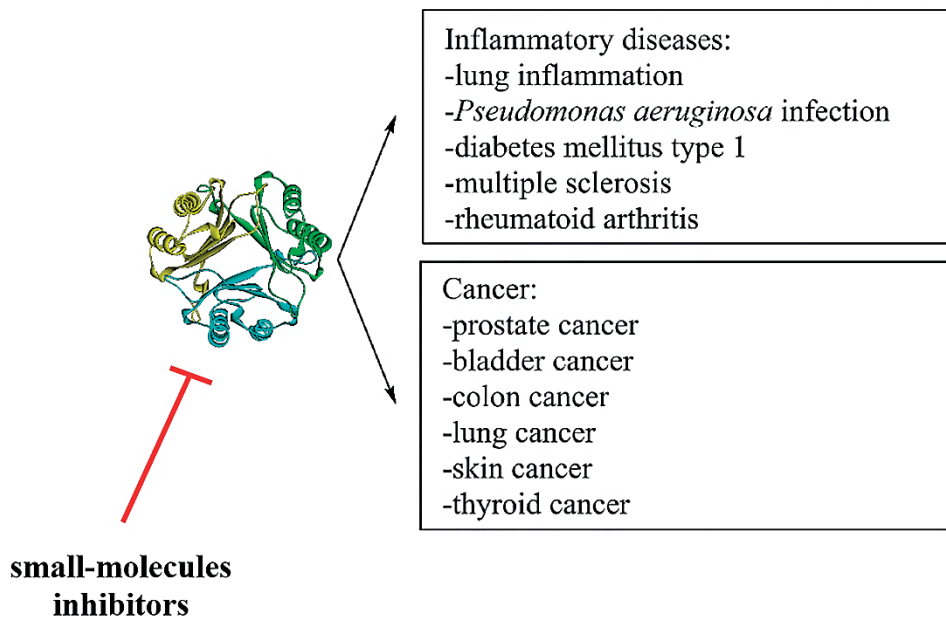
References

- [1] Laraia L, McKenzie G, Spring DR, Venkitaraman AR, Huggins DJ. Overcoming Chemical, Biological, and Computational Challenges in the Development of Inhibitors Targeting Protein-Protein Interactions. *Chem Biol* 2015;22:689–703. doi:10.1016/J.CHEMBIOL.2015.04.019.
- [2] Arkin MR, Tang Y, Wells JA. Small-molecule inhibitors of protein-protein interactions: progressing toward the reality. *Chem Biol* 2014;21:1102–14. doi:10.1016/j.chembiol.2014.09.001.
- [3] Bloom BR, Bennett B. Mechanism of a reaction in vitro associated with delayed-type hypersensitivity. *Science* 1966;153:80–2.
- [4] Nathan CF, Karnovsky ML, David JR. Alterations of macrophage functions by mediators from lymphocytes. *J Exp Med* 1971;133:1356–76. doi:10.1084/JEM.133.6.1356.
- [5] Bloom J, Sun S, Al-Abad Y. MIF, a controversial cytokine: a review of structural features, challenges, and opportunities for drug development. *Expert Opin Ther Targets* 2016;20:1463–75. doi:10.1080/14728222.2016.1251582.
- [6] O'Reilly C, Doroudian M, Mawhinney L, Donnelly SC. Targeting MIF in Cancer: Therapeutic Strategies, Current Developments, and Future Opportunities. *Inc Med Res Rev* 2016;36:440–60. doi:10.1002/med.21385.
- [7] Kok T, Wasielec AA, Cool RH, Melgert BN, Poelarends GJ, Dekker FJ. Small-molecule inhibitors of macrophage migration inhibitory factor (MIF) as an emerging class of therapeutics for immune disorders. *Drug Discov Today* 2018. doi:10.1016/j.drudis.2018.06.017.
- [8] Calandra T, Roger T. Macrophage migration inhibitory factor: a regulator of innate immunity. *Nat Rev Immunol* 2003;3:791–800. doi:10.1038/nri1200.
- [9] Leng L, Metz CN, Fang Y, Xu J, Donnelly S, Baugh J, et al. MIF Signal Transduction Initiated by Binding to CD74. *J Exp Med* 2003;197:1467–76. doi:10.1084/jem.20030286.
- [10] Poelarends GJ, Veetil VP, Whitman CP. The chemical versatility of the beta-alpha-beta fold: catalytic promiscuity and divergent evolution in the tautomerase superfamily. *Cell Mol Life Sci* 2008;65:3606–18. doi:10.1007/s00018-008-8285-x.
- [11] Merk M, Mitchell RA, Endres S, Bucala R. D-dopachrome tautomerase (D-DT or MIF-2): doubling the MIF cytokine family. *Cytokine* 2012;59:10–7. doi:10.1016/j.cyto.2012.03.014.
- [12] Benedek G, Meza-Romero R, Jordan K, Zhang Y, Nguyen H, Kent G, et al. MIF and D-DT are potential disease severity modifiers in male MS subjects. *Proc Natl Acad Sci U S A* 2017;114:E8421–9. doi:10.1073/pnas.1712288114.
- [13] Borghese F, Clanchy F IL. CD74: an emerging opportunity as a therapeutic target in cancer and autoimmune disease. *Expert Opin Ther Targets* 2011;15:237–51. doi:10.1517/14728222.2011.550879.
- [14] Strubin M, Berte C, Mach B. Alternative splicing and alternative initiation of translation explain the four forms of the Ia antigen-associated invariant chain. *EMBO J* 1986;5:3483–8.
- [15] Kok T, Wasielec AA, Dekker FJ, Poelarends GJ, Cool RH. High yield production of human invariant chain CD74 constructs fused to solubility-enhancing peptides and characterization of their MIF-binding capacities. *Protein Expr Purif* 2018;148:46–53. doi:10.1016/j.pep.2018.03.008.
- [16] Trivedi-Parmar V, Jorgensen WL. Advances and Insights for Small Molecule Inhibition of Macrophage Migration Inhibitory Factor. *J Med Chem* 2018: acs.jmedchem.8b00589. doi:10.1021/acs.jmedchem.8b00589.
- [17] Pantouris G, Syed MA, Fan C, Rajasekaran D, Cho TY, Rosenberg EM, et al. An Analysis of MIF Structural Features that Control Functional Activation of CD74. *Chem Biol* 2015;22:1197–205. doi:10.1016/j.chembiol.2015.08.006.
- [18] Eleftheriadis N, Neochoritis CG, Leus NGJ, van der Wouden PE, Dömling A, Dekker FJ. Rational Development of a Potent 15-Lipoxygenase-1 Inhibitor with *In Vitro* and *Ex Vivo* Anti-inflammatory Properties. *J Med Chem* 2015;58:7850–62. doi:10.1021/acs.jmedchem.5b01121.
- [19] Orita M, Yamamoto S, Katayama N, Aoki M, Takayama K, Yamagiwa Y, et al. Coumarin and chromen-4-one analogues as tautomerase inhibitors of macrophage migration inhibitory factor: discovery and X-ray crystallography. *J Med Chem* 2001;44:540–7. doi:10.1021/JM000386O.
- [20] Cournia Z, Leng L, Gandavadi S, Du X, Bucala R, Jorgensen WL. Discovery of Human Macrophage Migration Inhibitory Factor (MIF)-CD74 Antagonists via Virtual Screening. *J Med Chem* 2009;52:416–24. doi:10.1021/jm801100v.
- [21] Alam A, Pal C, Goyal M, Kundu MK, Kumar R, Iqbal MS, et al. Synthesis and bio-evaluation of human macrophage migration inhibitory factor inhibitor to develop anti-inflammatory agent. *Bioorg Med Chem* 2011;19:7365–73. doi:10.1016/j.bmc.2011.10.056.
- [22] Jorgensen WL, Gandavadi S, Du X, Hare AA, Trofimov A, Leng L, et al. Receptor agonists of macrophage migration inhibitory factor. *Bioorg Med Chem Lett* 2010;20:7033–6. doi:10.1016/j.bmcl.2010.09.118.

- [23] Ioannou K, Cheng KF, Crichlow G V, Birmipilis AI, Lolis EJ, Tsitsilonis OE, et al. ISO-66, a novel inhibitor of macrophage migration, shows efficacy in melanoma and colon cancer models. *Int J Oncol* 2014;45:1457–68. doi:10.3892/ijo.2014.2551.
- [24] Dziedzic P, Cisneros JA, Robertson MJ, Hare AA, Danford NE, Baxter RHG, et al. Design, Synthesis, and Protein Crystallography of Biaryltriazoles as Potent Tautomerase Inhibitors of Macrophage Migration Inhibitory Factor. *J Am Chem Soc* 2015;137:2996–3003. doi:10.1021/ja512112j.
- [25] Kok T, Wapenaar H, Wang K, Neochoritis CG, Zarganes-Tzitzikas T, Proietti G, et al. Discovery of chromenes as inhibitors of macrophage migration inhibitory factor. *Bioorg Med Chem* 2018;26:999–1005. doi:10.1016/J.BMC.2017.12.032.

Chapter 2

Small-molecule inhibitors of MIF as a potential class of therapeutics for inflammatory diseases and cancer



Publication in:

Kok T, Wasiel AA, Cool RH, Melgert BN, Poelarends GJ, Dekker FJ. Small-molecule inhibitors of macrophage migration inhibitory factor (MIF) as an emerging class of therapeutics for immune disorders. *Drug Discov Today* 2018. doi:10.1016/j.drudis.2018.06.017.

Abstract

Macrophage migration inhibitory factor (MIF) is an important cytokine for which an increasing number of functions is being described in the pathogenesis of inflammation and cancer. Nevertheless, the availability of potent and druglike MIF inhibitors that are well-characterized in relevant disease models remains limited. Highly potent and selective small molecule MIF inhibitors and validation of their use in relevant disease models will advance drug discovery. In this review we provide an overview of recent advances in the identification of MIF as a pharmacological target in the pathogenesis of inflammatory diseases and cancer. Based on that we give an overview of the current developments in the discovery and design of small molecule MIF inhibitors and define future aims in this field.

Keywords: macrophage migration inhibitory factor (MIF), inflammatory diseases, cancer, inhibitors

Introduction

Despite its discovery over 50 years ago in 1966 [1][2], the functions of the cytokine macrophage migration inhibitory factor (MIF) are still not fully elucidated. Initially, MIF was identified as a T cell-derived mediator that inhibits random movement of macrophages. Its activity was found to correlate with delayed-type hypersensitivity reactions, a prominent feature of several chronic diseases in humans [2]. In addition, MIF is released at sites of infection, causing macrophages to concentrate and carry out antigen processing and phagocytosis [3]. Today, MIF is recognized as a critical player in innate and adaptive immune responses that play a role in multiple diseases [4][5]. Therefore, the development of small molecule MIF inhibitors that interfere with its functions is quickly gaining importance.

The human MIF gene has been cloned and expressed for the first time in 1989 [6]. MIF is a relatively small protein that consists of 114 amino acids and has a molecular mass of 12,345 Da. Structural analysis of MIF revealed its striking similarities to bacterial enzymes from the tautomerase superfamily. Searching the human genome indicated that D-dopachrome tautomerase (D-DT) is the other gene with marked homology to MIF. Due to this similarity, D-DT is also referred to as MIF2 and an overlapping functional spectrum for MIF and D-DT has been suggested [7]. This should be taken into account in evaluation of MIF cytokine activities and in the development of small molecule MIF modulators.

MIF, a member of the tautomerase superfamily [8], is found across various organisms including bacteria, mice, plants, protozoa, helminths, molluscs, arthropods, and fish [9–11]. These tautomerase family members have similar enzyme activity involving an amino acid-terminal proline that acts as general base in keto-enol tautomerisation reactions of α -keto-carboxylates. In addition to its cytokine activity, MIF harbours keto-enol tautomerase and low-level dehalogenase activity, providing a functional link to other members of the tautomerase family [10]. MIF is a homotrimeric protein in which three monomers associate to form a symmetrical trimer (**Figure 1A**). Each MIF trimer has three tautomerase active sites at the interfaces of the monomer subunits. Characteristic for this family, MIF has a N-terminal proline (Pro-1), which is located within a hydrophobic pocket [12]. The residue Pro-1 was shown to be conserved between MIF and its bacterial homologues. Moreover, other invariant residues were identified as being clustered around the N-terminal proline. The evolutionary preservation of this region suggests its importance in the biological function of MIF [13]. Despite the lack of a known physiological substrate, it was shown that D-dopachrome (a stereoisomer of naturally occurring L-dopachrome), phenylpyruvate and *p*-hydroxyphenylpyruvate

are accepted as substrates by MIF (**Figure 1B**) [14][15]. A crystal structure of MIF in complex with *p*-hydroxyphenylpyruvate demonstrated that Pro-1 functions as a catalytic base in the tautomerase reaction [16]. It is well recognized that MIF's currently defined substrates either do not exist naturally *in vivo*, or do not exist at significant concentrations required for biological activity [17]. Nevertheless, small molecule modulators of MIF tautomerase activity may have an impact on MIF cytokine activity due to modulation of its conformation and/or ability to interact with other proteins.

Although MIF tautomerase activity may not be directly linked to its cytokine activity, it provides an opportunity for efficient screening of compound collections that could provide molecules that interfere with MIF cytokine activity. One of the best known targets to mediate MIF cytokine activity upon binding is the cluster of differentiation 74 (CD74) receptor [18]. Interestingly, recent findings demonstrate that MIF binding to CD74 occurs in the vicinity of the MIF tautomerase active site, which supports the idea that MIF tautomerase inhibitors may have potential to interfere with MIF cytokine function [19]. In this perspective, robust assays to test the ability of MIF tautomerase inhibitors to interfere with MIF cytokine functions *in vitro* and *in vivo* are highly important.

Functional cytokine roles of MIF and D-DT have been described in innate and adaptive immune responses [7][13]. It has been shown that MIF stimulates the production of pro-inflammatory mediators such as tumor necrosis factor (TNF α), interferon- γ (IFN γ), interleukins 1 β , 2, 6 and 8 (IL-1 β , IL-2, IL-6 and IL-8) and other effector cytokines [13]. The MIF-CD74 interaction is well known to initiate subsequent signaling cascades leading to cellular responses [18]. The biological functions of the CD74 receptor in immune diseases has recently been reviewed by Su *et al.* [20]. With respect to CD74 binding it is interesting to note that a difference has been reported between MIF and D-DT in a study by Merk *et al.* [21]. The same study indicates that MIF has a steeper dose-response ratio for macrophage migration inhibition and glucocorticoid overriding. This suggests an immune downregulatory role for D-DT in the presence of MIF. On the contrary, a recent study demonstrated that both MIF and D-DT are connected to disease progression of multiple sclerosis subjects [22]. This study and other studies as reviewed by Merk *et al.* [7] and O'Reilly *et al.* [5] indicate an overlapping activity spectrum for both cytokines.

Apart from the CD74 receptor MIF can also bind to chemokine receptors such as CXCR2, CXCR4 and CXCR7 to induce inflammatory and immune cell chemotaxis [23][24]. Given the pro-inflammatory activities, MIF is implicated in acute and chronic inflammatory diseases such as asthma, chronic obstructive pulmonary disease (COPD), rheumatoid arthritis, sepsis, diabetes, atherosclerosis

and cardiovascular diseases [13]. Many studies have investigated MIF as a biomarker for various diseases that have an inflammatory component, including systemic infections and sepsis, cancer, autoimmune diseases and different metabolic disorders, suggesting its important role in these diseases [25].

It should also be noted that MIF has been demonstrated to be post-translationally modified and that these modifications affect its biological functions [26]. MIF, but not D-DT, has a CXXC motif that can be oxidized to an intramolecular disulfide-bond. Oxidised MIF has also been proposed as a biomarker for different diseases [27]. Other studies indicate that oxidized MIF is the disease-related conformational isoform that could be employed for diagnosis and therapy [28][29]. It is to be expected that MIF redox behavior interferes with binding of small-molecule inhibitors. However, little is known about the structural consequences of these modifications in relation to inhibitor binding. Therefore, this represents an interesting and novel line of investigation.

Despite extensive studies on the functional role of MIF in multiple disease models, the identification and validation of the functional consequences of small molecule MIF tautomerase inhibitors is still in an early stage. The effects of such inhibitors have been investigated using the long-known standard MIF antagonist ISO-1 (**Table 1**) in *in vitro* assays and animal models [30]. Research on MIF antagonists is still in the preclinical stage and data on human disease are still observational [31], which indicates a need for further validation of MIF as a drug target.

In this review we aim to provide an overview of recent advances in the identification of MIF as a pharmacological target in the pathogenesis of inflammatory diseases and cancer (**Figure 1C**). Based on that we will provide an overview of the current developments in the discovery and design of small molecule MIF inhibitors and define future goals in this field.

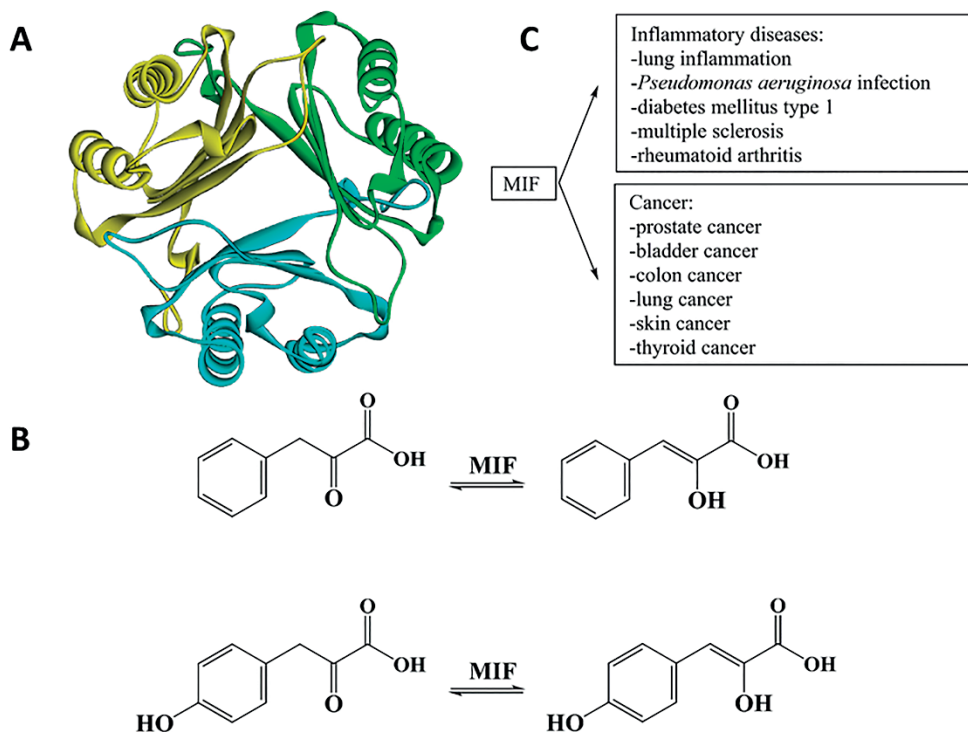


Figure 1. **A.** Crystal structure of MIF, showing that three monomers associate to form a symmetrical homotrimer (PDB 1CA7), **B.** MIF catalyses the tautomerisation of α -keto-carboxylates, **C.** Diseases for which a role of MIF has been described.

The role of MIF in pathogenesis of inflammatory diseases

Acute inflammation is a protective, beneficial, and self-limiting process during innate immune responses, but chronic inflammation is maladaptive and may result in tissue injury and dysfunction. For instance, some studies have shown that MIF plays an important role in the pathology of bladder inflammation. In bladder tissue substance P, an important inflammatory mediator, increases the levels of MIF. The important role of MIF was subsequently shown by administration of an anti-MIF antibody that could decrease substance P-induced inflammatory changes in bladder [32]. MIF was also shown to play a role in worsening of lung inflammation. High levels of MIF were reported to be detrimental for survival in a mouse model of pneumococcal pneumonia. Treatment of mice with a small-molecule inhibitor of MIF, designated MIF098 (Alissa-5) (**Table 2**), improved survival by reducing inflammatory responses [33]. In addition, higher MIF levels

were produced by alveolar macrophages in a mouse model for COPD as compared to those from healthy mice, and inhibition of MIF function by ISO-1 could block the corticosteroid-insensitive lung inflammation [34].

MIF also acts as an essential mediator of host immunity against various bacterial infections, however, its persistent or recurrent expression during chronic inflammatory disease stages can lead to loss of function and mortality. The involvement of MIF in the enhancement of biofilm formation by *Pseudomonas aeruginosa* was shown by the use of SCD-19, a small molecule inhibitor targeting MIF tautomerase activity. Application of this inhibitor resulted in lower bacterial burden in a mouse model of this infection as compared to untreated mice [35]. As another example, MIF promoter polymorphisms resulting in high MIF levels in cerebrospinal fluid of patients with streptococcal meningitis correlated with systemic complications and death [36]. Moreover, the authors of this study showed a reduction in bacterial load in a mouse model of pneumococcal pneumonia and sepsis after treatment with an anti-MIF antibody. From these studies it becomes clear that MIF plays a role in biofilm formation and mortality during bacterial infections, and it provides initial evidence that targeting MIF with small-molecule inhibitors has potential to interfere with such pathological conditions.

A relationship of MIF with autoimmune inflammatory disease has been observed in experimental autoimmune myocarditis. Early treatment of this disease with an anti-MIF antibody markedly delayed the onset of, and significantly reduced the severity of, this disease in rats [37]. The importance of MIF in the autoimmune inflammatory process has also been demonstrated for rheumatoid arthritis. It was observed that treatment with an anti-MIF antibody before immunization with type II collagen leads to delayed onset of arthritis in a mouse model of collagen-induced arthritis [38]. Altogether, these studies indicated that MIF correlates with disease severity in autoimmune inflammatory diseases and that treatment with anti-MIF antibodies has beneficial effects.

The role of MIF in pathogenesis of cancer

Inflammation and immunity play key roles in the onset and progression of cancer. Persistent or recurrent inflammation is related to development of cancer. In contrast, anti-cancer immune responses counteract the development and progression of cancer. From this perspective, the functional output of MIF as a key cytokine of the immune system can be connected to various aspects of oncology [39].

High serum levels of MIF are seen in cancer patients and tissues and MIF has consequently been proposed as a biomarker. In addition, high MIF levels correlate with poor prognosis in various carcinomas. Besides being involved in angiogenesis and thus indirectly in promoting tumour growth, the interaction of MIF with its receptors has been shown to initiate cancer promoting signal transduction pathways. For example, binding of MIF to CD74 can lead to stimulation of the ERK1/2 but also PI3K/AKT pathways and binding of MIF to the CXCR4 receptor was suggested to induce metastases [40].

Involvement of MIF in the development of prostate cancer was shown by studies with an androgen-independent prostate cancer cell line. In these studies, inhibition of MIF by ISO-1, anti-MIF antibody, or MIF siRNA resulted in decreased cell proliferation. ISO-1 significantly decreased tumor volume and tumor angiogenesis [41]. In another study with a prostate cancer cell line, treatment with anti-MIF antibodies was reported to reduce cell growth and in a xenograft mouse model of prostate cancer, anti-MIF antibodies were shown to limit tumor growth [42].

The involvement of MIF in the development of bladder cancer has also been described. MIF was reported to promote *in vitro* and *in vivo* bladder cancer progression via increasing cell proliferation and angiogenesis. The orally available MIF inhibitors, CPSI-2705 and -1306 (**Table 2**), have been shown to effectively decrease the growth and progression of bladder cancer *in vivo* [43].

A study on the role of MIF in the development of colon cancer in patients reported a positive correlation between MIF serum concentrations and colorectal cancer severity [44], thus indicating a potential use of MIF as biomarker. The same study demonstrated in a mouse model with colon carcinoma cell transplants that treatment with MIF inhibitor ISO-1 or anti-MIF antibodies resulted in significant reduction in the tumor burden, thus indicating a potential use of MIF directed therapeutics in cancer.

Furthermore, MIF has been indicated to be involved in the progression of lung cancer. Blocking the hydrophobic pocket that harbours MIF tautomerase activity, by a small molecule inhibitor of the isocoumarin class, SCD-19 (**Table 2**), significantly attenuated lung cancer growth [45].

Taken together, these studies demonstrate a positive correlation between MIF and the progression of cancer. Application of small molecule MIF inhibitors or anti-MIF antibodies attenuated cancer growth, thus indicating the potential of anti-MIF therapeutics in cancer [46][47][48].

Small-molecule inhibitors of MIF

Because of the essential involvement of MIF in the progression of numerous disorders with an inflammatory component, it is not surprising that attempts were made to find MIF directed therapeutics. One line of development is the application of biologicals, such as anti-MIF antibodies, as novel therapeutics. This approach has been used in many proof of concept studies [37] [38] [32] [41] [42] [44]. One clinical trial with an anti-MIF antibody has been reported, however no results have been revealed yet [49]. The other line of development is to generate MIF-binding small molecules with the aim to interfere with MIF functions. To develop MIF inhibitors, many studies resort to evaluating interference with MIF tautomerase activity. In this perspective, the evaluation of MIF tautomerase inhibitors for their interference with MIF cytokine functions in relevant disease models is highly important. Compared with biologicals, small molecule MIF inhibitors offer advantages such as lower manufacturing costs, non-immunogenic reaction and the possibility of oral administration. Therefore, this route of exploration gained tremendous interest. Here, we summarize the currently identified MIF tautomerase inhibitors and discuss the structure-activity relationship.

Inhibitors containing a chromen-4-one scaffold were identified in 2001 and their K_i values range between 0.04 and 7.4 μM . The most potent compound of this class is Orita-13 with a K_i of 0.04 μM [50]. However, a later investigation reported K_i values in the range of 13-22 μM for Orita-13 [51]. The phenol functionality in Orita-13 is also found in the MIF tautomerase substrates D-dopachrome and *p*-hydroxyphenylpyruvate and proved to be a successful design motif for MIF inhibitors (**Table 1**).

Isoxazolines as MIF inhibitors

The most frequently used reference inhibitor for MIF tautomerase activity is ISO-1, which was discovered in 2002. This inhibitor of the isoxazoline class was reported to inhibit MIF tautomerase activity in a dose-dependent manner. It binds at the same position as the substrate *p*-hydroxyphenylpyruvate with an IC_{50} of about 7 μM [52]. A later study described a K_i of 24 μM for inhibition of MIF tautomerase activity [51]. A MIF-CD74 binding study reported a maximum of 40% inhibition at 10 μM (**Table 1**) [53]. Further studies showed that inhibition of MIF by ISO-1 in a mouse model significantly reduced prostate cancer [41], colon cancer [44], and blocked melanoma cell growth [54]. Another study in a mouse model

showed that this MIF inhibitor blocks corticosteroid-insensitive lung inflammation [34]. In addition, ISO-1 was also reported to inhibit MIF activity in a mouse model of type 1 diabetes and to result in the delayed onset of this disease [55]. Altogether, ISO-1 is a valuable compound that is widely used as a reference inhibitor in the initial validation of small molecule MIF tautomerase inhibitors as potential therapeutics in diseases with an inflammatory component.

Another small molecule MIF tautomerase inhibitor with an isoxazoline scaffold is CPSI-1306 (**Table 2**). This inhibitor lacks the characteristic phenol functionality, which is advantageous for applications *in vivo*. Phenol functionalities are generally considered to be non-druglike because they are prone to phase II bioconjugation reactions thus resulting in quick inactivation and excretion in *in vivo* experiments. Oral administration of this inhibitor resulted in less severe symptoms in a mouse model for multiple sclerosis as compared to untreated mice [56]. Further small molecules with the same scaffold were synthesized and evaluated for MIF-inhibitory activity. The IC₅₀ of the most active compound, Alam-4b (**Table 1**), was 7.3 μM in a MIF tautomerase assay and this compound was shown to be nontoxic in a cell viability assay [57]. Subsequently, in 2014, another small molecule inhibitor of isoxazoline class, ISO-66 (**Table 1**), was reported. Its IC₅₀ in the MIF tautomerase assay was 1.5 μM and long-term administration of ISO-66 in a mouse model of colon cancer or melanoma was shown to be nontoxic and to decrease tumor burden significantly [58]. Thus, studies on MIF inhibitors with an isoxazoline scaffold demonstrate that the development and application of small molecule MIF inhibitors has potential to provide novel therapeutics.

1,2,3-triazoles as MIF inhibitors

In 2010, 1,2,3-triazole derivatives were reported as inhibitors of MIF. The most potent compounds, Jorgensen-3g and Jorgensen-3h (**Table 1**), showed IC₅₀ values of about 1 μM for MIF tautomerase activity and MIF-CD74 binding [59]. Subsequently, in 2015, improvements were made by synthesis of several optimized biaryltriazoles. This provided potent compounds with a phenolic hydroxyl group that bind to the MIF tautomerase active site. Nevertheless, some compounds had limited water solubility. The activity of this class of compounds was further improved by the addition of a fluorine atom adjacent to the phenolic hydroxyl group to enhance the hydrogen bond interaction with residue Asn-97 of MIF. This yielded the most potent compound, Dziedzic-3bb (**Table 1**), having a K_i value of

0.057 μM and a solubility that is in the normal range for orally available drugs [60].

The synthesis of fluorescently-labeled MIF inhibitors with a biaryltriazole scaffold was described in 2016. These inhibitors were used in a fluorescence polarization assay to assess the direct binding of inhibitors to the active site of MIF. The two most potent inhibitors, denoted Cisneros-3i and Cisneros-3j, were reported to have K_i 's of 0.057 and 0.034 μM in the tautomerase assay and K_d 's of 0.071 and 0.063 μM in the fluorescence polarization-based binding assay, respectively (**Table 1**) [61].

Covalent MIF inhibitors

The specific reactivity of the proline in the MIF active site provides opportunities to develop covalent inhibitors. In 2008, a compound of the phenylpyrimidine class, 4-IPP (**Table 2**), was reported to inactivate the MIF catalytic function by dehalogenation and formation of a covalent bond between C-4 of pyrimidine and the N-terminal nitrogen of Pro-1 in the MIF tautomerase active site. This compound also interferes with the biological functions of MIF as it was reported to irreversibly inhibit lung adenocarcinoma cell migration and anchorage-independent growth [62]. Later on, it was described that 4-IPP inhibits the growth of thyroid cancer cells by inducing apoptosis and mitotic cell death [63]. In 2009, isothiocyanates were discovered as irreversible MIF tautomerase inhibitors. The isothiocyanate BITC (**Table 2**) was shown to covalently modify the Pro-1 residue in the MIF active site. This drastically alters the MIF tertiary structure and results in loss of its tautomerase activity and in inhibition of MIF binding to CD74 [64].

The Woodward's reagent K is a classical heterocyclic electrophile with a specific reactivity [65][66]. Taking advantage of the specific reactivity of Woodward's Reagent K, covalent MIF inhibitors were developed. These inhibitors were shown to react with the active site Pro-1 of MIF and were applied for covalent labeling of MIF that proved to be selective. The covalent inhibitors were used as probes for labeling and imaging of MIF activities in living cells [67]. These examples demonstrate that it is possible to develop covalent active site-directed inhibitors of MIF that bind with a reasonable level of selectivity. Such inhibitors have great potential for labeling and imaging of enzyme activity *in vitro* and *in vivo*. In contrast to their application in imaging, covalent inhibitors are not preferred in pharmacotherapy due to concerns about their off-target effects.

Other type of MIF inhibitors

Apart from the isoxazolines and 1,2,3-triazoles, other types of reversible MIF inhibitors were also developed. In 2006, MIF inhibitors with a benzoxazinone scaffold were described and patented. The most potent compound, NVS-2, was reported to have an IC_{50} of 0.020 μM (**Table 2**) [68]. A later assay by Cisneros *et al.* reported a similar value for the K_i of 0.027 μM in the tautomerase assay and a K_d of 0.055 μM in the fluorescence polarization-based binding assay [61]. Subsequently, in 2010, substituted benzoxazol-2-ones were discovered as MIF antagonists (**Table 2**). One potent inhibitor from this class, MIF098 (Alissa-5), showed noncovalent inhibition in the MIF tautomerase assay, with an IC_{50} of around 0.010 μM . This inhibitor was further reported to attenuate MIF-dependent ERK phosphorylation in human synovial fibroblasts, which demonstrates possible use of MIF inhibition as therapy in rheumatoid arthritis [69].

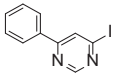
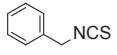
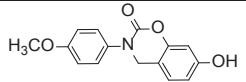
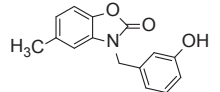
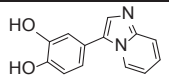
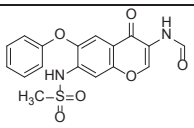
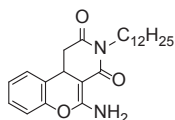
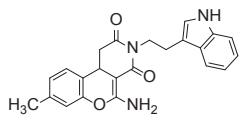
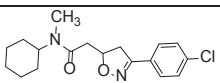
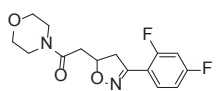
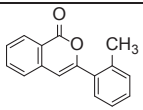
In 2012, an allosteric MIF tautomerase inhibitor p425 was identified in a high-throughput screening of a library consisting of 230,000 small molecules. However, this compound is a sulfonated azo compound (also known as pontamine sky blue), which has poor druglike properties [70]. Another study, in 2016, reported inhibitor K664-1 (**Table 2**) with a pyrimidazole scaffold as a novel MIF inhibitor with an IC_{50} of 0.16 μM in the MIF tautomerase assay [71]. This inhibitor provided protection to β -cells from cytokine-triggered apoptosis in a mouse model, which demonstrates its potential for the prevention of diabetes progression [72].

In 2016, compound T-614 (also known as iguratimod) was found to selectively inhibit MIF *in vitro* and *in vivo*. The compound has synergic effects with glucocorticoids to slow disease progression in a mouse model of multiple sclerosis. The IC_{50} of that compound in the MIF tautomerase assay was 6.81 μM (**Table 2**) [71]. Recently, novel types of MIF inhibitors were discovered using substitution-oriented screening (SOS). Inspired by the known chromen-4-one inhibitor Orita-13, a focused collection of compounds with a chromene scaffold was screened for MIF binding. In this study, inhibitors **10** and **17** (denoted Kok-10 and Kok-17, **Table 2**) provided IC_{50} values in the low micromolar range (18 and 6.2 μM , respectively) in the MIF tautomerase assay. The binding proved to be reversible and the enzyme kinetics suggested no direct interaction of these compounds with the substrate binding pocket [73].

Table 1. MIF inhibitors with a phenol functionality as the key structural element that presumably binds to the active site residue Asn-97 of MIF. TA = tautomerase assay, BA = binding assay MIF-CD74.

| Class | Compound | Structure | Activity, μM Reference(s) |
|----------------|----------------------------|-----------|--|
| chromen-4-one | Orita-13 | | $K_i = 0.04$ [50] (TA), $K_i = 17$ [60] (TA), $K_i = 13-22$ [51] (TA) |
| | ISO-1 | | $\text{IC}_{50} = 7$ [52] (TA), $\text{IC}_{50} = 24$ [51] (TA); Max. 40% inhibition [53] (BA) |
| isoxazoline | Alam-4b | | $\text{IC}_{50} = 7.3$ [57] (TA) |
| | ISO-66 | | $\text{IC}_{50} = 1.5$ [58] (TA) |
| | Jorgensen-3g | | $\text{IC}_{50} = 0.75$ [59] (TA); $\text{IC}_{50} = 0.9$ [59] (BA) |
| | Jorgensen-3h | | $\text{IC}_{50} = 1$ [59] (BA) |
| 1,2,3-triazole | Dziedzic-3bb (Cisneros-3i) | | Dziedzic-3bb: $K_i = 0.057$ [60] (TA) Cisneros-3i: $K_i = 0.057$ [61] (TA); $K_d = 0.071$ [61] (BA) |
| | Cisneros-3j | | $K_i = 0.034$ [61] (TA); $K_d = 0.063$ [61] (BA) |

Table 2. Covalent MIF inhibitors and MIF inhibitors with other structures. TA = tautomerase assay, BA = binding assay MIF-CD74.

| Class | Compound | Structure | Activity, μM Reference(s) |
|-------------------|-------------------|---|--|
| phenyl-pyrimidine | 4-IPP |  | $\text{IC}_{50} = 0.2\text{-}0.5$ [62] (TA) |
| isothiocyanate | BITC |  | $\text{IC}_{50} = 0.79$ [64] (TA) |
| benzoxazinone | NVS-2 |  | $\text{IC}_{50} = 0.020$ [68] (TA); $K_i = 0.027$ [61] (TA); $K_d = 0.055$ [61] (BA) |
| benzoxazol-2-one | MIF098 (Alissa-5) |  | $\text{IC}_{50} = 0.01$ [69] (TA) |
| pyrimidazole | K664-1 |  | $\text{IC}_{50} = 0.11$ [72] (TA); $K_i = 45$ [51] (TA), $K_i = 0.16$ [71] (TA) |
| | T-614 |  | $\text{IC}_{50} = 6.81$ [71] (TA) |
| chromene | Kok-10 |  | $\text{IC}_{50} = 18$ [73] (TA) |
| | Kok-17 |  | $\text{IC}_{50} = 6.2$ [73] (TA) |
| isoxazoline | CPSI-2705 |  | 2-10-fold more potent than ISO-1 [43] (TA) |
| | CPSI-1306 |  | 100-fold more potent than ISO-1 [43] (TA) |
| isocoumarin | SCD-19 |  | 100% inhibition at concentration of 100 μM [45] (TA) |

Future perspective of inhibitor development

Altogether it can be concluded that a diverse array of structures can be employed to develop MIF inhibitors that interact with MIF tautomerase activity via direct competition, via allosteric modulation of substrate binding, or via covalent binding. This provides a valuable starting points to design novel structural motifs that can be employed to interfere with MIF cytokine functions. Then, inhibitors of the enzymatic activity of MIF should also be evaluated in assays for binding to its cellular receptors such as CD74, CXCR2, CXCR4 and CXCR7 and/or in disease models. Within this context it is important to note that a study by Cisneros *et al.* in 2016 demonstrated that the reported IC_{50} 's of MIF tautomerase inhibitors were often not reproducible [51]. Most inhibitors were shown to be less potent than previously reported. As pointed out, for covalent or slow-tight binding inhibitors the IC_{50} 's are time dependent. Therefore, it is important to evaluate the reversibility of binding by recovery of enzyme activity in, for example, dilution experiments [74], which is too often neglected. Another complicating factor is the enzyme kinetics of the MIF tautomerase activity for its substrate *p*-hydroxyphenylpyruvate (4-HPP) that provides a sigmoidal curve, which cannot be fitted to a simple one-to-one binding model. Thus, the Michaelis-menten constant K_m cannot be derived easily and one needs to resort to $K_{half,app}$ [73] or $[S]_{0.5}$ [16]. This issue complicates the calculation of the equilibrium constant for inhibition (K_i) from IC_{50} values. Therefore, we argue to include enzyme dilution experiments and enzyme kinetic studies, or direct binding assays, if IC_{50} values are reported in order to provide a more complete analysis of MIF binding.

Conclusive remarks

MIF has been described to play a key role in the pathogenesis of inflammatory diseases and cancer. Small-molecule inhibitors of MIF have been developed and used in studies to investigate the biological role of MIF. Inhibitor ISO-1 is widely used as a reference compound for MIF inhibition in mouse models of lung inflammation, prostate cancer, colon cancer, melanoma and diabetes. Other small-molecule inhibitors also provided positive effects in various disease models. Altogether this indicates the potential of MIF inhibitors for development of novel therapeutics for diseases with an inflammatory component.

It is commonly presumed that MIF inhibitors identified in a MIF tautomerase assay have potential to interfere with MIF cytokine functions. Following this line of argumentation several classes of MIF tautomerase inhibitors

have been identified. The isoxazolines and the 1,2,3-triazoles are important classes of inhibitors from which potent MIF inhibitors were identified. Also covalent inhibitors that react with the active site Pro-1 of MIF have been identified and in one case used for activity-based labeling of MIF in living cells. Over time an increasing number of MIF inhibitors has been described, thus providing more insight in structure-activity relationship for MIF binding. A complicating factor in the analysis of MIF inhibitors proved to be covalent or slow-tight binding behavior that results in overestimation of the inhibitors potency. Also the sigmoidal enzyme kinetics for MIF tautomerase activity complicates analysis of MIF binding. We argue that anticipation of these issues is needed for successful further development of the field.

Ultimately, the identification of potent MIF inhibitors with favorable properties for drug discovery programs will enable the identification of novel therapeutics that target MIF functions in diseases with an inflammatory component. Furthermore, attention should be given toward the MIF structural homolog D-DT, which has been demonstrated to have an overlapping functional spectrum of action. This suggests that the combined or separate therapeutic targeting of D-DT and MIF could have additional advantages.

Conflict of Interest

The authors declare that they have no conflict of interest.

Acknowledgement

We thank the Directorate General of Higher Education Indonesia (DIKTI) for giving the grant 94.18/E4.4/2014, in collaboration with the University of Surabaya (Ubaya)-Indonesia and the University of Groningen (RuG)-The Netherlands (to TK). We acknowledge the European Research Council for providing ERC starting grant 309782 (to FJD) and the NWO for providing VIDI grants 723.012.005 (to FJD) and 700.56.421 (to GJP).

References

- [1] David JR. Its mediation by cell-free substances formed by lymphoid cell-antigen interaction. *Proc Natl Acad Sci U S A* 1966;56:72–7.
- [2] Bloom BR, Bennett B. Mechanism of a reaction in vitro associated with delayed-type hypersensitivity. *Science* 1966;153:80–2.
- [3] Nathan CF, Karnovsky ML, David JR. Alterations of macrophage functions by mediators from lymphocytes. *J Exp Med* 1971;133:1356–76. doi: 10.1084/Jem.133.6.1356.
- [4] Bloom J, Sun S, Al-Abed Y. MIF, a controversial cytokine: a review of structural features, challenges, and opportunities for drug development. *Expert Opin Ther Targets* 2016;20:1463–75. doi:10.1080/14728222.2016.1251582.
- [5] O'Reilly C, Doroudian M, Mawhinney L, Donnelly SC. Targeting MIF in Cancer: Therapeutic Strategies, Current Developments, and Future Opportunities. *Med Res Rev* 2016;36:440–60. doi:10.1002/med.21385.
- [6] Weiser WY, Temple PA, Witek-Giannotti JS, Remold HG, Clark SC, David JR. Molecular cloning of a cDNA encoding a human macrophage migration inhibitory factor. *Proc Natl Acad Sci U S A* 1989;86:7522–6.
- [7] Merk M, Mitchell RA, Endres S, Bucala R. D-dopachrome tautomerase (D-DT or MIF-2): doubling the MIF cytokine family. *Cytokine* 2012;59:10–7. doi:10.1016/j.cyto.2012.03.014.
- [8] Poelarends GJ, Veetil VP, Whitman CP. The chemical versatility of the beta-alpha-beta fold: catalytic promiscuity and divergent evolution in the tautomerase superfamily. *Cell Mol Life Sci* 2008;65:3606–18. doi:10.1007/s00018-008-8285-x.
- [9] Wasiel AA, Rozeboom HJ, Hauke D, Baas BJ, Zandvoort E, Quax WJ, et al. Structural and functional characterization of a macrophage migration inhibitory factor homologue from the marine cyanobacterium *Prochlorococcus marinus*. *Biochemistry* 2010;49:7572–81. doi:10.1021/bi1008276.
- [10] Wasiel AA, Baas B-J, Zandvoort E, Quax WJ, Poelarends GJ. Dehalogenation of an anthropogenic compound by an engineered variant of the mouse cytokine macrophage migration inhibitory factor. *ChemBiochem* 2012;13:1270–3. doi:10.1002/cbic.201200153.
- [11] Sparkes A, De Baetselier P, Roelants K, De Trez C, Magez S, Van Ginderachter JA, et al. The non-mammalian MIF superfamily. *Immunobiology* 2017;222:473–82. doi:10.1016/J.IMBIO.2016.10.006.
- [12] Suzuki M, Sugimoto H, Nakagawa A, Tanaka I, Nishihira J, Sakai M. Crystal structure of the macrophage migration inhibitory factor from rat liver. *Nat Struct Biol* 1996;3:259–66. doi:10.1038/nsb0396-259.
- [13] Calandra T, Roger T. Macrophage migration inhibitory factor: a regulator of innate immunity. *Nat Rev Immunol* 2003;3:791–800. doi:10.1038/nri1200.
- [14] Rosengren E, Åman P, Thelin S, Hansson C, Ahlfors S, Björk P, et al. The macrophage migration inhibitory factor MIF is a phenylpyruvate tautomerase. *FEBS Lett* 1997;417:85–8. doi:10.1016/S0014-5793(97)01261-1.
- [15] Donnelly SC, Bucala R. Macrophage migration inhibitory factor: a regulator of glucocorticoid activity with a critical role in inflammatory disease. *Mol Med Today* 1997;3:502–7. doi:10.1016/S1357-4310(97)01133-7.
- [16] Lubetsky JB, Swope M, Dealwis C, Blake P, Lolis E. Pro-1 of macrophage migration inhibitory factor functions as a catalytic base in the phenylpyruvate tautomerase activity. *Biochemistry* 1999;38:7346–54. doi:10.1021/bi990306m.
- [17] Cooke G, Armstrong ME, Donnelly SC. Macrophage migration inhibitory factor (MIF), enzymatic activity and the inflammatory response. *Biofactors* 2009;35:165–8. doi:10.1002/biof.27.
- [18] Leng L, Metz CN, Fang Y, Xu J, Donnelly S, Baugh J, et al. MIF Signal Transduction Initiated by Binding to CD74. *J Exp Med* 2003;197:1467–76. doi:10.1084/jem.20030286.
- [19] Pantouris G, Syed MA, Fan C, Rajasekaran D, Cho TY, Rosenberg EM, et al. An Analysis of MIF Structural Features that Control Functional Activation of CD74. *Chem Biol* 2015;22:1197–205. doi:10.1016/j.chembiol.2015.08.006.
- [20] Su H, Na N, Zhang X, Zhao Y. The biological function and significance of CD74 in immune diseases. *Inflamm Res* 2017;66:209–16. doi:10.1007/s00011-016-0995-1.
- [21] Merk M, Zierow S, Leng L, Das R, Du X, Schulte W, et al. The D-dopachrome tautomerase (DDT) gene product is a cytokine and functional homolog of macrophage migration inhibitory factor (MIF). *Proc Natl Acad Sci USA* 2011;108(34):E577–85. doi:10.1073/pnas.1102941108.
- [22] Benedek G, Meza-Romero R, Jordan K, Zhang Y, Nguyen H, Kent G, et al. MIF and D-DT are potential disease severity modifiers in male MS subjects. *Proc Natl Acad Sci U S A* 2017;114:E8421. doi:10.1073/PNAS.1712288114.

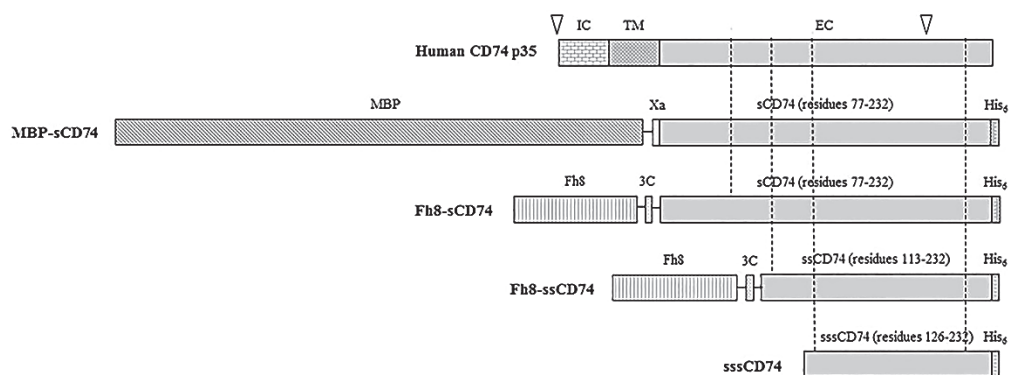
- [23] Weber C, Kraemer S, Drechsler M, Lue H, Koenen RR, Kapurniotu A, et al. Structural determinants of MIF functions in CXCR2-mediated inflammatory and atherogenic leukocyte recruitment. *Proc Natl Acad Sci U S A* 2008;105:16278–83. doi:10.1073/pnas.0804017105.
- [24] Bernhagen J, Krohn R, Lue H, Gregory JL, Zerneck A, Koenen RR, et al. MIF is a noncognate ligand of CXC chemokine receptors in inflammatory and atherogenic cell recruitment. *Nat Med* 2007;13:587–96. doi:10.1038/nm1567.
- [25] Grieb G, Kim B-S, Simons D, Bernhagen J, Pallua N. MIF and CD74 - Suitability as Clinical Biomarkers. *Mini-Reviews Med Chem* 2015;14:1125–31. doi:10.2174/1389557515666150203143317.
- [26] Schindler L, Dickerhof N, Hampton MB, Bernhagen J. Post-translational regulation of macrophage migration inhibitory factor: Basis for functional fine-tuning. *Redox Biol* 2018;15:135–42. doi:10.1016/j.redox.2017.11.028.
- [27] Schinagl A, Kerschbaumer RJ, Sabarth N, Douillard P, Scholz P, Voelkel D, et al. Role of the Cysteine 81 Residue of Macrophage Migration Inhibitory Factor as a Molecular Redox Switch. *Biochemistry* 2018;57:1523–32. doi:10.1021/acs.biochem.7b01156.
- [28] Thiele M, Kerschbaumer RJ, Tam FWK, Völkel D, Douillard P, Schinagl A, et al. Selective Targeting of a Disease-Related Conformational Isoform of Macrophage Migration Inhibitory Factor Ameliorates Inflammatory Conditions. *J Immunol* 2015;195:2343–52. doi:10.4049/jimmunol.1500572.
- [29] Schinagl A, Thiele M, Douillard P, Völkel D, Kenner L, Kazemi Z, et al. Oxidized macrophage migration inhibitory factor is a potential new tissue marker and drug target in cancer. *Oncotarget* 2016;7:73486–96. doi:10.18632/oncotarget.11970.
- [30] Al-Abed Y, VanPatten S. MIF as a disease target: ISO-1 as a proof-of-concept therapeutic. *Future Med Chem* 2011;3:45–63. doi:10.4155/fmc.10.281.
- [31] Bruchfeld A, Wendt M, Miller EJ. Macrophage Migration Inhibitory Factor in Clinical Kidney Disease. *Front Immunol* 2016;7:8. doi:10.3389/fimmu.2016.00008.
- [32] Meyer-Siegler KL, Vera PL. Intraluminal antibodies to macrophage migration inhibitory factor decrease substance P induced inflammatory changes in the rat bladder and prostate. *J Urol* 2004;172:1504–9.
- [33] Weiser JN, Roche AM, Hergott CB, LaRose MI, Connolly T, Jorgensen WL, et al. Macrophage Migration Inhibitory Factor Is Detrimental in Pneumococcal Pneumonia and a Target for Therapeutic Immunomodulation. *J Infect Dis* 2015;212:1677–82. doi:10.1093/infdis/jiv262.
- [34] Russell KE, Chung KF, Clarke CJ, Durham AL, Mallia P, Footitt J, et al. The MIF antagonist ISO-1 attenuates corticosteroid-insensitive inflammation and airways hyperresponsiveness in an ozone-induced model of COPD. *PLoS One* 2016;11:1–17. doi:10.1371/journal.pone.0146102.
- [35] Tynan A, Mawhinney L, Armstrong ME, O'Reilly C, Kennedy S, Caraher E, et al. Macrophage migration inhibitory factor enhances *Pseudomonas aeruginosa* biofilm formation, potentially contributing to cystic fibrosis pathogenesis. *FASEB J* 2017;31:5102–10. doi:10.1096/fj.201700463R.
- [36] Savva A, Brouwer MC, Roger T, Valls Serón M, Le Roy D, Ferwerda B, et al. Functional polymorphisms of macrophage migration inhibitory factor as predictors of morbidity and mortality of pneumococcal meningitis. *Proc Natl Acad Sci* 2016;113:3597–602. doi:10.1073/pnas.1520727113.
- [37] Matsui Y, Okamoto H, Jia N, Akino M, Uede T, Kitabatake A, et al. Blockade of macrophage migration inhibitory factor ameliorates experimental autoimmune myocarditis. *J Mol Cell Cardiol* 2004;37:557–66. doi:10.1016/J.YJMCC.2004.05.016.
- [38] Mikulowska A, Metz CN, Bucala R, Holmdahl R. Macrophage migration inhibitory factor is involved in the pathogenesis of collagen type II-induced arthritis in mice. *J Immunol* 1997;158:5514–7.
- [39] Nobre CCG, de Araújo JMG, Fernandes TAA de M, Cobucci RNO, Lanza DCF, Andrade VS, et al. Macrophage Migration Inhibitory Factor (MIF): Biological Activities and Relation with Cancer. *Pathol Oncol Res* 2017;23:235–44. doi:10.1007/s12253-016-0138-6.
- [40] Kindt N, Journe F, Laurent G, Saussez S. Involvement of macrophage migration inhibitory factor in cancer and novel therapeutic targets. *Oncol Lett* 2016;12:2247–53. doi:10.3892/ol.2016.4929.
- [41] Meyer-Siegler KL, Iczkowski K a, Leng L, Bucala R, Vera PL. Inhibition of macrophage migration inhibitory factor or its receptor (CD74) attenuates growth and invasion of DU-145 prostate cancer cells. *J Immunol* 2006;177:8730–9. doi:10.1073/jem.2006.04.016 [pii].
- [42] Hussain F, Freissmuth M, Völkel D, Thiele M, Douillard P, Antoine G, et al. Human anti-macrophage migration inhibitory factor antibodies inhibit growth of human prostate cancer cells in vitro and in vivo. *Mol Cancer Ther* 2013;12:1223–34. doi:10.1158/1535-7163.MCT-12-0988.
- [43] Choudhary S, Hegde P, Pruitt JR, Sielecki TM, Choudhary D, Scarpato K, et al. Macrophage migratory inhibitory factor promotes bladder cancer progression via increasing proliferation and angiogenesis. *Carcinogenesis* 2013;34:2891–9. doi:10.1093/carcin/bgt239.
- [44] He X-X, Chen K, Yang J, Li X-Y, Gan H-Y, Liu C-Y, et al. Macrophage migration inhibitory factor promotes colorectal cancer. *Mol Med* 2009;15:1–10. doi:10.2119/molmed.2008.00107.

- [45] Mawhinney L, Armstrong ME, O' Reilly C, Bucala R, Leng L, Fingerle-Rowson G, et al. Macrophage Migration Inhibitory Factor (MIF) Enzymatic Activity and Lung Cancer. *Mol Med* 2014;20:729–35. doi:10.2119/molmed.2014.00136.
- [46] Mangano K, Mazzon E, Basile MS, Di Marco R, Bramanti P, Mammanna S, et al. Pathogenic role for macrophage migration inhibitory factor in glioblastoma and its targeting with specific inhibitors as novel tailored therapeutic approach. *Oncotarget* 2018;9:17951–70. doi:10.18632/oncotarget.24885.
- [47] Lechien JR, Nassri A, Kindt N, Brown DN, Journe F, Saussez S. Role of macrophage migration inhibitory factor in head and neck cancer and novel therapeutic targets: A systematic review. *Head Neck* 2017;39:2573–84. doi:10.1002/hed.24939.
- [48] Wang S, Cen X, Liang X, Tang Y. Macrophage migration inhibitory factor: a potential driver and biomarker for head and neck squamous cell carcinoma. *Oncotarget* 2017;8:10650–61. doi:10.18632/oncotarget.12890.
- [49] Phase 1 Study of Anti-Macrophage Migration Inhibitory Factor (Anti-MIF) Antibody in Solid Tumors - Full Text View - ClinicalTrials.gov n.d. <https://clinicaltrials.gov/ct2/show/study/NCT01765790> (accessed February 20, 2018).
- [50] Orita M, Yamamoto S, Katayama N, Aoki M, Takayama K, Yamagiwa Y, et al. Coumarin and chromen-4-one analogues as tautomerase inhibitors of macrophage migration inhibitory factor: discovery and X-ray crystallography. *J Med Chem* 2001;44:540–7. doi: 10.1021/jm000386o
- [51] Cisneros JA, Robertson MJ, Valhondo M, Jorgensen WL. Irregularities in enzyme assays: The case of macrophage migration inhibitory factor. *Bioorg Med Chem Lett* 2016;26:2764–7. doi:10.1016/j.bmcl.2016.04.074.
- [52] Lubetsky JB, Dios A, Han J, Aljabari B, Ruzsicska B, Mitchell R, et al. The Tautomerase Active Site of Macrophage Migration Inhibitory Factor Is a Potential Target for Discovery of Novel Anti-inflammatory Agents. *J Biol Chem* 2002;277:24976–82. doi:10.1074/jbc.M203220200.
- [53] Cournia Z, Leng L, Gandavadi S, Du X, Bucala R, Jorgensen WL. Discovery of human macrophage migration inhibitory factor (MIF)-CD74 antagonists via virtual screening. *J Med Chem*. 2009;52(2):416–24. doi: 10.1021/jm801100v.
- [54] Tanese K, Hashimoto Y, Berkova Z, Wang Y, Samaniego F, Lee JE, et al. Cell Surface CD74–MIF Interactions Drive Melanoma Survival in Response to Interferon- γ . *J Invest Dermatol* 2015;135:2775–84. doi:10.1038/jid.2015.204.
- [55] Korf H, Breser L, Van Hoeck J, Godoy J, Cook DP, Stijlemans B, et al. MIF inhibition interferes with the inflammatory and T cell-stimulatory capacity of NOD macrophages and delays autoimmune diabetes onset. *PLoS One* 2017;12:e0187455. doi:10.1371/journal.pone.0187455.
- [56] Kithcart AP, Cox GM, Sielecki T, Short A, Pruitt J, Papenfuss T, et al. A small-molecule inhibitor of macrophage migration inhibitory factor for the treatment of inflammatory disease. *FASEB J* 2010;24:4459–66. doi:10.1096/fj.10-162347.
- [57] Alam A, Pal C, Goyal M, Kundu MK, Kumar R, Iqbal MS, et al. Synthesis and bio-evaluation of human macrophage migration inhibitory factor inhibitor to develop anti-inflammatory agent. *Bioorg Med Chem* 2011;19:7365–73. doi:10.1016/j.bmc.2011.10.056.
- [58] Ioannou K, Cheng KF, Crichlow G V, Birmpilis AI, Lolis EJ, Tsitsilonis OE, et al. ISO-66, a novel inhibitor of macrophage migration, shows efficacy in melanoma and colon cancer models. *Int J Oncol* 2014;45:1457–68. doi:10.3892/ijo.2014.2551.
- [59] Jorgensen WL, Gandavadi S, Du X, Hare AA, Trofimov A, Leng L, et al. Receptor agonists of macrophage migration inhibitory factor. *Bioorg Med Chem Lett* 2010;20:7033–6. doi:10.1016/j.bmcl.2010.09.118.
- [60] Dziedzic P, Cisneros JA, Robertson MJ, Hare AA, Danford NE, Baxter RHG, et al. Design, Synthesis, and Protein Crystallography of Biaryltriazoles as Potent Tautomerase Inhibitors of Macrophage Migration Inhibitory Factor. *J Am Chem Soc* 2015;137:2996–3003. doi:10.1021/ja512112j.
- [61] Cisneros JA, Robertson MJ, Valhondo M, Jorgensen WL. A Fluorescence Polarization Assay for Binding to Macrophage Migration Inhibitory Factor and Crystal Structures for Complexes of Two Potent Inhibitors. *J Am Chem Soc* 2016;138:8630–8. doi:10.1021/jacs.6b04910.
- [62] Winner M, Meier J, Zierow S, Rendon BE, Crichlow G V., Riggs R, et al. A Novel, Macrophage Migration Inhibitory Factor Suicide Substrate Inhibits Motility and Growth of Lung Cancer Cells. *Cancer Res* 2008;68:7253–7. doi:10.1158/0008-5472.CAN-07-6227.
- [63] Varinelli L, Caccia D, Volpi CC, Caccia C, De Bortoli M, Taverna E, et al. 4-IPP, a selective MIF inhibitor, causes mitotic catastrophe in thyroid carcinomas. *Endocr Relat Cancer* 2015;22:759–75. doi:10.1530/ERC-15-0299.
- [64] Ouertatani-Sakouhi H, El-Turk F, Fauvet B, Roger T, Roy D Le, Karpinar DP, et al. A new class of isothiocyanate-based irreversible inhibitors of macrophage migration inhibitory factor. *Biochemistry* 2009;48:9858–70. doi:10.1021/bi900957e.

- [65] Woodward RB, Olofson RA, Mayer H. A New Synthesis of Peptides. *J Am Chem Soc* 1961;83:1010–2. doi:10.1021/ja01465a072.
- [66] Woodward RB, Olofson RA. The Reaction of Isoxazolium Salts with Bases. *J Am Chem Soc* 1961;83:1007–9. doi:10.1021/ja01465a069.
- [67] Qian Y, Schürmann M, Janning P, Hedberg C, Waldmann H. Activity-Based Proteome Profiling Probes Based on Woodward's Reagent K with Distinct Target Selectivity. *Angew Chemie Int Ed* 2016;55:7766–71. doi:10.1002/anie.201602666.
- [68] Billich A, Lehr P, Gstach H. MIF-Inhibitors. United States Patent Application Publication 2007; US 20070219189A1.
- [69] Hare AA, Leng L, Gandavadi S, Du X, Cournia Z, Bucala R, et al. Optimization of N-benzyl-benzoxazol-2-ones as receptor antagonists of macrophage migration inhibitory factor (MIF). *Bioorg Med Chem Lett* 2010;20:5811–4. doi:10.1016/j.bmcl.2010.07.129.
- [70] Bai F, Asojo OA, Cirillo P, Ciustea M, Ledizet M, Aristoff PA, et al. A novel allosteric inhibitor of macrophage migration inhibitory factor (MIF). *J Biol Chem* 2012;287:30653–63. doi:10.1074/jbc.M112.385583.
- [71] Bloom J, Metz C, Nalawade S, Casabar J, Cheng KF, He M, et al. Identification of Iguratumod as an Inhibitor of Macrophage Migration Inhibitory Factor (MIF) with Steroid-sparing Potential. *J Biol Chem* 2016;291:26502–14. doi:10.1074/jbc.M116.743328.
- [72] Vujicic M, Nikolic I, Krajnovic T, Cheng KF, Vanpatten S, He M, et al. Novel inhibitors of macrophage migration inhibitory factor prevent cytokine-induced beta cell death. *Eur J Pharmacol* 2014;740:683–9. doi:10.1016/j.ejphar.2014.06.009.
- [73] Kok T, Wapenaar H, Wang K, Neochoritis CG, Zarganes-Tzitzikas T, Proietti G, et al. Discovery of chromenes as inhibitors of macrophage migration inhibitory factor. *Bioorg Med Chem* 2017;26(5):999–1005. doi:10.1016/j.bmc.2017.12.032.
- [74] Strelow J, Dewe W, Iversen PW, Brooks HB, Radding JA, McGee J, et al. Mechanism of Action Assays for Enzymes. Eli Lilly & Company and the National Center for Advancing Translational Sciences; 2004.

Chapter 3

High yield production of human CD74 as fusion proteins



Publication in:

Kok T, Wasiel AA, Dekker FJ, Poelarends GJ, Cool RH. High yield production of human invariant chain CD74 constructs fused to solubility-enhancing peptides and characterization of their MIF-binding capacities. *Protein Expr Purif* 2018;148:46–53. doi:10.1016/j.pep.2018.03.008.

Abstract

The HLA class II histocompatibility antigen gamma chain, also known as HLA-DR antigen-associated invariant chain or CD74, has been shown to be involved in many biological processes amongst which antigen loading and transport of MHC class II molecules from the endoplasmic reticulum to the Golgi complex. It is also part of a receptor complex for Macrophage Migration Inhibitory Factor (MIF), and participates in inflammatory signaling. The inhibition of MIF-CD74 complex formation is regarded as a potentially attractive therapeutic target in inflammation, cancer and immune diseases. In order to be able to produce large quantities of the extracellular moiety of human CD74, which has been reported to be unstable and protease-sensitive, different constructs were made as fusions with two solubility enhancers: the well-known maltose-binding domain and Fh8, a small protein secreted by the parasite *Fasciola hepatica*. The fusion proteins could be purified with high yields from *Escherichia coli* and were demonstrated to be active in binding to MIF. Moreover, our results strongly suggest that the MIF binding site is located in the sequence between the transmembrane and the membrane-distal trimerisation domain of CD74, and comprises at least amino acids 113-125 of CD74.

Key words: CD74, MIF, fusion proteins, solubility enhancers

Abbreviations

| | |
|----------|--|
| BSA | bovine serum albumin |
| CD74 | cluster of differentiation 74 |
| CLIP | class II-associated Ii peptide |
| ELISA | enzyme-linked immunosorbent assay |
| Fh8 | <i>Fasciola hepatica</i> 8-kDa antigen |
| Ii | invariant chain |
| MBP | maltose binding protein |
| MHCII | major histocompatibility complex class II molecules |
| MIF | macrophage migration inhibitory factor |
| PBS | phosphate-buffered saline |
| PCR | polymerase chain reaction |
| SDS PAGE | sodium dodecyl sulphate polyacrylamide gel electrophoresis |
| ITC | isothermal titration calorimetry |

Introduction

CD74 (Cluster of Differentiation 74), also referred to as HLA class II histocompatibility antigen gamma chain or HLA-DR antigen-associated invariant chain Ii, is a non-polymorphic type II transmembrane glycoprotein that has been demonstrated to perform a variety of cellular functions. It was initially identified in complex with major histocompatibility complex class II (MHCII) molecules and soon recognized for its role in antigen presentation via its involvement in assembly and subcellular trafficking of the MHCII complex [1]. The four isoforms of human CD74 differ in activity and cellular expression [2][3]. Due to an arginine motif in their N-terminal extension, isoforms p35 and p43 are retained in the endoplasmic reticulum (ER) except when they form a complex with MHCII molecules, in which this retention motif is masked so that the complex can traffic to post-ER compartments. Typically, the luminal domain of CD74 undergoes progressive proteolytic degradation in the endosomal/lysosomal system, finally leaving a fragment, the small class-II-associated invariant chain peptide (CLIP), attached to the MHC class II molecule. In contrast to p35 and p45, isoforms p33 and p41 do not have the ER retention signal allowing these isoforms to traffic in non-MHCII expressing cells [3].

In addition to its role in subcellular trafficking, a small portion of CD74 functions as a cellular receptor for the immune regulatory cytokine macrophage migration inhibitory factor (MIF). Although MIF can also bind to G-protein coupled receptors CXCR2, CXCR4 and CXCR7, the CD74-mediated signaling is recognized to play an important role in many diseases connected to inflammation, as well as cell proliferation and differentiation [4][5][6]. Recently, serum levels of not only MIF but also the soluble, circulating version of CD74 were reported to be related to liver and respiratory diseases [7][8]. Taken together, the MIF-CD74 interaction and the related signaling pathway have become attractive targets for novel therapies, as also illustrated by the humanized monoclonal anti-CD74 antibody milatuzumab that recently received orphan drug designation from the Food and Drug Administration in the USA for the treatment of multiple myeloma and chronic lymphocytic leukemia [9]. Excellent descriptions of the biological and structural aspects of CD74 can be found in two recent reviews [2] [10].

In the light of CD74's fate in the endosomal/lysosomal system, it may not be surprising that the study of the binding of MIF to CD74 is hampered by the partially unstable structure of CD74; only the trimerisation domain within the extracellular moiety appears to have a stable structure [11]. In addition, the production yield of the extracellular moiety of CD74 in bacterial cells is not very high [12]. The application of fusion technology via the use of affinity fusion tags,

in particular solubility enhancing peptides, is frequently used to improve the yield of active, pure protein [13][14][15]. We have tested two affinity tags: the well-documented maltose-binding protein (MBP) and the recently reported small EF-hand protein Fh8 from the parasitic trematode *Fasciola hepatica*. MBP is a large (43 kDa), highly soluble protein of *E. coli* that acts as a solubility enhancer tag [16]. For purification, MBP fusion proteins can bind to immobilized amylose resins and be eluted using maltose [17]. Similar to MBP, the small (8 kDa) protein Fh8 combines solubility enhancing properties to the possibility of affinity chromatography [18][19][20].

In this study we made use of the MBP and Fh8 fusion partners to obtain a high yield of soluble CD74 and characterized the purified fusion proteins for binding to MIF. In addition to the fused proteins, we also tested the cleaved products for their binding activity. The results allowed us to conclude that the extracellular moiety of CD74 between the transmembrane region and the membrane-distal trimerisation domain, in particular amino acids 113-125, is involved in binding of MIF.

Materials and methods

Procedures for restriction enzyme digestions, ligation, transformation, and other standard molecular biology manipulations were performed as described by Sambrook *et al.* [21]. The PCR was carried out in a DNA thermal cycler model GS-1 (Biolegio, The Netherlands). DNA sequencing was performed by Macrogen, Korea. Proteins were analyzed by gel electrophoresis using 10% sodium dodecyl sulphate polyacrylamide gels (SDS-PAGE; Invitrogen, The Netherlands). The gels were stained with InstantBlue protein stain (Expedeon, UK). Protein markers used for SDS-PAGE were PageRuler Prestained Protein Ladder marker (Thermo Scientific, The Netherlands) or SeeBlue Plus2 Prestained marker (Invitrogen, The Netherlands).

Protein concentrations were determined by the Pierce™ Coomassie Protein Assay (Thermo Fischer Scientific, The Netherlands) using bovine serum albumin as a reference. Molar concentrations of MIF and CD74 proteins refer to the concentrations of their subunits.

Molecular weight analysis of purified proteins or proteins extracted from SDS-PAGE gels were performed by electrospray ionization-mass spectrometry using a Sciex API 3000 triple quadrupole mass spectrometer (AB Sciex, Canada), housed in the Mass Spectrometry Facility at the University of Groningen.

Plasmids and bacterial strains

The plasmid and bacterial strain used for MIF production in this study was pET20b(+) (Addgene, UK) and *E. coli* BL21 (DE3), respectively [22]. The plasmid and bacterial strains used for CD74 production were pET20b(+) and *Rosetta-gami* 2(DE3) (Novagen, Germany) for MBP the fusion proteins; and pET14b (Addgene, UK) and *E. coli* BL21 star (DE3) pRARE2 (Thermo Fisher Scientific, The Netherlands) for the Fh8 fusion proteins.

DNA manipulations

(i) Construction of pET20b-MBP-sCD74 expression vector. Plasmid pCR T7/CT TOPO encoding the extracellular domain of human CD74 with a C-terminal His-tag was a kind gift from Prof. Richard Bucala [4].

The MBP-sCD74 fusion construct was generated by the overlap extension PCR method. The first DNA fragment, containing the MBP gene and the sequence encoding the factor Xa cleavage site, was amplified by PCR using pMAL-c2X vector as a template and a pair of primers: MBP-EXT-Fw (5'-CAG CGA **CAT ATG** AAA ATC GAA GAA GGT AAA CTG GTA ATC-3'; *NdeI* site in bold) and MBP-FUS-Rv (5'-ACG ACC TTC GAT GAA TTC TGA AAT CCT TCC CTC GAT CCC GAG GTT-3'; nucleotide sequence encoding the factor Xa cleavage site is underlined). The second fragment, containing the sCD74 gene was amplified using pET20b (sCD74) as a template. Plasmid pET20b-sCD74 was made as follows: the CD74 gene was amplified (primers: CD74-Fw: 5'-CAG CGA **CAT ATG** CAG GGC CGG CTG GAC AAA CTG ACA GTC ACC-3', *NdeI* site in bold; and CD74-Rv: 5'-CTG ATG GAT **CTC GAG** CAT GGG GAC TGG GCC CAG ATC CTG CTT-3', *XhoI* site in bold) and, after *NdeI/XhoI*-digestion, ligated into the pET20b vector. The sCD74 gene fragment was amplified from this plasmid using the following primers: MBP-FUS-Fw (5'-AAC CTC GGG ATC GAG GGA AGG ATT TCA GAA TTC ATC GAA GGT CGT CAG GGC CGG CTG GAC AAA CTG ACA GTC ACC TC-3'; nucleotide sequences for factor Xa cleavage site underlined) and CD74-Rv. The two fragments generated in the first round of PCR were fused in the second round using MBP-EXT-Fw and CD74-Rv primers. After digestion with *NdeI* and *XhoI* and purification, this fragment was ligated into the pET20b vector cleaved with the same restriction enzymes. The newly constructed expression vector was denoted pET20b-MBP-sCD74 and its fidelity was confirmed by DNA sequencing.

(ii) Construction of pCoBo-Fh8-sCD74 and pCoBo-Fh8-ssCD74 expression vectors. For production of Fh8-fused proteins, a modified pET15b vector was created that contains two multiple cloning sites separated by a 3C cleavage sequence in the following manner: (1) The *Hind*III site in pET15b was removed by mutagenesis; (2) oligonucleotides were designed with restriction sites *Age*I and *Kpn*I followed by a DNA stretch encoding the rhinovirus 3C proteolytic site (LEVLFQ/GP) and with a *Nco*I sequence on each end of the oligonucleotides, allowing cloning into the *Nco*I site of pET15b. The oligos were designed in such a manner that the “upstream” *Nco*I site closest to the T7 promoter would be lost. The proper orientation of this insert in the modified plasmid was checked by restriction analysis and sequencing; (3) The DNA encoding Fh8 was amplified from plasmid pD454-Fh8 (DNA2.0 Inc., USA) using the following primers carrying *Age*I and *Kpn*I restriction sites (in bold), respectively: Fh8AQUAFwd (5'-TTA AGA AGG AGA TAT ACC ATG CAA ACC **GGT** ATG CCG AGC GTT CAA GAA G-3') and Fh8AQUARev (5'-TTG AAA AAG CAC TTC AAG ACC TCC **GGT ACC** AGA TGT GCC GCT GCT CAG-3'). The DNA fragment was cloned into the modified pET15b vector cleaved with *Age*I and *Kpn*I using AQUA cloning [23]; (4) Oligonucleotides were designed to insert a new multiple cloning site comprising restriction sites *Bam*HI, *Hind*III, *Nde*I, *Sml*I, *Xho*I, *Sma*I, *Xma*I, with an upstream *Nco*I site and a dysfunctional *Bam*HI site downstream. The hybridised oligos were ligated in the plasmid cleaved with *Nco*I and *Bam*HI. This plasmid was named pCoBo-Fh8.

The CD74 gene on the pET20b-MBP-sCD74 plasmid was amplified using the following primers: CD74-Fwd (5'-GCA TCA GGA TCC ATT GGA GCA AAT **AAG CTT** CGG CTG GAC AAA CTG AC-3') and CD74-Rev (5'-TTG TTA GCA GCC GGA TCG TCA TTA **CCC GGG** GG ATC TCA GTG GTG GTG-3') for Fh8-sCD74; and CD74-Fwd (5'-GCA TCA GGA TCC ATT GGA GCA AAT **AAG CTT** CTG CTG ATG CAG GCG-3') and CD74-Rev (5'-TTG TTA GCA GCC GGA TCG TCA TTA **CCC GGG** GG ATC TCA GTG GTG GTG-3') for Fh8-ssCD74, carrying *Hind*III and *Sma*I restriction sites (bold). After digestion, the DNA fragment was ligated into the pCoBo-Fh8 vector cleaved with *Hind*III and *Sma*I, resulting in pCoBo-Fh8-sCD74 and pCoBo-Fh8-ssCD74, respectively. The inserts of all constructs were checked by DNA sequencing.

Protein production and purification

(i) Production and purification of CD74 fusion proteins. The pET20b-MBP-sCD74 and pCoBo-Fh8-sCD74 were transformed into *Rossetta-gami 2* (DE3) and

BL21 Star (DE3) +pRARE2 strain, respectively. For protein production, overnight pre-cultures were used to inoculate 1 L 2YT medium in a 5 L Erlenmeyer flask. Cultures were then grown until $OD_{600} \sim 0.5$. Isopropyl β -thiogalactopyranoside was added to a final concentration of 50 μ M and the cultures were incubated overnight at 20°C. Cells were harvested by centrifugation (3500 \times g, 15 min, 4°C), washed with 0.9% NaCl and the cell pellet stored at -20°C until further use. In a typical purification experiment, 10 g cell pellets from a 1 L culture were thawed and suspended in 15 mL of lysis buffer (50 mM Tris-HCl, 10% glycerol, pH 7.4) supplemented with 1 tablet protease inhibitor (Roche, The Netherlands), 19 mg EDTA and 19 mg EGTA. Cells were disrupted by sonication for 6 \times 30 s while cooled in ice-water (with 90 s rest in between each cycle) at a 50% duty cycle and 240 W output using a Branson sonifier model 450 (Branson Ultrasonics Corporation, USA), after which cell debris was removed by centrifugation (34,000 \times g, 60 min, 4°C). The cell free extract (supernatant) was incubated overnight at 4°C with 5 mL cOmplete HisTrap purification resin (Roche Life Science, The Netherlands), pre-equilibrated with lysis buffer. The non-bound proteins were removed as flow through by gravity flow. The column was then washed with 50 mL lysis buffer followed by 12 mL HT elution buffer (50 mM Tris-HCl, 500 mM imidazole, 10% glycerol, pH 7.4). Fractions were analyzed by SDS PAGE and those containing CD74 fusion proteins pooled.

HisTrap-purified MBP-fused CD74 proteins was applied to a gravity column containing 5 mL MBPTrap resin, pre-equilibrated with MT buffer (50 mM Tris-HCl, 10% glycerol, pH 7.4). After an overnight incubation at 4°C while mixing on a rotor, the non-bound proteins were removed from the column with 50 mL of MT buffer. Bound protein was eluted with 3.5 mL MT elution buffer (50 mM Tris-HCl, 10 mM maltose, 10% glycerol, pH 7.4). Fractions were analyzed by SDS PAGE, those containing CD74 fusion proteins were pooled, aliquoted, snapfrozen and stored in aliquots at -80°C.

Fh8-fused CD74 proteins could be further purified by a 5 mL octyl sepharose column (GE Healthcare, The Netherlands) at 10°C as described [12]. In short, the protein was dialysed against OS buffer (50 mM Tris-HCl, 150 mM NaCl, 5 mM $CaCl_2$, 10% glycerol, pH 7.6) and loaded on a 5-mL octyl sepharose column (GE Healthcare, The Netherlands), pre-equilibrated with OS buffer. After washing with low $CaCl_2$ -buffer (25 mM Tris-HCl, 75 mM NaCl, 2.5 mM $CaCl_2$, 10% glycerol, pH 7.6), the protein was eluted with 50 mM Tris, 5 mM EDTA, 10% glycerol, pH 7.6. Fractions were analyzed by SDS PAGE, those containing Fh8-fusion proteins were pooled, aliquoted, snapfrozen and stored in aliquots at -80°C.

(ii) Factor Xa cleavage of MBP-sCD74. The cleavage of the MBP-sCD74 fusion protein was performed in 50 mM Tris-HCl, 10% glycerol supplemented with 50 mM NaCl and 2 mM CaCl₂ at pH 7.4 by factor Xa protease (NEB, The Netherlands) with a mass/volume ($\mu\text{g}/\mu\text{L}$) ratio MBP-sCD74:factor Xa of 25:1, 3 hours incubation period at 4°C. The cleaved product was purified using cOmplete His-Trap purification resin. Fractions were analyzed by SDS PAGE, those containing sCD74 were pooled, aliquoted, snapfrozen and stored in aliquots at -80°C.

(iii) 3C cleavage of Fh8-ssCD74. The cleavage of the Fh8-ssCD74 fusion protein was performed in 50 mM Tris-HCl, 10% glycerol supplemented with 150 mM NaCl at pH 7.4 by 3C PreScission protease (GE Healthcare, The Netherlands) with a mass/volume ($\mu\text{g}/\mu\text{L}$) ratio Fh8-ssCD74:3C of 100:1, 1 hour at 4°C. The cleaved product was purified using octyl sepharose resin (GE Healthcare, The Netherlands) followed by cOmplete His-Trap purification resin, as described above. Fractions were analyzed by SDS PAGE, those containing ssCD74 were pooled, aliquoted, snapfrozen and stored in aliquots at -80°C. Protein sssCD74, produced by overnight incubation of Fh8-ssCD74 with 3C Precision protease at 4°C, was purified using cOmplete HisTrap resin.

(iv) Peptides MBP and Fh8. Proteins MBP was purchased from ProSpec-Tany TechnoGene Ltd (Germany). Fh8 was produced with pCoBo-Fh8 and purified using octyl sepharose resin.

(v) Production and purification of MIF. MIF was produced in BL21(DE3) in a similar manner as MBP-sCD74. After harvesting, cells were resuspended in lysis buffer supplemented with 1 tablet protease inhibitor (Roche, The Netherlands). Cell free extract was obtained as described earlier for MBP-sCD74 and incubated overnight at 4°C with 5 mL cOmplete His-Trap purification resin (Roche, The Netherlands), which had previously been equilibrated with the lysis buffer. The non-bound proteins were removed as flow through by gravity flow. The column was washed with 50 mL lysis buffer followed by 12 mL elution buffer (50 mM Tris-HCl, 500 mM imidazole, 10% glycerol, pH 7.4). Fractions were analyzed by SDS PAGE and those containing MIF were pooled, aliquoted, snap-frozen and stored at -80°C.

Analysis of proteins using size exclusion chromatography

MIF and CD74 proteins were analysed separately on an analytical size exclusion column. 20 μL of a 1 mg/mL protein solution was injected and run at 0.2 mL/min on a 3 ml Superdex200 5/150 column (GE Healthcare), equilibrated with PBS, pH 7.4, at 10 °C. To calibrate the column, the elution volumes of five marker proteins (GE Healthcare) were determined under identical conditions: thyroglobulin (669 kDa), ferritin (440 kDa), aldolase (158 kDa), conalbumin (75 kDa), and ovalbumin (43 kDa).

Binding assays

Enzyme-linked immunosorbent assay (ELISA)

The sCD74 proteins were characterised for MIF binding in an ELISA test. Wells in 96-well plates were coated with 100 μL of 300 nM MIF in phosphate-buffered saline (PBS) [400 ng/well]. After washing with 200 μL buffer PBS+Tween 0.05% and blocking with commercial blocker (Rockland, The Netherlands), 100 μL of 500 nM sCD74 was added, and the system was incubated for 30 min at room temperature. After the wells were washed and blocked, mouse anti-MBP mAb (Sigma-Aldrich, The Netherlands) or rabbit anti-CD74 pAb (Sinobiological, The Netherlands) was added. The bound complexes were detected after washing by the addition of goat anti-mouse horseradish peroxidase conjugate (Thermo Fisher Scientific, The Netherlands) or goat anti-rabbit horseradish peroxidase conjugate (Life Technologies, The Netherlands), and tetra methylbenzidine (Thermo Fisher Scientific, The Netherlands) as its substrate. After ~10 min the reaction was stopped by the addition of 1M H_2SO_4 and the absorbance at 450 nm measured. The specificity of binding was confirmed by using 100 μL of 500 nM MBP in PBS, and 100 μL of 500 nM Fh8 in PBS as controls. Each experiment was done in triplicate and repeated at least two times.

A dose-dependent ELISA was performed with sCD74 concentration ranging from 3 to 3200 nM (for MBP-sCD74) and 12 to 3200 nM (for Fh8-ssCD74). The corrected absorbance at 450 nm was then plotted against logarithm of concentration to find the dissociation constant of the binding.

Isothermal Titration Calorimetry (ITC)

Binding of MIF to CD74 was measured by ITC model ITC200 (Malvern, UK) at 25°C, 1000 rpm stirring speed, 120 seconds spacing between each injection. The cell was filled with 200 μ L of 40-85 μ M MBP-sCD74 in PBS and titrated with 20 consecutive injections of 2 μ L 70-220 μ M MIF in PBS. A cell filled with PBS only titrated with MIF and a cell filled with fusion protein titrated with PBS only were used as control.

Results and Discussion

Even though MIF was one of the first cytokines to have been described, many details of its signaling activities still have to be elucidated. Nevertheless, the involvement of receptor CD74 has been proven in many MIF-related diseases and this receptor has been recognised as a major pharmaceutical target. The interaction between MIF and CD74 was *in vitro* demonstrated to be located in the extracellular moiety of CD74 [4][24]. However, the unstable and protease-prone character of the extracellular moiety of CD74 has hampered further characterisation. Several attempts to obtain a good production of the extracellular moiety of CD74 with a C-terminal His-tag in bacteria resulted in low yields of soluble protein [12]. As a consequence, we have tried to tackle this problem by fusing CD74 to solubility-enhancing peptides. Two different solubility enhancing peptides were used: the large, but well characterised MBP protein [14] and the recently reported small protein Fh8 [16][17][18]. **Figure 1** presents a schematic overview of the fusion proteins encoded by the constructs that were made, and their corresponding amino acid sequences.

Production and purification of CD74 proteins

The fragments of the human CD74 gene as cloned into the expression vectors were not codon-optimized for bacterial expression. Therefore, we used *E.coli* strains that were transformed with the plasmid pRARE2 supplying tRNAs for 7 rare codons (AGA, AGG, AUA, CUA, GGA, CCC, and CGG), e.g. the strains *Rossetta-gami 2* (DE3) and BL21 Star (DE3) + pRARE2. This allowed high production yields of soluble MBP-sCD74, Fh8-sCD74 and Fh8-ssCD74 (**Figure 2**).

Fusion protein MBP-sCD74 was successfully purified by affinity chromatography using a HisTrap column followed by a MBP-Trap column. Mass

spectrometric analysis of the major band running just below the 62 kDa marker protein (**Figure 3**, lane 3) gave a mass of 62.326 kDa which corresponds to the calculated MW of 62.319 kDa. MS analysis of the tryptic digestion of the protein confirmed the identity of MBP-sCD74 by >90 % coverage. About ~60 mg of purified MBP-sCD74 was obtained from one liter of culture. Mass analysis of a contaminating protein running above the 14 kDa marker protein (**Figure 3**, lane 3) showed this to be a 14.711 kDa peptide, corresponding to a degradation product with a proteolytic cleavage between residues Pro112 and Leu113 of CD74. This deviates from previously observed cleavage sites in this region [25][26], a difference that is likely to be related to differences in *E. coli* strains and growth conditions that were used, and /or to the N- or C-terminally located His-tag leading to purification of different fragments. The proteolytic sensitivity is supported by the NMR study of fragment 133-208 of CD74, which showed that amino acids directly flanking the trimerisation domain are disordered [27]. In line with this, the CLIP region (residues 97-119) appears as a linear peptide without secondary structure in complex with MHCII molecules [28][29][30][31].

The large size of MBP (42 kDa) made us decide to also construct a fusion of sCD74 with the much smaller Fh8 protein, an EF-hand protein of 8 kDa that shows calcium-dependent binding to hydrophobic resins. The Fh8-sCD74 fusion protein was first purified by affinity chromatography on a HisTrap column. Similar to MBP-sCD74, purification of Fh8-sCD74 on the cOmplete HisTrap column resulted in a approximately 90% pure protein with an experimentally determined mass of 29.604 kDa, corresponding to the calculated mass of 29.605 kDa. The yield of Fh8-sCD74 was 30 mg per liter culture. Mass analysis of the contaminant protein running above the 14 kDa marker protein in the SDS-PAGE gel (**Figure 3**, lane 2) demonstrated this protein to have a mass of 14.711 kDa, similar to the contamination found in the MBP-sCD74 protein batch. Unfortunately, the octyl sepharose column did not improve the purity of the fusion protein. The difficulty to remove degradation products from fusion products are most likely due to the multimeric character of CD74: cleavage in loop regions does not necessarily affect trimer formation of CD74-derived proteins nor their chromatographic behaviour.

In an attempt to create a more protease-stable fragment of sCD74, a plasmid encoding fusion protein Fh8-ssCD74 (CD74 residues 113-232) was constructed (**Figure 1**). Production of this protein and purification on a cOmplete HisTrap column (**Figure 3**, lane 1) resulted in the high yield of 75 mg of ~95% pure protein per liter of culture with an experimentally determined mass of 25.461 kDa, corresponding to the calculated mass of 25.462 kDa. As anticipated, the previously observed contaminant of 14.711 kDa was not found in this protein batch.

In order to obtain the non-fused sCD74, fusion protein MBP-sCD74 was cleaved with factor Xa, followed by purification on a HisTrap column. This resulted in a mixture of sCD74 and lower molecular weight products (**Figure 3**, lane 5). Apparently, the MBP-sCD74 fusion protein is prone to cleavage with factor Xa at additional sites. Attempts to improve the purity of sCD74 by size exclusion and ion exchange chromatography were unsuccessful.

Similarly, 3C-mediated cleavage of Fh8-ssCD74 and subsequent purification of ssCD74 also resulted in a mixture of proteins of slightly smaller mass (results not shown). Also here, chromatography attempts to recover ssCD74 using HisTrap as a highly purified protein were not successful. Further experimentation indicated that a stable cleavage product of ssCD74, denoted as sssCD74, was obtained after overnight incubation at 4°C with 3C protease. Mass spectrometry analysis demonstrated that the molecular weight of this product was 13.343 kDa, corresponding to residues 126-232 with C-terminal His-tag, thus lacking almost the whole region up to the membrane-distal trimerisation domain of CD74 (**Figure 1**). This fragment could be highly purified with a cOmplete HisTrap column (**Figure 3**, lane 6). Noteworthy, fragment sssCD74 is comparable to the 18 kDa proteolytic fragment K3, that retains the ability to bind to MHCII molecules, and, like sssCD74, starts at residue Gly126 but has a C-terminal truncation [32].

When analyzed on an analytical size exclusion column, the fusion proteins MBP-sCD74, Fh8-sCD74 and Fh8-ssCD74 eluted earlier than expected (**Figure 4**). Although expected to run as trimers with molecular weights 186.9, 88.8, and 77.5 kDa, respectively, they eluted between the reference proteins ferritin (MW 440 kDa) and aldolase (158 kDa). At first impression, this seems to indicate that the fusion proteins form hexameric instead of trimeric structures. However, since fusion partners MBP and Fh8 are considered to be stable monomers, and since the elution volumes of cleaved products sCD74 and sssCD74 correspond to the expected elution volumes of their trimeric versions (60.9 and 39.9 kDa, respectively), this behaviour is more likely to be a consequence of increased hydrodynamic shapes of the trimeric fusion proteins. Such behaviour is not unexpected for fusion proteins that consist of two well-defined domains separated by an intrinsically disordered moiety. Our results suggest that all CD74 proteins used in this study are mostly present in a homotrimeric form. However, the chromatograms of the three fusion proteins show more than one peak indicating some heterogeneity. Fh8-sCD74 shows two major peaks which are not easily explained. MBP-sCD74 and Fh8-sCD74 show a small peak at c. 40 kDa, which can be interpreted as the trimer of the 14.711 kDa contamination. As expected, the elution volume of MIF fits to its trimeric form (40.3 kDa; **Figure 4**).

MIF binding capacities of CD74 proteins

The MIF binding capacities of the different CD74 proteins were assessed by ELISA. As depicted in **Figure 5A** and **B**, all fusion proteins of CD74 were able to bind to this cytokine. The lack of MIF binding to the MBP and Fh8 polypeptides demonstrated that the interactions of the CD74 fusion proteins with MIF are a consequence of the presence of CD74 and not of the fusion partners. Interestingly, at a concentration of 500 nM, fusion protein Fh8-ssCD74 gave a lower MIF-binding response than Fh8-sCD74 (**Figure 5B**) indicating that deletion of residues 77-112 of CD74 only partially affects the binding to MIF. The binding capacity of 500 nM non-fused sCD74 itself is also shown in **Figure 5C**. Deletion of residues 77-125 in the luminal moiety up to the membrane-distal trimerisation domain resulted in a complete loss of MIF binding capacity as is demonstrated by the lack of binding of 500 nM purified protein sssCD74 (**Figure 5C**). This is not due to a loss of structural stability since both sCD74 and sssCD74 behave as trimeric proteins during size exclusion chromatography (**Figure 4**). These results thus strongly suggest that the MIF-binding region lies N-terminal to the membrane-distal trimerisation domain of CD74.

These biochemical results differ from the results of a docking experiment in which amino acid sequences YGNMT and RHSLE within the trimerisation domain were predicted to be involved in the binding to MIF [33]. The docking experiment – as it is depending on three-dimensional structures - was performed with the crystal structures of MIF (PDB ID: 1MIF) and the membrane-distal trimerisation domain of CD74 (PDB ID: 1HIE), hence excluding the disordered region N-terminal to the trimerisation domain. Our results, especially the lack of interaction of sssCD74 with MIF in our ELISA assay (**Figure 5C**), indicate that the membrane-distal CD74 trimerisation domain is not or only weakly involved in the interaction with MIF, and is not sufficient for a high affinity interaction.

In order to get further insight in the formation of a complex between MIF and CD74, we performed a dose-dependent ELISA with MBP-sCD74 and Fh8-ssCD74 (**Figure 6**). Whereas the binding isotherm of MBP-sCD74 leads to an EC₅₀-value of approximately 110 nM, Fh8-ssCD74 leads to a 2.5-fold higher value of approximately 280 nM, suggesting that removal of residues 77-112 of CD74 is affecting but not destructing the interaction with MIF. Together with the lack of MIF-binding by sssCD74 (i.e. amino acids 126-232), these results indicate that CD74 amino acids 113-125 are of primary importance for the interaction with MIF, and that the amino acids N-terminal to this region add to the binding ability. ITC binding kinetics measurements confirmed that MIF binds to MBP-sCD74 (**Figure 7**). Complex formation is an exothermic reaction with a reaction enthalpy (ΔH) of

$-(2.5 \pm 0.5) \cdot 10^6$ cal/mol. This low enthalpy value made obtaining solid data of ITC experimentation rather difficult. The apparent dissociation constant (K_D) was 1.3 ± 0.1 μ M. This affinity is lower than the EC_{50} -value obtained with ELISA.

Earlier SPR measurements of the interaction between MIF and sCD74 have resulted in significantly higher reported affinities of 0.23 or 9 nM, depending on the experimental configuration [4]. We note, however, that the lack of details in this SPR study does not allow a direct comparison. Interestingly, the same study also shows a sandwich ELISA that seems to point at an EC_{50} value in the submicromolar range of sCD74, which is comparable to our ELISA results. The affinity measurements thus show considerable variety, which may be caused by different complex formation between these multimeric proteins under different experimental conditions. As Leng *et al.* [4] pointed out: based on the serum concentration of MIF, one would expect a nanomolar range affinity for its receptor. In that light it should be noted that the *in vitro* results have been obtained with bacterially produced proteins. The native proteins, with possible post-translational modifications on MIF and CD74 (e.g. oxidation and glycosylation [34]) may have different affinities. In addition, the transmembrane domain of CD74 is also able to trimerize [35][36] and thus may bring extra stability and raise the affinity for MIF.

Interestingly, the molar binding ratio in our ITC experiment was found to be 0.29 ± 0.03 . Assuming all MBP-sCD74 and MIF molecules to be active, this molar ratio indicates that a complex of a trimeric MIF with 3 trimers of MBP-sCD74 is formed. This suggests that MIF initiates signaling by clustering the trimeric CD74 receptor into a larger network that is needed to overcome the threshold for initiation of the signaling cascade.

Conclusions

Our research demonstrated that the luminal portion of CD74 can be produced at high yields in a bacterial expression system when fused to the solubility enhancing proteins MBP and Fh8. The purified fusion proteins were demonstrated to bind to MIF. The extracellular region from the transmembrane domain up to the membrane-distal trimerisation domain of CD74 appears to be essential for this interaction, with amino acids 113-125 being an important region, as demonstrated by the binding assays with different constructs.

The successful production of functional CD74 in high quantities, whether as a fusion protein or as cleaved product, is the first step in further characterisation of its structural features and of the elucidation of the binding mechanism of

mammalian MIF and MIF homologues to this receptor. Moreover, it will stimulate our search for clinically relevant inhibitors of the MIF-CD74 interaction.

Acknowledgements

We thank Prof. Richard Bucala, Yale/New haven Hospital, for kindly providing the human CD74 gene. We acknowledge Jan Ytzen van de Meer, Bas Vriezelaar, Angela Asselman, Ykelien Boersma, Ronald van Merkerk, Laura Sampedro and Gea Schuurman-Wolters for assistance and support given during our research. This work was supported by a grant 94.18/E4.4/2014 from Directorate General of Higher Education Indonesia (DIKTI) in collaboration with the University of Surabaya (Ubaya), Indonesia and the University of Groningen (RuG), The Netherlands.

Author contribution statement

FJD and GJP conceived and supervised the project, TK and AAW with the assistance of RHC designed the experiments. TK and AAW performed the experiments. TK with the assistance of RHC analyzed and interpreted the data. TK and RHC wrote the paper. GJP and FJD gave input for revisions of the manuscript.

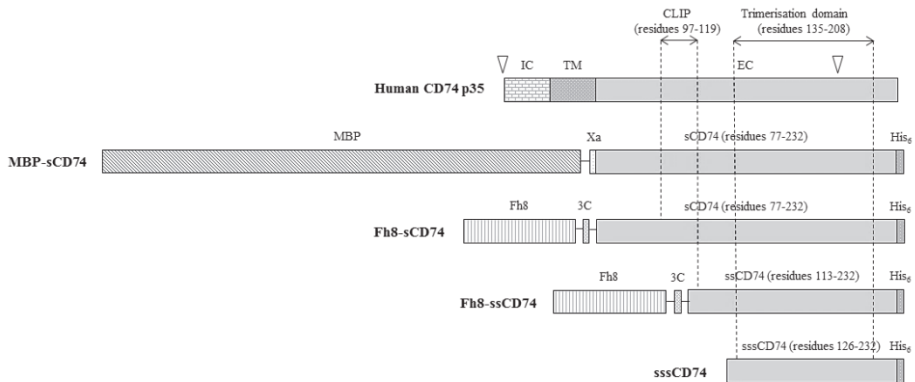
References

- [1] F. Borghese, F. IL Clanchy, CD74: an emerging opportunity as a therapeutic target in cancer and autoimmune disease, *Expert Opin. Ther. Targets.* 15 (2011) 237–251. doi:10.1517/14728222.2011.550879.
- [2] B. Schroder, The multifaceted roles of the invariant chain CD74 - More than just a chaperone, *Biochim. Biophys. Acta - Mol. Cell Res.* 1863 (2016) 1269–1281. doi:10.1016/j.bbamer.2016.03.026.
- [3] M. Strubin, C. Berte, B. Mach, Alternative splicing and alternative initiation of translation explain the four forms of the Ia antigen-associated invariant chain, *EMBO J.* 5 (1986) 3483–8.
- [4] L. Leng, C.N. Metz, Y. Fang, J. Xu, S. Donnelly, J. Baugh, T. Delohery, Y. Chen, R.A. Mitchell, R. Bucala, MIF Signal Transduction Initiated by Binding to CD74, *J. Exp. Med.* 197 (2003) 1467–1476. doi:10.1084/jem.20030286.
- [5] K.L. Meyer-Siegler, K. a Iczkowski, L. Leng, R. Bucala, P.L. Vera, Inhibition of macrophage migration inhibitory factor or its receptor (CD74) attenuates growth and invasion of DU-145 prostate cancer cells, *J. Immunol.* 177 (2006) 8730–8739. doi:177/12/8730.
- [6] H. Su, N. Na, X. Zhang, Y. Zhao, The biological function and significance of CD74 in immune diseases, *Inflamm. Res.* 66 (2017) 209–216. doi:10.1007/s00011-016-0995-1.
- [7] D.N. Assis, L. Leng, X. Du, C.K. Zhang, G. Grieb, M. Merk, A.B. Garcia, C. McCrann, J. Chapiro, A. Meinhardt, Y. Mizue, D.J. Nikolic-Paterson, J. Bernhagen, M.M. Kaplan, H. Zhao, J.L. Boyer, R. Bucala, The Role of Macrophage Migration Inhibitory Factor in Autoimmune Liver Disease, *Hepatology.* 59 (2014) 580–591. doi:10.1002/hep.26664.
- [8] G. Wu, Y. Sun, K. Wang, Z. Chen, X. Wang, F. Chang, T. Li, Relationship between elevated soluble CD74 and severity of experimental and clinical ALI / ARDS, *Nat. Publ. Gr.* (2016) 1–20. doi:10.1038/srep30067.
- [9] M. Podhorecka, J. Markowicz, A. Szymczyk, J. Pawlowski, Target therapy in hematological malignances: new monoclonal antibodies, *Int. Sch. Res. Not.* 2014 (2014) 1–16. doi:10.1155/2014/701493.
- [10] R. Lindner, Invariant Chain Complexes and Clusters as Platforms for MIF Signaling, *Cells.* 6 (2017) 6. doi:10.3390/cells6010006.
- [11] G. Pantouris, M.A. Syed, C. Fan, D. Rajasekaran, T.Y. Cho, E.M. Rosenberg, R. Bucala, V. Bhandari, E.J. Lolis, E.J. Lolis, An Analysis of MIF Structural Features that Control Functional Activation of CD74, *Chem. Biol.* 22 (2015) 1197–205. doi:10.1016/j.chembiol.2015.08.006.
- [12] A.A. Wasiel, Macrophage Migration Inhibitory Factor Cell Surface Receptor, Enzymatic Activities and Evolutionary History of A Multifunctional Cytokine, PhD thesis, University of Groningen, The Netherlands (2013), ISBN 978-90-367-6152-9.
- [13] D. Esposito, D.K. Chatterjee, Enhancement of soluble protein expression through the use of fusion tags, *Curr. Opin. Biotechnol.* 17 (2006) 353–358. doi:10.1016/j.copbio.2006.06.003.
- [14] R.B. Kapust, D.S. Waugh, Escherichia coli maltose-binding protein is uncommonly effective at promoting the solubility of polypeptides to which it is fused, *Protein Sci.* 8 (1999) 1668–1674. doi:10.1110/ps.8.8.1668.
- [15] S. Costa, A. Almeida, A. Castro, L. Domingues, Fusion tags for protein solubility, purification, and immunogenicity in Escherichia coli: The novel Fh8 system, *Front. Microbiol.* 5 (2014) 1–20. doi:10.3389/fmicb.2014.00063.
- [16] J.D. Fox, R.B. Kapust, D.S. Waugh, Single amino acid substitutions on the surface of Escherichia coli maltose-binding protein can have a profound impact on the solubility of fusion proteins, *Protein Sci.* 10 (2001) 622–630. doi:10.1110/ps.45201.
- [17] K.D. Pryor, B. Leiting, High-Level Expression of Soluble Protein in Escherichia coli Using a His6-Tag and Maltose-Binding-Protein Double-Affinity Fusion System, *Protein Expr. Purif.* 10 (1997) 309–319. doi:10.1006/prep.1997.0759.
- [18] S.J. Costa, A. Almeida, A. Castro, L. Domingues, H. Besir, The novel Fh8 and H fusion partners for soluble protein expression in Escherichia coli: A comparison with the traditional gene fusion technology, *Appl. Microbiol. Biotechnol.* 97 (2013) 6779–6791. doi:10.1007/s00253-012-4559-1.

- [19] S.J. Costa, E. Coelho, L. Franco, A. Almeida, A. Castro, L. Domingues, The Fh8 tag: A fusion partner for simple and cost-effective protein purification in *Escherichia coli*, *Protein Expr. Purif.* 92 (2013) 163–170. doi:10.1016/j.pep.2013.09.013.
- [20] H. Fraga, T.Q. Faria, F. Pinto, A. Almeida, R.M.M. Brito, A.M. Damas, FH8 - A small EF-hand protein from *Fasciola hepatica*, *FEBS J.* 277 (2010) 5072–5085. doi:10.1111/j.1742-4658.2010.07912.x.
- [21] J. Sambrook, E.F. Fritsch, T. Maniatis, *Molecular Cloning: A Laboratory Manual*, 2nd ed., Cold Spring Harbor Laboratory Press, Cold Spring Harbor, NY (1989).
- [22] A.A. Wasiel, H.J. Rozeboom, D. Hauke, B.J. Baas, E. Zandvoort, W.J. Quax, A.M. Thunnissen, G.J. Poelarends, Structural and functional characterization of a macrophage migration inhibitory factor homologue from the marine cyanobacterium *Prochlorococcus marinus*, *Biochemistry.* 49 (2010) 7572–7581. doi:10.1021/bi1008276.
- [23] H.M. Beyer, P. Gonschorek, S.L. Samodelov, M. Meier, W. Weber, M.D. Zurbriggen, AQUA cloning: A versatile and simple enzyme-free cloning approach, *PLoS One.* 10 (2015) 1–20. doi:10.1371/journal.pone.0137652.
- [24] X. Shi, L. Leng, T. Wang, W. Wang, X. Du, J. Li, C. McDonald, Z. Chen, J.W. Murphy, E. Lolis, P. Noble, W. Knudson, R. Bucala, CD44 Is the Signaling Component of the Macrophage Migration Inhibitory Factor-CD74 Receptor Complex, *Immunity.* 25 (2006) 595–606. doi:10.1016/j.immuni.2006.08.020.
- [25] S. Park, S. Sadegh-nasseritt, D.C. Wiley, Invariant chain made in *Escherichia coli* has an exposed N-terminal segment that blocks antigen binding to HLA-DR1 and a trimeric C-HLA-DR1 C-terminal that binds empty HLA-DR1, *Proc. Natl. Acad. Sci.* 92 (1995) 11289–11293.
- [26] A. Jasanoff, S.J. Park, D.C. Wiley, Direct observation of disordered regions in the major histocompatibility complex class II-associated invariant chain., *Proc. Natl. Acad. Sci. USA.* 92 (1995) 9900–4. doi:10.1073/pnas.92.21.9900.
- [27] S. Günther, A. Schlundt, J. Sticht, Y. Roske, U. Heinemann, K.-H. Wiesmüller, G. Jung, K. Falk, O. Röttschke, C. Freund, Bidirectional binding of invariant chain peptides to an MHC class II molecule, *Proc. Natl. Acad. Sci. USA.* 107 (2010) 22219–24. doi:10.1073/pnas.1014708107.
- [28] A. Jasanoff, G. Wagner, D.C. Wiley, Structure of a trimeric domain of the MHC class II-associated chaperonin and targeting protein Ii. *EMBO J.* 17 (1998), 6812–6818
- [29] A. Jasanoff, S. Song, A.R. Dinner, G. Wagner, D.C. Wiley, One of two unstructured domains of Ii becomes ordered in complexes with MHC class II molecules, *Immunity.* 10 (1999) 761–768. doi:10.1016/S1074-7613(00)80075-8.
- [30] P. Ghosh, M. Amaya, E. Mellins, D.C. Wiley, The structure of an intermediate in class II MHC maturation: CLIP bound to HLA-DR3, *Nature.* 378 (1995) 457–62. doi:10.1038/378457a0.
- [31] C.A. Painter, M.P. Negroni, K.A. Kellersberger, Z. Zavala-Ruiz, J.E. Evans, L.J. Stern, Conformational lability in the class II MHC 310 helix and adjacent extended strand dictate HLA-DM susceptibility and peptide exchange, *Proc. Natl. Acad. Sci. USA.* 108 (2011) 19329–34. doi:10.1073/pnas.1108074108.
- [32] J.R. Newcomb, C. Carboy-newcomb, P. Cresswell, Trimeric Interactions of the Invariant Chain and Its Association with Major Histocompatibility Complex Class II $\alpha\beta$ Dimers, *J. Bio. Chem.* 271 (1996) 24249–24256.
- [33] R. Meza-romero, G. Benedek, L. Leng, R. Bucala, P. Rd, O. Health, N. Haven, O. Health, Predicted structure of MIF/CD74 and RTL1000/CD74 complexes, *Metab. Brain Dis.* 31 (2016) 249–255. doi:10.1007/s11011-016-9798-x.
- [34] L. Schindler, N. Dickerhof, M.B. Hampton, J. Bernhagen, Post-translational regulation of macrophage migration inhibitory factor: Basis for functional fine-tuning, *Redox Biol.* 15 (2018) 135–142. doi:10.1016/J.REDOX.2017.11.028.
- [35] A. Kukol, J. Torres, I.T. Arkin, A Structure for the Trimeric MHC Class II-associated Invariant Chain Transmembrane Domain, *J. Mol. Biol.* 320 (2002) 1109–1117. doi:10.1016/S0022-2836(02)00563-6.
- [36] Ann M. Dixon, Bradford J. Stanley, Erin E. Matthews, and Jessica P. Dawson, Donald M. Engelman, Invariant Chain Transmembrane Domain Trimerization: A Step in MHC Class II Assembly, *Biochemistry.* 45 (2006). doi:10.1021/BI052112E.

Figures

A.



B.

MBP-sCD74

*MKIEEGKLVIVWINGDKGYNGLAEVGKFKFEDTGIKVTVEHPDKLEEFQVAATGDGPDIIFWAHDRFGGYAQSGLLAEITPDKAFQDKLYPFTWDVAVRY
NGKLIAYPIAVEALSILYNKDLLPNPPKTWEEIPALDKELKAKGKSALMFNLQEPYFTWPLAADGGYAFKYENGYDIKDVGVNDNAGAKGLTFLVDLIGN
KHMNADTDYSIAEAFNKGETAMTINGPWAWNSNIDTSKVNYGVTVLPTFRGQPSKPFVGLSAGINAASPKNELAKEFLENYLLTDEGLEAVNKDKPLG
AVALKSYEEELAKDPRIATMENAQKGEIMPNIPQMSAFWYAVRTAVINAASGRQTVDEALKDAQTNSSSNNNNNNNNNNLGIEGRISFIEGRARLD
KLTVTSQNLQLENLRMKLPKPKPKVSKMRMATPLLMQALPMGALPQGPQMKNATKYGNMTEDEVHMHLLQNADPLKVYPPPLKGSFPENLRHLKNT
METIDWKVFESWMHHWLLFEMSRHSLEQKPTDAPPKESLELEDPSSGLGVTKQDLGVPVPMLEHHHHHH*

Fh8-sCD74

*MQTGMPSVQVEKLLHVLDNRNGDGKVSAEELKAFADDSKCPLDSNKIKAFIKEHDKNKGKLDLDELVSILSSGTSGTGGLEVLFGQGGPAMAASGSIGA
NKILLMQALPMGALPQGPQMKNATKYGNMTEDEVHMHLLQNADPLKVYPPPLKGSFPENLRHLKNTMETIDWKVFESWMHHWLLFEMSRHSLEQK
RHLKNTMETIDWKVFESWMHHWLLFEMSRHSLEQKPTDAPPKESLELEDPSSGLGVTKQDLGVPVPMLEHHHHHH*

Fh8-ssCD74

*MQTGMPSVQVEKLLHVLDNRNGDGKVSAEELKAFADDSKCPLDSNKIKAFIKEHDKNKGKLDLDELVSILSSGTSGTGGLEVLFGQGGPAMAASGSIGA
NKILLMQALPMGALPQGPQMKNATKYGNMTEDEVHMHLLQNADPLKVYPPPLKGSFPENLRHLKNTMETIDWKVFESWMHHWLLFEMSRHSLEQK
PTDAPPKESLELEDPSSGLGVTKQDLGVPVPMLEHHHHHH*

sssCD74

*GPMQKNATKYGNMTEDEVHMHLLQNADPLKVYPPPLKGSFPENLRHLKNTMETIDWKVFESWMHHWLLFEMSRHSLEQKPTDAPPKESLELEDPSSG
LGVTKQDLGVPVPMLEHHHHHH*

Figure 1. A. Schematic presentation of human CD74 isoform p35 and CD74-derived proteins used in this study. IC = intracellular (residues 1-46), TM = transmembrane (residues 47-73), EC = extracellular (residues 74-232), the inverted triangles indicate where isoforms p33, p35, p41 and p43 differ. Xa = factor Xa cleavage site, 3C = 3C protease cleavage site, His₆ = (His)₆-tag. B. Amino acid sequences of CD74-derived proteins used in this study. The sequences of the solubility enhancing peptides MBP and Fh8 are in italics, the proteolytic sites are underlined, and the CD74 sequences are presented in bold. Sequences of CD74 that are dotted or dashed underlined represent the CLIP region and the membrane-distal trimerisation domain, respectively.

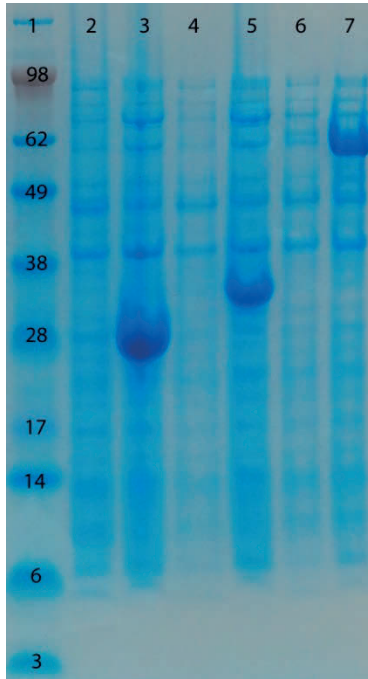


Figure 2. Overproduction of CD74 fusion proteins. Lane 1: marker proteins with the indicated molecular weights. Lanes 2 and 3: cell lysate before and after overproduction of Fh8-ssCD74 (MW 25.0 kDa), respectively. Lanes 4 and 5: cell lysate before and after overproduction of Fh8-sCD74 (MW 29.6 kDa), respectively. Lanes 6 and 7: cell lysate before and after overproduction of MBP-sCD74 (MW 62.3 kDa), respectively.

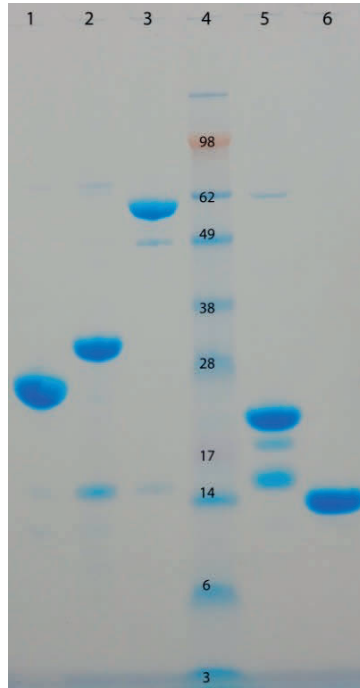


Figure 3. SDS gel of different purified CD74 proteins. Fh8-ssCD74 (lane 1), Fh8-sCD74 (lane 2), MBP-sCD74 (lane 3), sCD74 (lane 5), and sssCD74 (lane 6). Lane 4 contains the protein markers with indication of the molecular weights.

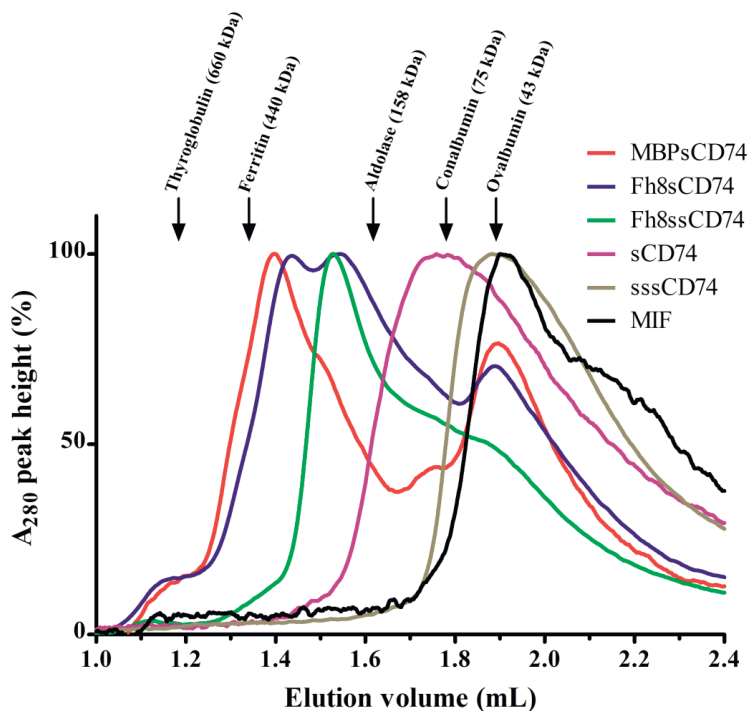


Figure 4. Size exclusion chromatography of MIF and CD74-derived proteins. Purified proteins were separately analyzed on a 3 mL gel filtration column (Superdex200 5/150) by injecting 20 μ L of a 1 mg/mL protein solution onto the column equilibrated with PBS, pH 7.4, at 10 $^{\circ}$ C. Each chromatogram was normalised to its absorbance at 280 nm. The column was also calibrated with 20 μ L of 1 mg/mL solutions of five marker proteins: thyroglobulin (669 kDa), ferritin (440 kDa), aldolase (158 kDa), conalbumin (75 kDa), and ovalbumin (43 kDa). The elution volumes of these marker proteins (1.19; 1.34; 1.61; 1.78; and 1.89 ml, respectively) are indicated with arrows.

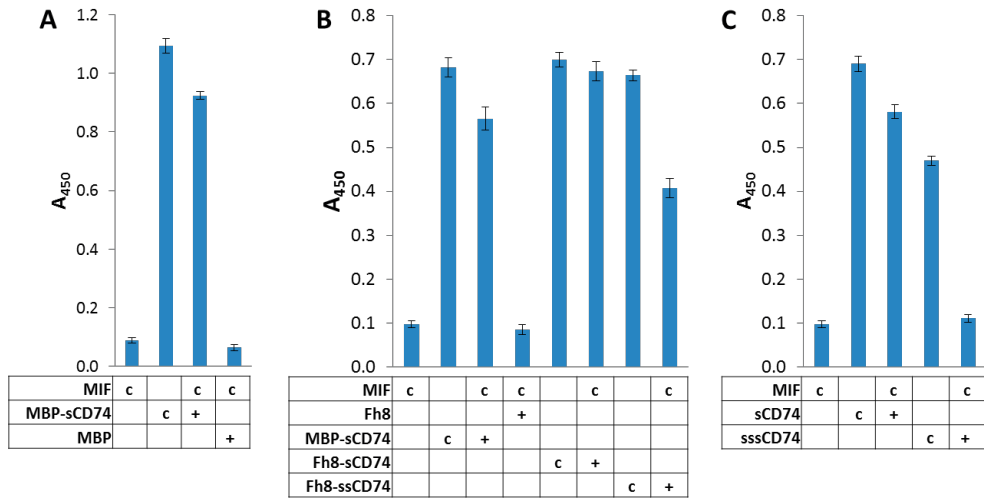


Figure 5. ELISA binding observation between MIF and sCD74 fusion proteins. **A.** MIF with 500 nM MBP-sCD74 and controls using mouse anti-MBP mAb for detection. **B.** MIF with 500 nM MBP-sCD74, Fh8-sCD74 or Fh8-ssCD74 and controls using rabbit anti-CD74 pAb for detection. **C.** MIF with 500 nM sCD74 or sssCD74 and controls using rabbit anti-CD74 pAb for detection.

c: protein used for coating (300 nM MIF or 500 nM of other proteins);

+: protein tested for binding to MIF

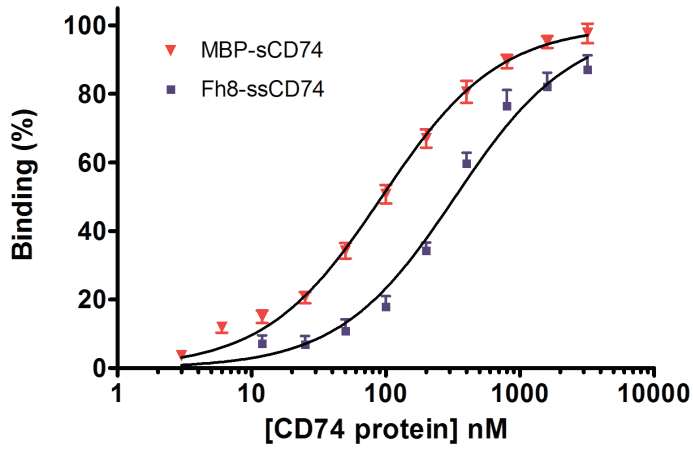


Figure 6. Dose-dependent ELISA of MIF binding to CD74 fusion proteins. The interaction was determined between 300 nM coated MIF and different concentrations of MBP-sCD74 or Fh8-ssCD74, and revealed with α MBP or α CD74 antibodies, respectively.

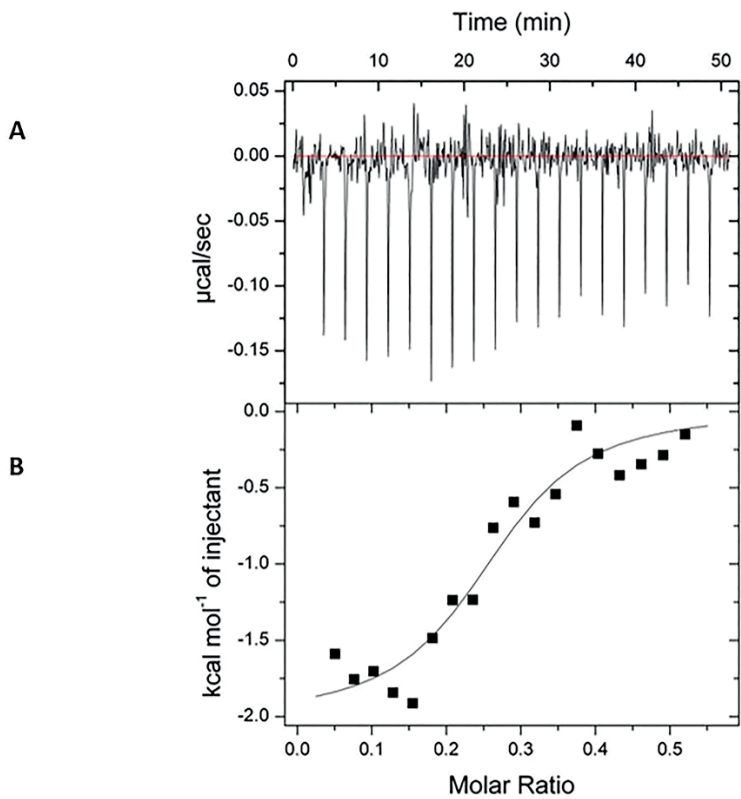
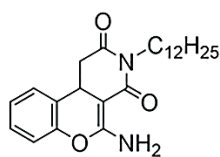
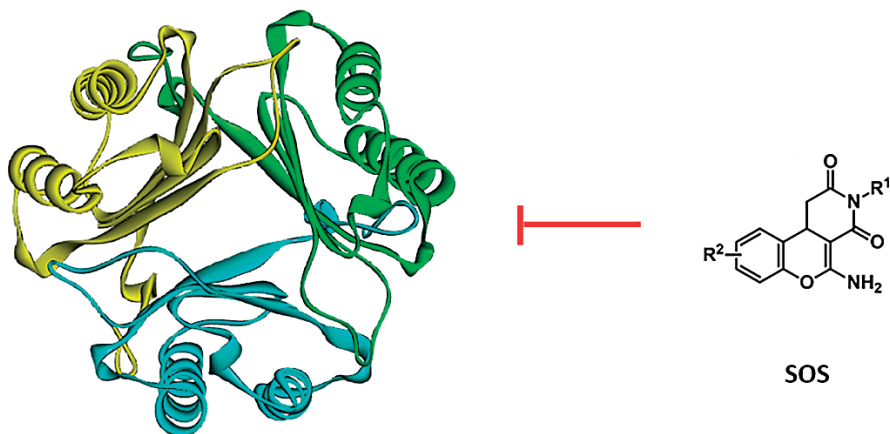


Figure 7. ITC measurement of MIF binding to MBP-sCD74. MBP-sCD74 41 μM in cell was titrated by MIF 72 μM . **A.** Heat flow as a function of time. **B.** Reaction enthalpy versus molar ratio.

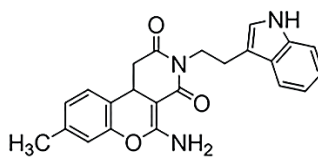
Chapter 4

Development of chromenes as MIF inhibitors



Kok-10

IC₅₀ = 18 μM



Kok-17

IC₅₀ = 6.2 μM

Publication in:

Kok T, Wapenaar H, Wang K, Neochoritis CG, Zarganes-Tzitzikas T, Proietti G, Eleftheriadis N, Kurpiewska K, Kalinowska-Tłuścik J, Cool RH, Poelarends GJ, Dömling A, Dekker FJ. Discovery of chromenes as inhibitors of macrophage migration inhibitory factor. *Bioorg Med Chem* 2018;26:999–1005. doi:10.1016/J.BMC.2017.12.032.

Abstract

Macrophage migration inhibitory factor (MIF) is an essential signaling cytokine with a key role in the immune system. Binding of MIF to its molecular targets such as, among others, the cluster of differentiation 74 (CD74) receptor plays a key role in inflammatory diseases and cancer. Therefore, the identification of MIF binding compounds gained importance in drug discovery. In this study, we aim to discover novel MIF binding compounds by screening of a focused compound collection for inhibition of its tautomerase enzyme activity. Inspired by the known chromen-4-one inhibitor Orita-13, a focused collection of compounds with a chromene scaffold was screened for MIF binding. The library was synthesized using versatile cyanoacetamide chemistry to provide diversely substituted chromenes. The screening provided inhibitors with IC_{50} 's in the low micromolar range. Kinetic evaluation suggested that the inhibitors were reversible and did not bind in the binding pocket of the substrate. Thus, we discovered novel inhibitors of the MIF tautomerase activity, which may ultimately support the development of novel therapeutic agents against diseases in which MIF is involved.

Keywords: Macrophage migration inhibitory factor, chromenes, inhibitor, enzyme kinetics

Introduction

Macrophage migration inhibitory factor (MIF) is a central cytokine of the immune system. It is expressed in immune cells such as T-cells, macrophages, basophiles, eosinophils and B-cells [1]. Unlike other cytokines, MIF is constitutively expressed and stored in cytoplasmic pools and rapidly released in response to stimuli [2]. Upon release, MIF interacts with surface receptors on B-cells, T-cells, macrophages and some epithelial cells, which induce pro-inflammatory signal transduction. MIF has been shown to interact with the type II cluster of differentiation 74 (CD74) receptor, which is the invariant chain of the major histocompatibility complex II (MHCII). CD74 does not seem to have an intracellular signaling domain and is, therefore, expected to initiate intracellular signaling by recruiting other membrane receptors such as CD44, CXCR2 and CXCR4 [3-5]. These interactions are important for the role of MIF in inflammatory signaling. In addition, MIF has also been suggested as a target in cancer due to its downregulation of p53 and its overexpression in several cancer cell types [6-10]. It was shown that neutralization of MIF through antibodies or genetic deletion was beneficial in several inflammatory disease models and a small-molecule inhibitor of MIF was able to reduce tumor growth in mouse models [11-15]. Taken together these data indicate that development of MIF binding molecules has potential for drug discovery for inflammatory diseases and cancer.

MIF is a small protein of 115 amino acids, weighing approximately 12.4 kDa and exists predominantly in a homotrimeric form. One human homologue has been described, D-Dopachrome Tautomerase (D-DT or MIF2), which shows a similar function to MIF [16]. MIF has structural similarity to two bacterial enzymes: 4-oxalocrotonate tautomerase (4-OT) and 5-carboxymethyl-2-hydroxyumuconate isomerase [17]. Inspired by these similarities, it was discovered that MIF not only functions as a cytokine, but has enzymatic activity as well. It has been shown to catalyze the interconversion of enol and keto isomers of D-Dopachrome and phenylpyruvate [18]. One residue particularly important for this activity is the N-terminal proline which acts as a catalytic base in the tautomerase reaction [19]. Screening for inhibitors of MIF tautomerase activity has been recognized as an efficient way to identify MIF binding compounds that can be further investigated in more advanced disease models where MIF has been shown to play a role. A well-known inhibitor of the MIF tautomerase activity is the isoxazoline (*S,R*)-3-(4-hydroxyphenyl)-4,5-dihydro-5-isoxazole acetic acid methyl ester (ISO-1, **Figure 1**). ISO-1 is a competitive inhibitor of the MIF tautomerase activity and has beneficial effects in several disease models such as sepsis, chronic obstructive pulmonary disease (COPD) and cancer [15, 20-23]. Based on ISO-1,

several other MIF inhibitors have been developed, among which are the biaryltriazoles [24-28]. Using a structure-based virtual screening method, Orita-13 containing a chromen-4-one scaffold was identified as a MIF inhibitor [26, 29]. Additionally, covalent MIF inhibitors have been described, such as TP, as probes suitable for activity-based protein profiling [30]. Taken together, several small-molecule binders of MIF have been developed (**Figure 1**), but the identification of novel structural classes remains needed for a better understanding of the structural requirements for binding and to provide a broader basis for drug discovery.

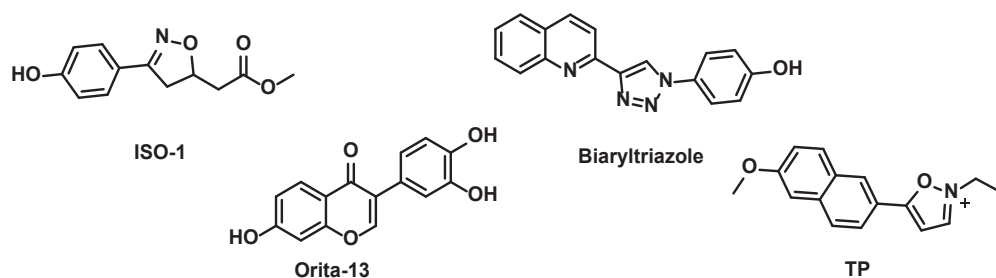


Figure 1. Known MIF tautomerase activity inhibitors “ISO-1”, a “biaryltriazole” from [26], “Orita-13” and activity-based probe “TP”.

Here, we describe the identification of novel MIF binders inspired by the chromen-4-one scaffold of Orita-13. A focused compound collection of 57 compounds was synthesized using cyanoacetamide-based chemistry. Screening of this library for inhibition of MIF tautomerase activity provided 6 inhibitors with potencies in the low micromolar range. The structural motif that was identified expands the number of scaffold available for further development of MIF inhibitors towards applications in disease models.

Materials and methods

Chemistry general

All the reagents and solvents were purchased from Sigma-Aldrich, AK Scientific, Fluorochem, Abcr GmbH, or Acros and were used without further purification. All microwave irradiation reactions were carried out in a Biotage Initiator™ Microwave Synthesizer. Thin layer chromatography was performed on Millipore precoated silica gel plates (0.20 mm thick, particle size 25 μm). Nuclear magnetic resonance spectra were recorded on Bruker Avance 500 or 600 spectrometers ^1H NMR (500 MHz; 600 MHz), ^{13}C NMR (126 MHz; 151 MHz).

Chemical shifts for ^1H NMR were reported as δ values and coupling constants were in hertz (Hz). The following abbreviations were used for spin multiplicity: s = singlet, br s = broad singlet, d = doublet, t = triplet, q = quartet, quin = quintet, dd = doublet of doublets, ddd = doublet of doublet of doublets, m = multiplet. Chemical shifts for ^{13}C NMR were reported in ppm relative to the solvent peak. Flash chromatography was performed on a Reveleris[®] X2 Flash Chromatography system, using Grace[®] Reveleris Silica flash cartridges (12 grams). Mass spectra were measured on a Waters Investigator Supercritical Fluid Chromatograph with a 3100 MS Detector (ESI) using a solvent system of methanol and CO_2 on a Viridis silica gel column (4.6 x 250 mm, 5 μm particle size) or Viridis 2-ethyl pyridine column (4.6 x 250 mm, 5 μm particle size). High resolution mass spectra were recorded using a LTQ-Orbitrap-XL (Thermo Scientific, The Netherlands) at a resolution of 60000@m/z400.

General procedure for the synthesis of 1-57

To a stirred solution of 2*H*-chromen-2-one (1.0 mmol) in dry ethanol (5 mL), the corresponding cyanoacetamide (1.0 mmol) and sodium ethoxide (0.2 mmol) were added. The reaction mixture was stirred at room temperature for 24 hours. The precipitate was filtered off and washed with cold ethanol (2 x 5 mL), yielding the final compounds without further purification in yield ranging from 35 to 81 %. The characterization of all compounds can be found in the supporting information.

Single crystal x-ray structure determination

X-ray diffraction data for a single crystal of compound **7** was collected using a SuperNova (Rigaku-Oxford Diffraction) four circle diffractometer with a mirror monochromator and a microfocus $\text{MoK}\alpha$ radiation source ($\lambda = 0.71073 \text{ \AA}$). Additionally, the diffractometer was equipped with a CryoJet HT cryostat system (Oxford Instruments) allowing low temperature experiments, performed at 130 (2) K. The obtained data was processed with CrysAlisPro software.^{S1} The phase problem was solved by direct methods using SIR2004.^{S2} Parameters of models were refined by full-matrix least-squares on F^2 using SHELXL-2014/6.^{S3} Calculations were performed using WinGX integrated system (ver. 2014.1).^{S4} Figure was prepared with Mercury 3.7 software.^{S5}

All non-hydrogen atoms were refined anisotropically. All hydrogen atoms attached to carbon atoms were positioned with the idealised geometry and refined using the riding model with the isotropic displacement parameter $U_{\text{iso}}[\text{H}] = 1.2$ (or 1.5 (methyl groups only)) $U_{\text{eq}}[\text{C}]$. Positions of hydrogen atoms linked to N2 were defined on the difference Fourier map and refined with no additional restraints. The molecular geometry (asymmetric unit) observed in the crystal structure is shown in **Figure S1**. Crystal data and structure refinement results for presented crystal structure are shown in **Table S1**. Crystallographic data have been deposited with the Cambridge Crystallographic Data Centre as supplementary publication no. CCDC 1575884.

MIF tautomerase activity assay

Tautomerase activity inhibition of MIF by the synthesized chromene compounds was measured using recombinantly expressed His-tagged MIF, which was purified with cOmplete His-Trap purification resin (Roche, The Netherlands). The assay was done following the procedure of Dziejczak *et al.* [26]. 4-hydroxyphenyl pyruvate (4-HPP) was used as substrate to quantify tautomerase activity. Stock solutions of 10 mM 4-HPP were made in 50 mM ammonium acetate buffer pH 6.0, and incubated overnight at room temperature to allow equilibration between keto and enol form. Further dilutions of the substrate were made in the same acetate buffer. Inhibitor stock solutions had a concentration of 10 mM in DMSO. The inhibitor stock solutions were diluted in 0.4 M boric acid pH 6.2 to give final concentration in the screening assay of 25 and 50 μM . For the IC_{50} assay final concentrations of 250 – 0 μM or 100 – 0 μM or 25 – 0 μM in 5% DMSO, with 2 or 1.6 fold dilution series were applied. The control contained 5% DMSO as a vehicle control. This amount did not influence the MIF tautomerase activity. In the assays 50 μL of mixtures of MIF (dilution in 0.2 M boric acid pH 6.2, to give a final concentration of 340 nM) and the synthesized compounds were put in a UV-star F bottom 96-well plate. The enzymatic reaction was started by addition of 50 μL 4-HPP (to give a final concentration of 0.5 mM), and the increase of absorbance at 306 nm was followed over time using a Spectrostar Omega BMG Labtech plate reader. The positive control contained all the components excluding inhibitor (but including 5% DMSO), and the negative control was as the positive control without MIF. The data obtained were analyzed by firstly taking the slopes of the linear part of the increased absorbance over the time (that is the velocity of the enzymatic reaction), then normalizing them to the positive and negative control to give percentage of inhibition.

Enzyme kinetic evaluation

To evaluate the reversibility of MIF tautomerase inhibition by the discovered chromene inhibitors, preincubation experiments were conducted using inhibitor **10** and **17**. The inhibitors (125 – 0 μM , 1.6 fold dilution series in 5% DMSO) were preincubated with the enzyme (340 nM) for 2 minutes (the time of preincubation in the regular IC_{50} assays) and 40 minutes prior to adding the substrate and starting the enzymatic reaction. Then the IC_{50} curves were made as described above.

Dilution experiments were performed using inhibitor **10**. To do this, an initial mixture with a relatively high concentration of MIF (34 μM) and the inhibitor (125 μM in 5% DMSO) was made. Subsequently, this mixture was diluted 100 times in a solution containing the substrate 4-HPP (0.5 mM) and boric acid. A control assay was done following the same procedure without inhibitor, but containing 5 % DMSO. The enzyme activity was measured as described before. The absorbance was plotted against time.

To further investigate the mechanism of inhibition, kinetic experiments were conducted using inhibitor **10**. The velocity of the enzymatic reaction was measured at increasing concentrations of 4-HPP (0 - 2.56 mM, 1.25 x dilution) in the presence of MIF (340 nM) and inhibitor (0, 6.25 or 12.5 μM). The velocity of the reaction was plotted against the concentration of 4-HPP using GraphPad Prism 5.0. The curve was plotted using enzyme kinetics-allosteric sigmoidal, yielding the $V_{\text{max app.}}$, Hill slope and $K_{\text{prime app.}}$. The concentration of 4-HPP that gives half of V_{max} (K_{half}) was calculated from the K_{prime} using the following equation:

$$K_{\text{half}} = \frac{\text{Hill slope}}{\sqrt{K_{\text{prime}}}}$$

Results and discussion

Chemistry

A library of approximately 60 fused amino-2H-chromenopyridine-diones was synthesized using methods as initially described by Rosati *et al.* (**Figure 2A**) [31, 32]. The alignment of Orita-13 with the amino-2H-chromenopyridine-dione scaffold can be detected by checking the stereoscopic view of Orita-13, which indicates the potential of this library for MIF binding (**Figure 2B**). These scaffolds combine a series of interesting features besides the chromene core, such as the amino group in 5-position and a fused piperidinodione ring. Moreover, the possibility to increase the diversity with two points of diversification and the rigid

core structure attributed to the selection of this scaffold. It was possible to get the crystal structure of compound **7** revealing an intramolecular hydrogen bond between the exocyclic amine and the carbonyl group. This led to coplanarity between the fused rings, which provides interesting possibilities for the type of interactions under investigation (**Figure 2C**, **Figure S1**, **Scheme S1**).

Starting from our broad experience with cyanoacetamide chemistry in heterocycle synthesis [33-36], we elaborated on the synthesis of Rosati *et al.* [31], using a number of different cyanoacetamides and suitably substituted 2*H*-chromenes. Thus, we designed and synthesized a highly diverse medium sized library in a medicinal chemistry frame utilizing aliphatic and aromatic substituents, heterocycles, hydrogen bond donors and acceptors. In addition, we enhanced the solubility of specific compounds with the introduction of morpholino substituents. The reactions proceeded under mild conditions with a plethora of different cyanoacetamides in good to very good yields in a parallel manner.

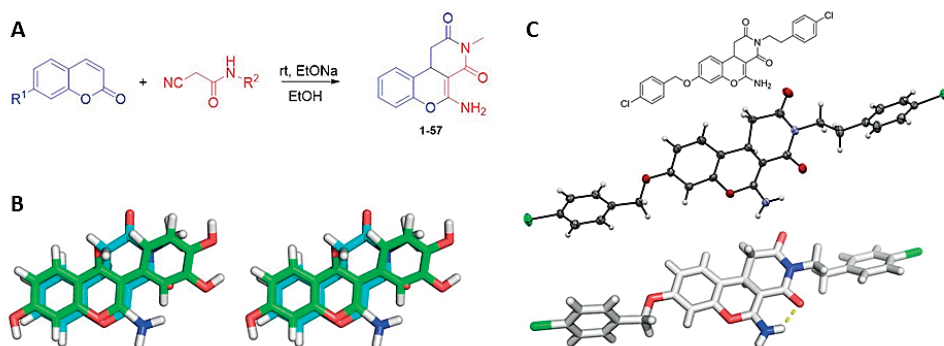


Figure 2. A. Synthesis of fused amino-2*H*-chromenopyridine-diones. B. Stereoscopic view of the 3D-alignment of Orita-13 (green) with the amino-2*H*-chromenopyridine-dione scaffold (cyan). C. Structure of compound **7**, Molecular geometry observed in the crystal structures of compound **7**, showing the atom labelling scheme and an intramolecular hydrogen bond between the exocyclic amine and the carbonyl group is formed.

Biological evaluation

The compounds were tested for inhibition of the MIF tautomerase activity using a spectrophotometric assay based on the absorbance detection of the enzymatic enol product of 4-hydroxy phenylpyruvate (4-HPP) after reaction with boric acid [26]. First, a single point screening was done at a concentration of 25 μ M and 50 μ M and the compounds showing more than 50% inhibition of enzyme activity at 25 μ M were tested for IC₅₀ values (**Figure S2**, **Figure S3**).

The investigation started with 4-chlorobenzoyloxy chromene derivatives, bearing various aliphatic or aromatic substituents on the R¹ position (compounds **1-8**, **Table 2**). Short aliphatic substituents (**1 - 3**) showed less than 50% inhibition at 25 μM, whereas compound **4** carrying a longer aliphatic substituent provided an IC₅₀ of 7.1 ± 0.4 μM. The compounds with aromatic substituent (**5 - 8**) also showed inhibition, of which a 4-chlorophenethyl substituent (**7**, IC₅₀ = 13 ± 1.0 μM) and an indole with ethyl spacer (**8**, IC₅₀ = 8.0 ± 0.5 μM) gave the best results. This suggests that lipophilic interactions are important for the inhibition of MIF. Next, these active derivatives (**4**, **7** and **8**) were further investigated. To investigate whether the bulky 4-chlorobenzoyloxy was necessary, it was removed (R² = H) or replaced with several smaller substituents such as 3-Me, 4-Me or 3-OEt on the R² position (**Table 1**). In case of the long dodecane substituent (**9 - 11**), when smaller substitutions on position R² were introduced, activity did not improve. In contrast, introducing smaller substitutions on R² in case of compounds with a 4-chlorophenethyl on position R¹ (**12 - 13**) caused a loss of activity. Concerning the indole substituted compounds (**14 - 17**), a methyl substituent improved slightly the activity, but others were not active. Several other compounds were synthesized combining different types of R¹ position, such as morpholines, naphthalenes, furans, thiophenes or aliphatic chains with different heteroatoms (**Table 2**), but these did not lead to an improved inhibition. The IC₅₀ value of reference MIF inhibitor ISO-1 was determined under the conditions used for the chromene compounds. The IC₅₀ value of ISO-1 was within the range reported in literature [37]. The activity of Orita-13 has been reported to be similar to ISO-1 [27]. The most potent chromene compounds were active at lower concentrations compared to the reference compound ISO-1. Therefore, compounds **10** and **17** were taken for further investigation.

Table 1. Inhibition of MIF tautomerase activity by synthesized compounds of a chromene scaffold and reference compound ISO-1. IC₅₀ values were given as mean ± standard deviation of at least 2 independent experiments. ND = not determined.

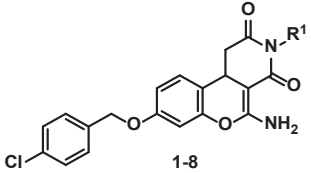
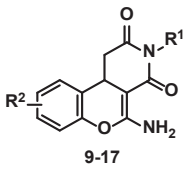
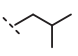
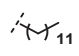
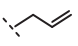
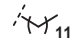
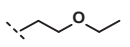
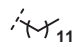
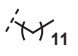
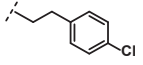
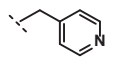
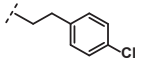
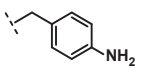
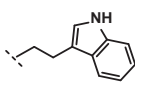
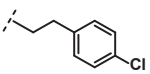
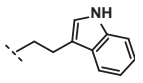
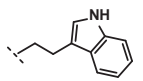
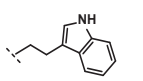
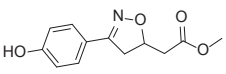
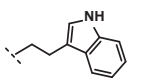
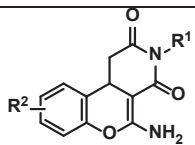
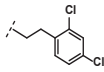
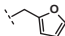
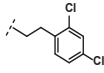
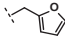
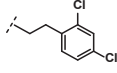
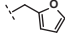
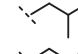
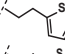
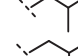
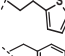
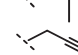
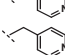
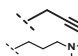
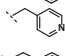
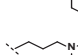
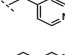
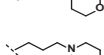
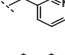
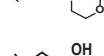
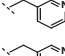
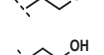
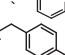
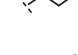
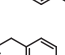
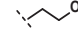
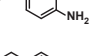
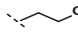
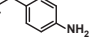
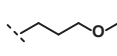
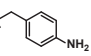
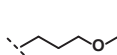
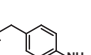
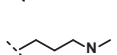
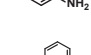
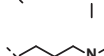
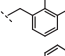
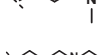
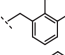
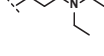
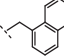
|  1-8 | | | |  9-17 | | | | |
|--|---|-----------------------|-----------------------|---|---|----------------|-----------------------|-----------------------|
| Compound | R ¹ | % inhibition at 25 μM | IC ₅₀ (μM) | Compound | R ¹ | R ² | % inhibition at 25 μM | IC ₅₀ (μM) |
| 1 |  | 40% | ND | 9 |  | 3-OEt | 60% | 21 ± 2.1 |
| 2 |  | 10% | ND | 10 |  | H | 60% | 18 ± 3.5 |
| 3 |  | 10% | ND | 11 |  | 4-Me | 50% | ND |
| 4 |  | 80% | 7.1 ± 1.0 | 12 |  | H | 15% | ND |
| 5 |  | 15% | ND | 13 |  | 3-Me | 5% | ND |
| 6 |  | 45% | ND | 14 |  | 3-OEt | 10% | ND |
| 7 |  | 80% | 13 ± 1.1 | 15 |  | H | 15% | ND |
| 8 |  | 70% | 8.0 ± 1.0 | 16 |  | 4-Me | 25% | ND |
| ISO-1 |  | | 79 ± 3.7 | 17 |  | 3-Me | 55% | 6.2 ± 0.6 |

Table 2. Additional chromene compounds tested for inhibition of MIF. Percent inhibition at 25 μM is given as mean of at least 2 independent experiments.

|  | | | | | | | |
|---|---|----------------|----------------------------------|----------|---|----------------|----------------------------------|
| Compound | R ¹ | R ² | % inhibition at 25 μM | Compound | R ¹ | R ² | % inhibition at 25 μM |
| 18 |  | 3-OEt | 30% | 38 |  | 3-OMe | 0% |
| 19 |  | 4-Me | 20% | 39 |  | H | 0% |
| 20 |  | 3-Me | 20% | 40 |  | 4-Me | 15% |
| 21 |  | 3-OEt | 10% | 41 |  | 3-OMe | 15% |
| 22 |  | 3-OMe | 15% | 42 |  | 4-Me | 10% |
| 23 |  | 4-Me | 0% | 43 |  | 3-OEt | 0% |
| 24 |  | 3-OMe | 0% | 44 |  | 3-OMe | 0% |
| 25 |  | 3-Me | 0% | 45 |  | 4-Me | 0% |
| 26 |  | 3-OEt | 0% | 46 |  | 3-Me | 0% |
| 27 |  | 3-OMe | 0% | 47 |  | 3-OEt | 10% |
| 28 |  | 4-Me | 0% | 48 |  | 3-OMe | 0% |
| 29 |  | 3-OMe | 0% | 49 |  | 4-Me | 0% |
| 30 |  | H | 0% | 50 |  | 3-OEt | 0% |
| 31 |  | 4-Me | 0% | 51 |  | 3-OMe | 0% |
| 32 |  | 3-OEt | 0% | 52 |  | H | 0% |
| 33 |  | 3-OMe | 0% | 53 |  | 4-Me | 10% |
| 34 |  | 3-Me | 0% | 54 |  | 3-Me | 0% |
| 35 |  | 3-OMe | 0% | 55 |  | 3-OEt | 50% |
| 36 |  | 3-Me | 0% | 56 |  | 3-OMe | 25% |
| 37 |  | 4-Me | 0% | 57 |  | 3-Me | 35% |

Kinetic evaluation

To investigate the reversibility of the inhibition of MIF by the discovered inhibitors, a preincubation assay was performed with **10** and **17**. The inhibitors were preincubated with MIF for 2 or 40 minutes before initiating the enzymatic reaction. Then, the IC₅₀ curve was made as described before. No difference in IC₅₀ was observed between incubation times, suggesting that the inhibition was not time-dependent on the investigated time scale (**Figure 3A**, **Figure S4**). To further investigate reversibility we performed dilution experiments with compound **10** in which the inhibitor and enzyme were preincubated at a high concentration (10 x IC₅₀) before dilution in a substrate solution to 10 x below the IC₅₀ of the inhibitor. In combination with an irreversible inhibitor, the enzyme will show no activity after dilution. With a reversible inhibitor, however, the activity of the enzyme can be recovered [38]. The dilution assay with compound **10** showed that the activity of MIF could be recovered after dilution (**Figure 3B**), which is consistent with reversible inhibition as observed in the preincubation assay.

To further investigate the mechanism of inhibition of the inhibitors, a kinetic evaluation of compound **10** was done (**Figure 3C**). The velocity of the enzyme reaction was measured at increasing concentrations of the substrate (HPP) in the presence of different concentrations of inhibitor **10**. From this curve, the apparent maximum velocity ($V_{\max \text{ app.}}$), the hill slope and the concentration of HPP that gave half of $V_{\max \text{ app.}}$ ($K_{\text{half app.}}$) were determined. The experiment showed a sigmoidal curve with a Hill slope larger than 1, not following Michaelis-Menten kinetics, which is in line with observations from Lubetsky *et al.* [39]. The K_{half} values were consistent with the values reported by Lubetsky *et al.* (denoted as $[S]_{0.5}$). An increasing concentration of compound **10** gave a decrease in $V_{\max \text{ app.}}$. The change in $K_{\text{half app.}}$ is less pronounced. This indicates that there is no direct competition between the substrate HPP and the inhibitor **10**. This observation is in contrast to the binding mode described for Orita-13 that has been shown to bind the MIF active site [29].

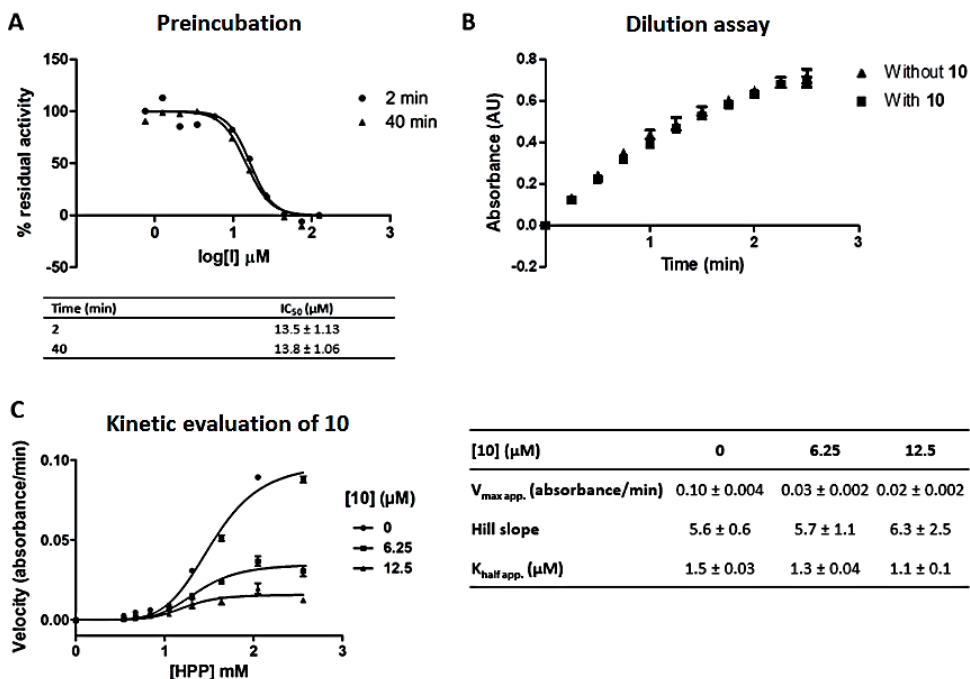


Figure 3. A. MIF (340 nM) was preincubated with compounds **10** (125 – 0 μM) for 2 or 40 minutes prior to starting the enzyme reaction by adding the substrate. No significant change in IC₅₀ value was observed. B. MIF (34 μM) was incubated with a concentration of 125 μM of compound **10**. Subsequently, this mixture was diluted 100x with the substrate and the enzyme activity was monitored. Diluting the inhibitor recovered the enzyme activity. C. The velocity of the enzyme reaction was measured at increasing concentrations of the substrate (HPP) in the presence of different concentrations of inhibitor **10**. The V_{max app.}, Hill slope and K_{half app.} were determined for each inhibitor concentration.

Conclusions and future perspectives

MIF binding to its molecular targets plays a key role in inflammatory processes and cancer. Therefore, MIF binders are considered to be potential therapeutics. In this study, we employed the MIF tautomerase enzymatic activity to identify MIF binding compounds that could potentially interfere with MIF functions. Using cyanoacetamide chemistry a focused compound collection with a chromene scaffold was synthesized and subsequently screened for inhibition of MIF tautomerase activity. This enabled identification of several novel MIF inhibitors with IC₅₀'s in the low micromolar range. Kinetic evaluation suggested that compound **10** and **17** were reversible inhibitors and that inhibitor **10** does not bind in direct competition with the substrate HPP. Taken together, a novel structural class of MIF inhibitors has been identified that could be used to further

investigate the tautomerase activity of MIF and may ultimately lead to the development of novel therapeutic agents.

Acknowledgements

We thank Directorate General of Higher Education Indonesia (DIKTI) in collaboration with the University of Surabaya (Ubaya), Indonesia and the University of Groningen (RuG), The Netherlands, for giving a grant 94.18/E4.4/2014. We acknowledge the European Research Council for providing an ERC starting grant (309782) and the NWO for providing a VIDI grant (723.012.005) to F. J. Dekker. Research in Dömling research group was supported by the US National Institutes of Health (NIH) (2R01GM097082-05). Funding has been received from the European Union's Horizon 2020 research and innovation program under MSC ITN "Accelerated Early staGe drug dIScovery" (AEGIS, grant agreement No. 675555) and CoFund ALERT (grant agreement No. 665250). We thank the European Regional Development Fund in the framework of the Polish innovation Economy Operational Program (contract no. POIG.02.01.00-12-023/08) for financial support of J. Kalinowska-Tłuścik.

References

- [1] Calandra, T. and T. Roger, Macrophage migration inhibitory factor: a regulator of innate immunity. *Nature reviews.Immunology*, 2003. **3**(10): p. 791-800.
- [2] Calandra, T., et al., The macrophage is an important and previously unrecognized source of macrophage migration inhibitory factor. *The Journal of experimental medicine*, 1994. **179**(6): p. 1895-1902.
- [3] Shi, X., et al., CD44 is the signaling component of the macrophage migration inhibitory factor-CD74 receptor complex. *Immunity*, 2006. **25**(4): p. 595-606.
- [4] Leng, L., et al., MIF signal transduction initiated by binding to CD74. *The Journal of experimental medicine*, 2003. **197**(11): p. 1467-1476.
- [5] Bernhagen, J., et al., MIF is a noncognate ligand of CXC chemokine receptors in inflammatory and atherogenic cell recruitment. *Nature medicine*, 2007. **13**(5): p. 587-596.
- [6] Gordon-Weeks, A.N., et al., Macrophage migration inhibitory factor: a key cytokine and therapeutic target in colon cancer. *Cytokine & growth factor reviews*, 2015. **26**(4): p. 451-461.
- [7] Tomiyasu, M., et al., Quantification of macrophage migration inhibitory factor mRNA expression in non-small cell lung cancer tissues and its clinical significance. *Clinical cancer research : an official journal of the American Association for Cancer Research*, 2002. **8**(12): p. 3755-3760.
- [8] Xu, X., et al., Overexpression of macrophage migration inhibitory factor induces angiogenesis in human breast cancer. *Cancer letters*, 2008. **261**(2): p. 147-157.
- [9] Munaut, C., et al., Macrophage migration inhibitory factor (MIF) expression in human glioblastomas correlates with vascular endothelial growth factor (VEGF) expression. *Neuropathology and applied neurobiology*, 2002. **28**(6): p. 452-460.
- [10] Shimizu, T., et al., High expression of macrophage migration inhibitory factor in human melanoma cells and its role in tumor cell growth and angiogenesis. *Biochemical and biophysical research communications*, 1999. **264**(3): p. 751-758.
- [11] Bernhagen, J., et al., MIF is a pituitary-derived cytokine that potentiates lethal endotoxaemia. *Nature*, 1993. **365**(6448): p. 756-759.
- [12] Bozza, M., et al., Targeted disruption of migration inhibitory factor gene reveals its critical role in sepsis. *The Journal of experimental medicine*, 1999. **189**(2): p. 341-346.
- [13] de Jong, Y.P., et al., Development of chronic colitis is dependent on the cytokine MIF. *Nature immunology*, 2001. **2**(11): p. 1061-1066.
- [14] Mikulowska, A., et al., Macrophage migration inhibitory factor is involved in the pathogenesis of collagen type II-induced arthritis in mice. *Journal of immunology (Baltimore, Md.: 1950)*, 1997. **158**(11): p. 5514-5517.
- [15] Ioannou, K., et al., ISO-66, a novel inhibitor of macrophage migration, shows efficacy in melanoma and colon cancer models. *International journal of oncology*, 2014. **45**(4): p. 1457-1468.
- [16] Merk, M., et al., D-dopachrome tautomerase (D-DT or MIF-2): doubling the MIF cytokine family. *Cytokine*, 2012. **59**(1): p. 10-17.
- [17] Suzuki, M., et al., Crystal structure of the macrophage migration inhibitory factor from rat liver. *Nature structural biology*, 1996. **3**(3): p. 259-266.
- [18] Rosengren, E., et al., The macrophage migration inhibitory factor MIF is a phenylpyruvate tautomerase. *FEBS letters*, 1997. **417**(1): p. 85-88.
- [19] Lubetsky, J.B., et al., Pro-1 of macrophage migration inhibitory factor functions as a catalytic base in the phenylpyruvate tautomerase activity. *Biochemistry*, 1999. **38**(22): p. 7346-7354.
- [20] Lubetsky, J.B., et al., The tautomerase active site of macrophage migration inhibitory factor is a potential target for discovery of novel anti-inflammatory agents. *The Journal of biological chemistry*, 2002. **277**(28): p. 24976-24982.
- [21] Al-Abed, Y., et al., ISO-1 binding to the tautomerase active site of MIF inhibits its pro-inflammatory activity and increases survival in severe sepsis. *The Journal of biological chemistry*, 2005. **280**(44): p. 36541-36544.
- [22] Russell, K.E., et al., The MIF Antagonist ISO-1 Attenuates Corticosteroid-Insensitive Inflammation and Airways Hyperresponsiveness in an Ozone-Induced Model of COPD. *PloS one*, 2016. **11**(1): p. e0146102.
- [23] Al-Abed, Y. and S. VanPatten, MIF as a disease target: ISO-1 as a proof-of-concept therapeutic. *Future medicinal chemistry*, 2011. **3**(1): p. 45-63.

- [24] Balachandran, S., et al., Synthesis and biological activity of novel MIF antagonists. *Bioorganic & medicinal chemistry letters*, 2011. **21**(5): p. 1508-1511.
- [25] Alam, A., et al., Synthesis and bio-evaluation of human macrophage migration inhibitory factor inhibitor to develop anti-inflammatory agent. *Bioorganic & medicinal chemistry*, 2011. **19**(24): p. 7365-7373.
- [26] Dziedzic, P., et al., Design, synthesis, and protein crystallography of biaryltriazoles as potent tautomerase inhibitors of macrophage migration inhibitory factor. *Journal of the American Chemical Society*, 2015. **137**(8): p. 2996-3003.
- [27] Cisneros, J.A., et al., A Fluorescence Polarization Assay for Binding to Macrophage Migration Inhibitory Factor and Crystal Structures for Complexes of Two Potent Inhibitors. *Journal of the American Chemical Society*, 2016. **138**(27): p. 8630-8638.
- [28] Jorgensen, W.L., et al., Receptor agonists of macrophage migration inhibitory factor. *Bioorganic & medicinal chemistry letters*, 2010. **20**(23): p. 7033-7036.
- [29] Orita, M., et al., Coumarin and chromen-4-one analogues as tautomerase inhibitors of macrophage migration inhibitory factor: discovery and X-ray crystallography. *Journal of medicinal chemistry*, 2001. **44**(4): p. 540-547.
- [30] Qian, Y., et al., Activity-Based Proteome Profiling Probes Based on Woodward's Reagent K with Distinct Target Selectivity. *Angew Chem Int Ed Engl*, 2016. **55**(27): p. 7766-71.
- [31] Rosati, O., et al., Synthesis of 5-Amino-1,10b-dihydro-2H-chromeno[3,4-c]pyridine-2,4(3H)-diones from Coumarins and Cyanoacetamides under Basic Conditions. *Synthesis-stuttgart*, 2010. **2**: p. 239-248.
- [32] Curini, M., et al., Preparation of 2-Amino-4H-chromene Derivatives from Coumarins in Basic Media. *Eur. J. Org. Chem.*, 2006(3): p. 746-751.
- [33] Wang, K., E. Herdtweck, and A. Dömling, Cyanoacetamides (IV): versatile one-pot route to 2-quinoline-3-carboxamides. *ACS combinatorial science*, 2012. **14**(5): p. 316-322.
- [34] Wang, K., et al., Cyanoacetamide multicomponent reaction (I): Parallel synthesis of cyanoacetamides. *Journal of combinatorial chemistry*, 2009. **11**(5): p. 920-927.
- [35] Wang, K., D. Kim, and A. Dömling, Cyanoacetamide MCR (III): three-component Gewald reactions revisited. *Journal of combinatorial chemistry*, 2010. **12**(1): p. 111-118.
- [36] Wang, K., E. Herdtweck, and A. Dömling, One-pot synthesis of 2-amino-indole-3-carboxamide and analogous. *ACS combinatorial science*, 2011. **13**(2): p. 140-146.
- [37] Cisneros, J.A., et al., Irregularities in enzyme assays: The case of macrophage migration inhibitory factor. *Bioorg Med Chem Lett*, 2016. **26**(12): p. 2764-2767.
- [38] Strelow, J., et al., Mechanism of Action Assays for Enzymes, in *Assay Guidance Manual*, G.S. Sittampalam, et al., Editors. 2004: Bethesda (MD).
- [39] Lubetsky, J.B., et al., Pro-1 of macrophage migration inhibitory factor functions as a catalytic base in the phenylpyruvate tautomerase activity. *Biochemistry*, 1999. **38**(22): p. 7346-54.

Supplementary Figures

Crystal structure of compound 7

Copies of the data can be obtained, free of charge, on application to CCDC, 12 Union Road, Cambridge CB2 1EZ, UK. (fax: +44-(0)1223-336033 or e-mail: deposit@ccdc.cam.ac.uk)

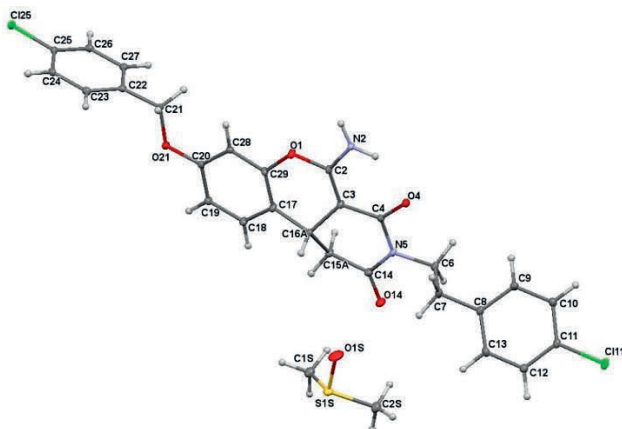


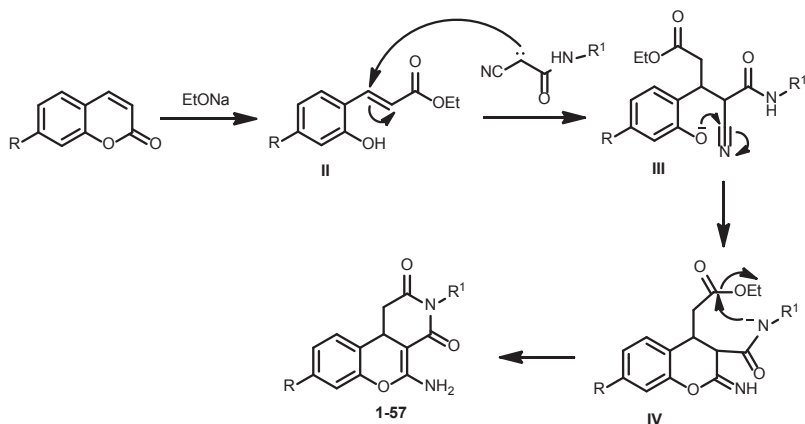
Figure S1. Molecular geometry observed in the crystal structures of compound 7, showing the atom labelling scheme. This compound crystallise as a solvate in the ration 1:1 (compound 7:DMSO). The positional disorder of C15 and C16 atoms were defined, with site occupancy 76% and 24% for alternative conformers A and B, respectively (here only the most abundant conformation is presented). Displacement ellipsoids of non-hydrogen atoms are drawn at the 30% probability level. H atoms are presented as small spheres with an arbitrary radius.

Table S1. Crystal data and structure refinement results for compound 7.

| Compound 7 | |
|--|--|
| Empirical moiety formula | C ₂₇ H ₂₂ Cl ₂ N ₂ O ₄ , C ₂ H ₆ O S |
| Formula weight [g/mol] | 587.49 |
| Crystal system | Triclinic |
| Space group | P $\bar{1}$ |
| Unit cell dimensions | a = 9.8209(5) Å b = 12.2263(8) Å c = 12.4634(13) Å α = 70.821(8)° β = 78.730(6)° γ = 78.721(5)° |
| Volume [Å ³] | 1372.2(2) |
| Z | 2 |
| D _{calc} [Mg/m ³] | 1.422 |
| μ [mm ⁻¹] | 0.356 |
| F(000) | 612 |
| Crystal size [mm ³] | 0.6 x 0.5 x 0.2 |
| Θ range | 2.95° to 28.66° |
| Index ranges | -12 ≤ h ≤ 13, -15 ≤ k ≤ 14, -15 ≤ l ≤ 14 |
| Refl. Collected | 9636 |
| Independent reflections | 6167 [R(int) = 0.0288] |
| Completeness [%] to Θ | 99.8 (Θ 25.2°) |
| Absorption correction | Multi-scan |
| T _{min} and T _{max} | 0.713 and 1.000 |
| Data/ restraints/parameters | 6167 / 0 / 381 |
| GooF on F ² | 1.040 |
| Final R indices [I > 2 σ (I)] | R1 = 0.0453, wR2 = 0.0957 |
| R indices (all data) | R1 = 0.0719, wR2 = 0.1141 |
| $\Delta\rho_{\max}$, $\Delta\rho_{\min}$ [e · Å ⁻³] | 0.31 and -0.32 |

Plausible mechanism of the formation of derivatives 1-57

The process takes place through the initial formation of coumaric derivative **II** and the subsequent Michael-type addition under basic conditions of the cyanoacetamide carbanion to **II** to give the intermediate **III**. In the final step, the intermediate **III** is converted into the iminochromene derivative **IV** through an intramolecular attack of the anion on the phenolic oxygen atom to the carbon of the nitrile bond. Finally, the adducts **1-57** were formed via cyclization between the amide and the carboxy ester side chain (**Scheme S1**).



Scheme S1. Plausible mechanism of the formation of derivatives **1-57**

Biological evaluation

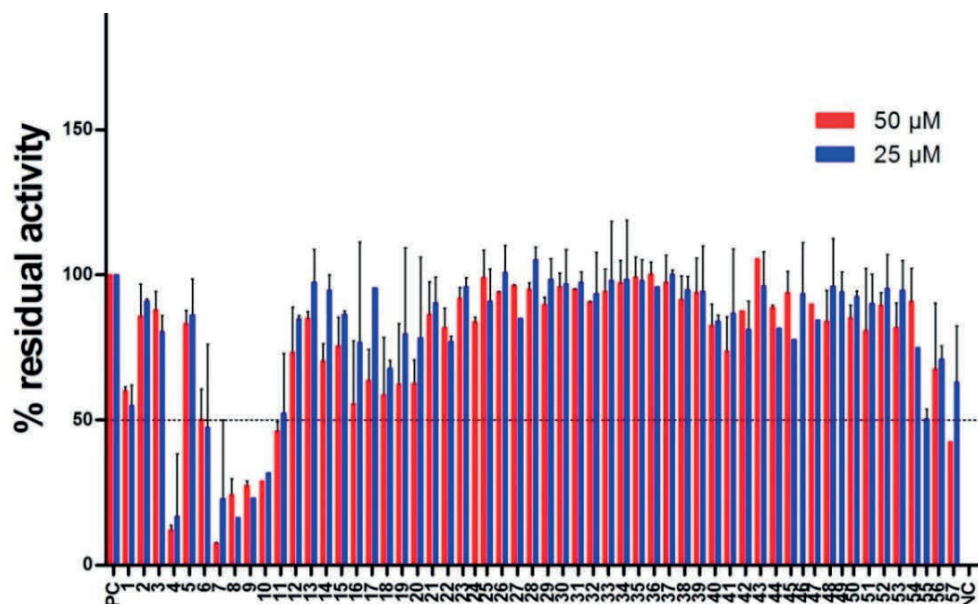


Figure S2. Single point screening of chromene compounds at 50 and 25 μM in the presence of 0.5 mM 4-HPP, 340 nM MIF and 0.2 M boric acid.

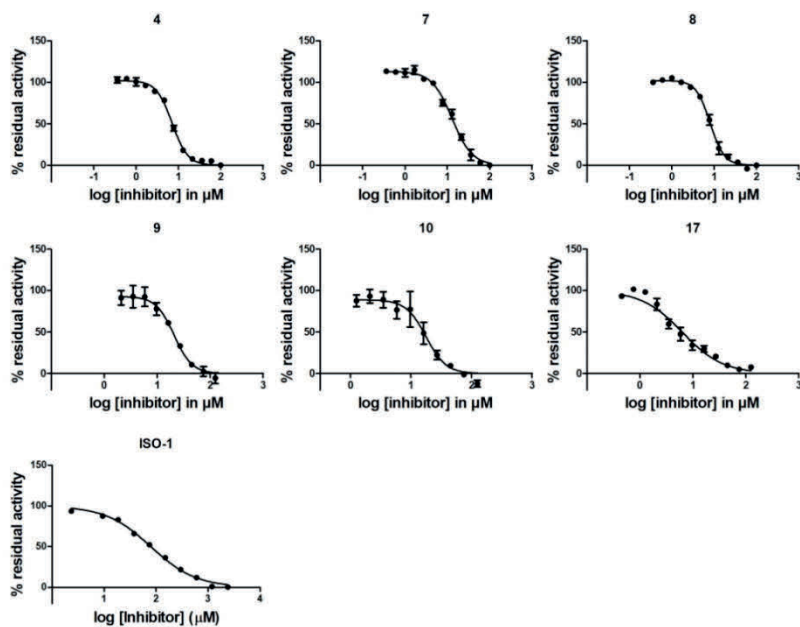


Figure S3. IC_{50} curves of the hits from the screening and ISO-1. The compounds were tested for inhibition of MIF tautomerase activity (MIF 340 nM, 4-HPP 0.5 mM) at 125 - 0 μM or 100 - 0 μM .

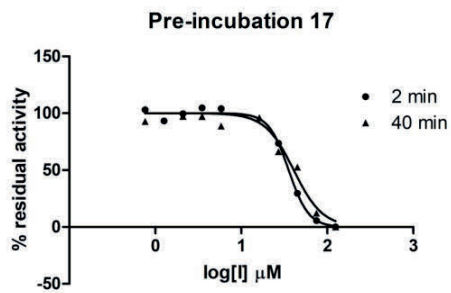
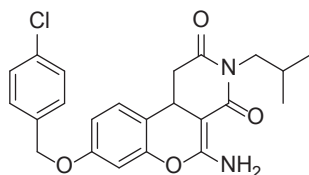


Figure S4. MIF (340 nM) was preincubated with compounds **17** (125 – 0 μM) for 2 or 40 minutes prior to starting the enzyme reaction by adding the substrate. No significant change in IC_{50} value was observed.

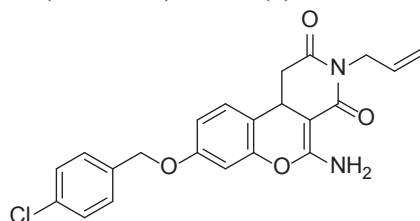
Characterization of compounds 1-57

5-Amino-8-(4-chlorobenzoyloxy)-3-isobutyl-1*H*-chromeno[3,4-*c*]pyridine-2,4(3*H*,10*bH*)-dione (1)



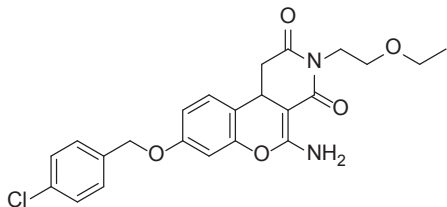
Light brown solid; ^1H NMR (500 MHz, $\text{DMSO-}d_6$) δ [ppm] 7.46 (d, $J = 10.0$ Hz, 2H), 7.43 (d, $J = 10.0$ Hz, 2H), 7.30 (d, $J = 10.0$ Hz, 1H), 6.78 (dd, $J = 10.0, 5.0$ Hz, 1H), 6.58 (d, $J = 10.0$ Hz, 1H), 5.10 (s, 2H), 3.87 (dd, $J = 10.0, 5.0$ Hz, 1H), 3.60 (dd, $J = 10.0, 5.0$ Hz, 1H), 3.46 (dd, $J = 10.0, 5.0$ Hz, 1H), 3.18 (dd, $J = 15.0, 5.0$ Hz, 1H), 0.78 (d, $J = 5.0$ Hz, 3H), 0.77 (d, $J = 5.0$ Hz, 3H). MS (ESI): Calcd for $\text{C}_{23}\text{H}_{23}\text{ClN}_2\text{O}_4$ (m/z): 426.1346, found: 426.8927.

3-Allyl-5-amino-8-(4-chlorobenzoyloxy)-1*H*-chromeno[3,4-*c*]pyridine-2,4(3*H*,10*bH*)-dione (2)



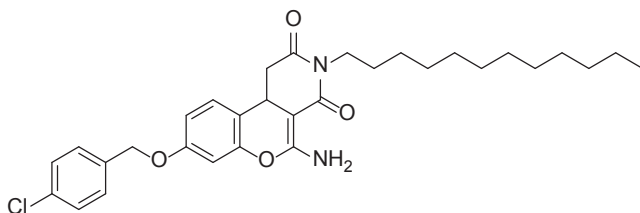
Brown solid; ^1H NMR (600 MHz, $\text{DMSO-}d_6$) δ [ppm] 8.20 (brs, 2H), 7.46 (s, 4H), 7.35 (d, $J = 8.4$ Hz, 1H), 6.84 (dd, $J = 8.4, 2.4$ Hz, 1H), 6.62 (d, $J = 2.4$ Hz, 1H), 5.76-5.83 (m, 1H), 5.15 (s, 2H), 5.00-5.05 (m, 2H), 4.83 (dd, $J = 15.0, 5.4$ Hz, 1H), 4.24 (dd, $J = 15.0, 4.8$ Hz, 1H), 3.94 (dd, $J = 13.8, 4.2$ Hz, 1H), 3.23 (dd, $J = 15.6, 4.2$ Hz, 1H), 2.55 (t, $J = 15.0$ Hz, 1H). MS (ESI): Calcd for $\text{C}_{22}\text{H}_{19}\text{ClN}_2\text{O}_4$ (m/z): 410.1033, found: 410.1029.

5-Amino-8-(4-chlorobenzoyloxy)-3-(2-ethoxyethyl)-1H-chromeno[3,4-c]pyridine-2,4(3H,10bH)-dione (3)



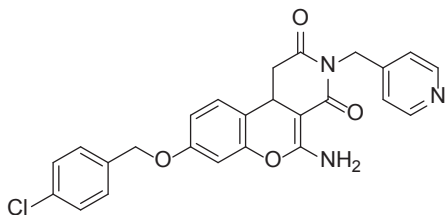
Brown solid; $^1\text{H NMR}$ (600 MHz, $\text{DMSO-}d_6$) δ [ppm] 8.20 (brs, 2H), 7.32 (d, $J = 8.4$ Hz, 1H), 6.82 (dd, $J = 8.4, 2.4$ Hz, 1H), 6.26 (d, $J = 2.4$ Hz, 1H), 5.13 (s, 2H), 3.92-3.97 (m, 1H), 3.87 (dd, $J = 13.8, 3.6$ Hz, 1H), 3.75-3.80 (m, 1H), 3.30 (m, 4H), 3.19 (dd, $J = 15.6, 4.2$ Hz, 1H), 1.07 (t, $J = 6.6$ Hz, 3H). MS (ESI): Calcd for $\text{C}_{23}\text{H}_{23}\text{ClN}_2\text{O}_5$ (m/z): 442.1295, found: 442.1288.

5-Amino-8-(4-chlorobenzoyloxy)-3-dodecyl-1H-chromeno[3,4-c]pyridine-2,4(3H,10bH)-dione (4)



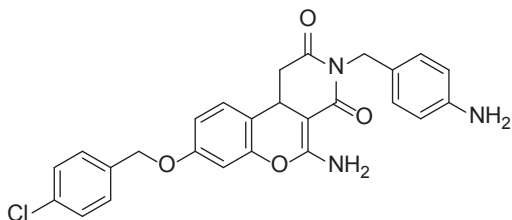
Brown solid; $^1\text{H NMR}$ ($\text{DMSO-}d_6$, 500 MHz) δ [ppm] 8.20 (brs, 2H), 7.46 (s, 4H), 7.35 (d, $J = 8.4$ Hz, 1H), 6.84 (dd, $J = 8.4, 2.4$ Hz, 1H), 6.62 (d, $J = 2.4$ Hz, 1H), 5.15 (s, 2H), 3.87 (dd, $J = 13.8, 4.2$ Hz, 1H), 3.70-3.77 (m, 1H), 3.57-3.63 (m, 1H), 3.19 (dd, $J = 15.6, 4.2$ Hz, 1H), 2.55 (t, $J = 15.0$ Hz, 1H), 1.42-1.46 (m, 2H), 1.15-1.25 (m, 18H), 0.85 (t, $J = 6.6$ Hz, 3H); $^{13}\text{C NMR}$ (126 MHz, $\text{DMSO-}d_6$) δ [ppm] 170.5, 167.1, 160.1, 157.9, 149.0, 135.9, 135.3, 132.5, 129.7, 129.4, 128.5, 128.0, 115.3, 112.7, 112.6, 111.8, 111.8, 102.0, 101.9, 101.7, 73.0, 69.0, 68.6, 31.3, 29.1, 28.8, 28.8, 27.9, 26.5, 22.1, 14.0. HRMS: Calcd for $\text{C}_{31}\text{H}_{39}\text{ClN}_2\text{O}_4$ (m/z): $[\text{M}+1]^+$ 539.25984, found: 539.26727.

**5-Amino-8-(4-chlorobenzoyloxy)-3-(pyridin-4-ylmethyl)-1*H*-chromeno[3,4-
c]pyridine-2,4(3*H*,10*bH*)-dione (5)**



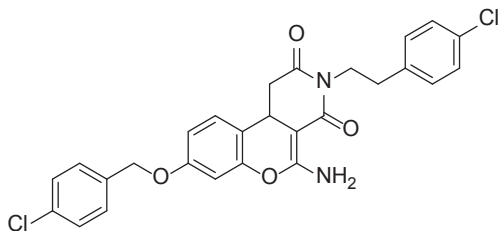
Brown solid; ¹H NMR (600 MHz, DMSO-*d*₆) δ [ppm] 8.47 (d, *J* = 6.0 Hz, 2H), 7.48 (s, 4H), 7.38 (d, *J* = 6.0 Hz, 1H), 7.20 (d, *J* = 6.0 Hz, 2H), 6.85 (dd, *J* = 8.4, 2.4 Hz, 1H), 6.64 (d, *J* = 2.4 Hz, 1H), 5.15 (s, 2H), 4.99 (d, *J* = 15.6 Hz, 1H), 4.86 (d, *J* = 15.6 Hz, 1H), 4.05 (dd, *J* = 13.8, 4.2 Hz, 1H), 3.23 (dd, *J* = 15.6, 4.2 Hz, 1H), 2.68 (t, *J* = 15.0 Hz, 1H). MS (ESI): Calcd for C₂₅H₂₀ClN₃O₄ (m/z): 461.1142, found: 461.1138.

**5-Amino-3-(4-aminobenzyl)-8-(4-chlorobenzoyloxy)-1*H*-chromeno[3,4-
c]pyridine-2,4(3*H*,10*bH*)-dione (6)**



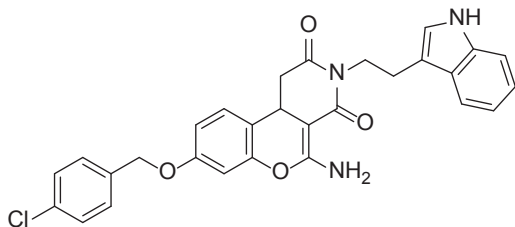
Brown solid; ¹H NMR (600 MHz, DMSO-*d*₆) δ [ppm] 8.20 (brs, 2H), 7.47 (s, 4H), 7.34 (d, *J* = 9.0 Hz, 1H), 6.94 (d, *J* = 7.8 Hz, 2H), 6.93 (dd, *J* = 9.0, 3.0 Hz, 1H), 6.61 (d, *J* = 2.4 Hz, 1H), 6.46 (d, *J* = 8.4 Hz, 2H), 5.14 (s, 2H), 4.93 (s, 2H), 4.76 (d, *J* = 7.8 Hz, 1H), 4.69 (d, *J* = 7.8 Hz, 1H), 3.89 (dd, *J* = 13.8, 4.2 Hz, 1H), 3.22 (dd, *J* = 15.6, 4.8 Hz, 1H), 2.54 (t, *J* = 15.0 Hz, 1H). MS (ESI): Calcd for C₂₆H₂₂ClN₃O₄ (m/z): 475.1299, found: 475.1291.

5-Amino-8-(4-chlorobenzoyloxy)-3-(4-chlorophenethyl)-1*H*-chromeno[3,4-*c*]pyridine-2,4(3*H*,10*bH*)-dione (7)



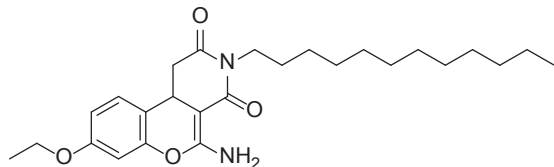
Light brown solid; ^1H NMR (DMSO-*d*₆, 500 MHz) δ [ppm] 7.46 (s, 4H), 7.34 (s, 1H), 7.33 (d, *J* = 8.4 Hz, 2H), 7.23 (d, *J* = 8.4 Hz, 2H), 6.83 (dd, *J* = 8.4, 3.0 Hz, 1H), 6.62 (d, *J* = 2.4 Hz, 1H), 5.14 (s, 2H), 3.92-3.95 (m, 1H), 3.77-3.85 (m, 2H), 3.19 (dd, *J* = 15.6, 4.2 Hz, 1H), 2.72-2.80 (m, 2H), 2.73 (t, *J* = 15.0 Hz, 1H) ppm; ^{13}C NMR (126 MHz, DMSO-*d*₆) δ [ppm] 170.4, 167.0, 160.2, 149.0, 138.1, 135.9, 135.3, 132.7, 132.5, 130.8, 130.5, 130.4, 129.8, 129.4, 128.5, 128.4, 128.3, 128.2, 128.1, 115.2, 113.0, 112.7, 112.6, 73.0, 69.0, 68.6, 68.2. HRMS: Calcd for C₂₇H₂₂Cl₂N₂O₄ (*m/z*): [*M*+1]⁺ 509.09566, found: 509.10278.

3-(2-(1*H*-Indol-3-yl)ethyl)-5-amino-8-(4-chlorobenzoyloxy)-1*H*-chromeno[3,4-*c*]pyridine-2,4(3*H*,10*bH*)-dione (8)



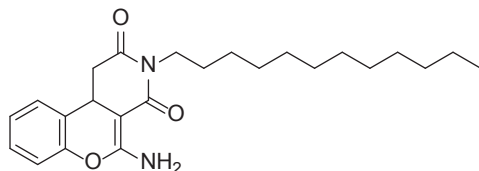
Brown solid; ^1H NMR (DMSO-*d*₆, 500 MHz) δ [ppm] 10.83 (s, 1H), 7.67 (d, *J* = 8.4 Hz, 1H), 7.49 (s, 4H), 7.35 (d, *J* = 8.4 Hz, 1H), 7.34 (d, *J* = 7.8 Hz, 1H), 7.17 (s, 1H), 7.07 (t, *J* = 7.8 Hz, 1H), 7.00 (t, *J* = 7.8 Hz, 1H), 6.84 (dd, *J* = 9.0, 2.4 Hz, 1H), 6.63 (d, *J* = 2.4 Hz, 1H), 5.15 (s, 2H), 3.98-4.08 (m, 1H), 3.86-3.93 (m, 2H), 3.22 (dd, *J* = 15.6, 4.2 Hz, 1H), 2.80-2.92 (m, 2H), 2.56 (t, *J* = 7.8 Hz, 1H). ^{13}C NMR (126 MHz, DMSO-*d*₆) δ [ppm] 170.4, 162.0, 161.3, 160.3, 155.3, 144.4, 144.3, 136.3, 135.4, 132.7, 129.8, 129.5, 128.6, 127.2, 122.8, 122.8, 121.0, 118.3, 116.3, 113.0, 112.7, 112.6, 111.5, 111.4, 101.7, 101.7, 69.0, 25.3, 24.9. HRMS: Calcd for C₂₉H₂₄ClN₃O₄ (*m/z*): [*M*+1]⁺ 514.14553, found: 514.15259.

5-Amino-3-dodecyl-8-ethoxy-1*H*-chromeno[3,4-*c*]pyridine-2,4(3*H*,10*bH*)-dione (9)



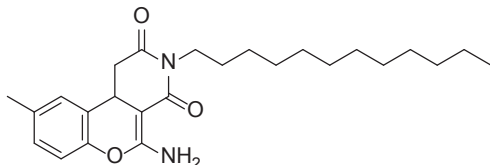
Brown solid; ¹H NMR (DMSO-*d*₆, 500 MHz) δ [ppm] 8.23 (brs, 2H), 7.31 (d, J = 8.4 Hz, 1H), 6.74 (dd, J = 8.4, 2.4 Hz, 1H), 6.53 (d, J = 2.4 Hz, 1H), 4.03 (q, J = 6.6 Hz, 2H), 3.87 (dd, J = 13.8, 4.2 Hz, 1H), 3.70-3.77 (m, 1H), 3.58-3.63 (m, 1H), 3.18 (dd, J = 15.6, 4.2 Hz, 1H), 2.49 (t, J = 15.0 Hz, 1H), 1.40-1.50 (m, 2H), 1.33 (t, J = 6.6 Hz, 3H), 1.18-1.29 (m, 18H), 0.85 (t, J = 6.6 Hz, 3H); ¹³C NMR (126 MHz, DMSO-*d*₆) δ [ppm] 170.5, 167.2, 160.1, 148.0, 144.4, 129.5, 128.0, 114.7, 112.7, 112.4, 111.33, 73.1, 64.0, 63.4, 31.3, 29.2, 29.1, 29.0, 28.80, 28.76, 27.9, 26.5, 26.3, 25.6, 25.3, 22.1, 14.5, 14.4, 14.0. HRMS: Calcd for C₂₆H₃₈N₂O₄ (m/z): [M+1]⁺ 443.28316, found: 443.29013.

5-Amino-3-dodecyl-1*H*-chromeno[3,4-*c*]pyridine-2,4(3*H*,10*bH*)-dione (10)



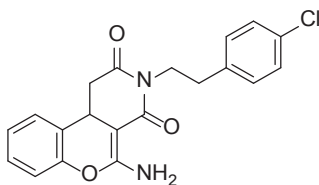
Brown solid; ¹H NMR (500 MHz, DMSO-*d*₆) δ [ppm] 8.12 (br s, 2H), 7.41 (d, J = 7.8 Hz, 1H), 7.28 (t, J = 7.8 Hz, 1H), 7.15 (t, J = 7.8 Hz, 1H), 7.02 (d, J = 7.8 Hz, 1H), 3.98 (dd, J = 13.8, 3.6 Hz, 1H), 3.71-3.75 (m, 1H), 3.59-3.63 (m, 1H), 3.23 (dd, J = 15.6, 4.8 Hz, 1H), 2.56 (t, J = 14.4 Hz, 1H), 1.40-1.50 (m, 2H), 1.18-1.30 (m, 18H), 0.85 (t, J = 6.6 Hz, 3H) ppm; ¹³C NMR (126 MHz, DMSO-*d*₆) δ [ppm] 170.4, 167.1, 160.2, 148.4, 128.4, 127.2, 124.7, 123.1, 115.7, 72.8, 31.3, 29.1, 29.0, 28.8, 27.9, 26.5, 26.0, 22.1, 14.0. HRMS: Calcd for C₂₄H₃₄N₂O₃ (m/z): [M+1] 399.25694, found: 399.26407.

5-Amino-3-dodecyl-9-methyl-1*H*-chromeno[3,4-*c*]pyridine-2,4(3*H*,10*bH*)-dione (11)



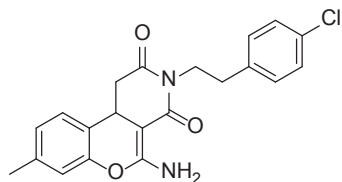
Yellow solid; ¹H NMR (600 MHz, DMSO-*d*₆) δ [ppm] 8.10 (brs, 1H), 7.23 (s, 1H), 7.08 (d, *J* = 8.4 Hz, 1H), 6.92 (d, *J* = 7.8 Hz, 1H), 3.93 (dd, *J* = 14.4, 4.2 Hz, 1H), 3.71-3.78 (m, 1H), 3.58-3.63 (m, 1H), 3.21 (dd, *J* = 15.6, 4.2 Hz, 1H), 2.54 (t, *J* = 14.4 Hz, 1H), 2.28 (s, 3H), 1.40-1.50 (m, 2H), 1.18-1.30 (m, 18H), 0.85 (t, *J* = 6.6 Hz, 3H). MS (ESI): Calcd for C₂₅H₃₆N₂O₃ (*m/z*): 412.2726, found: 412.2733.

5-Amino-3-(4-chlorophenethyl)-1*H*-chromeno[3,4-*c*]pyridine-2,4(3*H*,10*bH*)-dione (12)



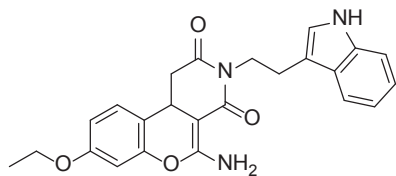
Brown solid; ¹H NMR (600 MHz, DMSO-*d*₆) δ [ppm] 8.20 (brs, 2H), 7.42 (d, *J* = 7.8 Hz, 1H), 7.34 (d, *J* = 8.4 Hz, 2H), 7.28 (t, *J* = 7.8 Hz, 1H), 7.22 (d, *J* = 8.4 Hz, 2H), 7.16 (t, *J* = 7.8 Hz, 1H), 7.02 (d, *J* = 7.8 Hz, 1H), 7.00 (d, *J* = 8.4 Hz, 2H), 6.69 (d, *J* = 8.4 Hz, 2H), 3.90-3.98 (m, 2H), 3.78-3.84 (m, 1H), 3.22 (dd, *J* = 15.6, 4.8 Hz, 1H), 2.70-2.80 (m, 2H), 2.55 (t, *J* = 14.4 Hz, 1H). MS (ESI): Calcd for C₂₀H₁₇ClN₂O₃ (*m/z*): 368.0928, found: 368.0921.

5-Amino-3-(4-chlorophenethyl)-8-methyl-1H-chromeno[3,4-c]pyridine-2,4(3H,10bH)-dione (13)



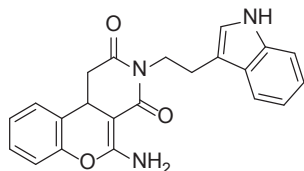
Brown solid; $^1\text{H NMR}$ (600 MHz, $\text{DMSO-}d_6$) δ [ppm] 8.10 (s, 2H), 7.35 (d, $J = 8.4$ Hz, 2H), 7.31 (d, $J = 7.8$ Hz, 1H), 7.27 (d, $J = 8.4$ Hz, 2H), 6.99 (d, $J = 7.8$ Hz, 1H), 6.85 (s, 1H), 3.81-3.97 (m, 3H), 3.20 (dd, $J = 15.6, 4.2$ Hz, 1H), 2.74-2.78 (m, 2H), 2.63 (t, $J = 15.0$ Hz, 1H), 2.28 (s, 3H). MS (ESI): Calcd for $\text{C}_{21}\text{H}_{19}\text{ClN}_2\text{O}_3$ (m/z): 382.1084, found: 382.8395.

3-(2-(1H-Indol-3-yl)ethyl)-5-amino-8-ethoxy-1H-chromeno[3,4-c]pyridine-2,4(3H,10bH)-dione (14)



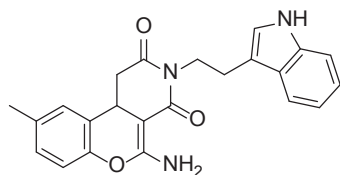
Light brown solid; $^1\text{H NMR}$ (600 MHz, $\text{DMSO-}d_6$) δ [ppm] 10.83 (s, 1H), 7.68 (d, $J = 7.8$ Hz, 1H), 7.33 (d, $J = 8.4$ Hz, 2H), 7.17 (s, 1H), 7.07 (t, $J = 7.2$ Hz, 1H), 7.00 (t, $J = 8.4$ Hz, 1H), 6.75 (dd, $J = 8.4, 2.4$ Hz, 1H), 6.54 (d, $J = 2.4$ Hz, 1H), 4.01 (q, $J = 7.2$ Hz, 2H), 4.00-4.03 (m, 1H), 3.85-3.92 (m, 2H), 3.22 (dd, $J = 15.6, 4.2$ Hz, 1H), 2.82-2.92 (m, 2H), 2.55 (t, $J = 14.4$ Hz, 1H), 1.33 (t, $J = 7.2$ Hz, 3H). MS (ESI): Calcd for $\text{C}_{24}\text{H}_{23}\text{N}_3\text{O}_4$ (m/z): 417.1689, found: 417.1682.

3-(2-(1*H*-Indol-3-yl)ethyl)-5-amino-1*H*-chromeno[3,4-*c*]pyridine-2,4(3*H*,10*bH*)-dione (15)



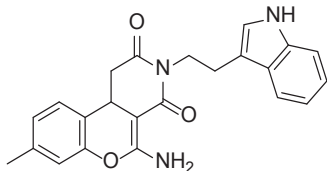
Brown solid; ¹H NMR (600 MHz, DMSO-*d*₆) δ [ppm] 10.82 (s, 1H), 8.20 (brs, 1H), 7.68 (d, *J* = 7.8 Hz, 1H), 7.44 (d, *J* = 7.8 Hz, 1H), 7.35 (d, *J* = 7.8 Hz, 1H), 7.30 (t, *J* = 7.2 Hz, 1H), 7.18 (s, 1H), 7.17 (t, *J* = 8.4 Hz, 1H), 7.08 (t, *J* = 7.2 Hz, 1H), 7.05 (d, *J* = 7.8 Hz, 1H), 7.01 (t, *J* = 7.2 Hz, 1H), 4.01-4.06 (m, 1H), 3.99 (dd, *J* = 14.4, 4.2 Hz, 1H), 3.86-3.92 (m, 1H), 3.26 (dd, *J* = 15.6, 4.2 Hz, 1H), 2.82-2.94 (m, 2H), 2.61 (t, *J* = 15.6 Hz, 1H). MS (ESI): Calcd for C₂₂H₁₉N₃O₃ (m/z): 373.1426, found: 373.1429.

3-(2-(1*H*-indol-3-yl)ethyl)-5-amino-9-methyl-1*H*-chromeno[3,4-*c*]pyridine-2,4(3*H*,10*bH*)-dione (16)



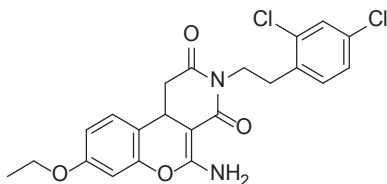
Brown solid; ¹H NMR (600 MHz, DMSO-*d*₆) δ [ppm] 10.83 (s, 1H), 7.68 (d, *J* = 7.8 Hz, 1H), 7.34 (d, *J* = 7.8 Hz, 1H), 7.25 (s, 1H), 7.18 (s, 1H), 7.09 (t, *J* = 7.2 Hz, 1H), 7.08 (t, *J* = 8.4 Hz, 1H), 7.01 (t, *J* = 7.2 Hz, 1H), 6.93 (d, *J* = 8.4 Hz, 1H), 4.00-4.03 (m, 1H), 3.95 (dd, *J* = 13.8, 4.2 Hz, 1H), 3.86-3.91 (m, 1H), 3.25 (dd, *J* = 15.0, 4.2 Hz, 1H), 2.82-2.92 (m, 2H), 2.60 (t, *J* = 14.4 Hz, 1H), 2.29 (s, 3H). MS (ESI): Calcd for C₂₃H₂₁N₃O₃ (m/z): 387.1583, found: 387.1583.

3-(2-(1*H*-Indol-3-yl)ethyl)-5-amino-8-methyl-1*H*-chromeno[3,4-*c*]pyridine-2,4(3*H*,10*bH*)-dione (17)



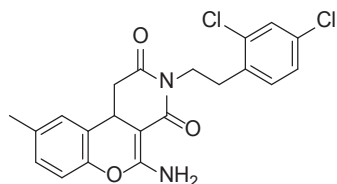
Yellow solid; ^1H NMR (500 MHz, $\text{DMSO-}d_6$) δ [ppm] 10.85 (s, 1H), 8.20 (brs, 2H), 7.68 (d, $J = 7.8$ Hz, 1H), 7.34 (d, $J = 7.8$ Hz, 1H), 7.29 (d, $J = 7.8$ Hz, 1H), 7.17 (s, 1H), 7.07 (t, $J = 7.2$ Hz, 1H), 7.00 (d, $J = 7.2$ Hz, 1H), 6.99 (d, $J = 7.2$ Hz, 1H), 6.86 (s, 1H), 4.02 (td, $J = 11.4, 5.4$ Hz, 1H), 3.93 (dd, $J = 13.8, 5.4$ Hz, 1H), 3.89 (td, $J = 11.4, 5.4$ Hz, 1H), 3.24 (dd, $J = 15.6, 4.2$ Hz, 1H), 2.81-2.92 (m, 2H), 2.57 (t, $J = 15.0$ Hz, 1H), 2.29 (s, 3H); ^{13}C NMR (126 MHz, $\text{DMSO-}d_6$) δ [ppm] 170.5, 167.2, 160.4, 148.3, 138.2, 136.3, 127.3, 127.0, 125.5, 122.7, 121.0, 120.0, 118.3, 116.0, 111.5, 111.4, 73.0, 25.8, 24.1, 20.5. HRMS: Calcd for $\text{C}_{23}\text{H}_{21}\text{N}_3\text{O}_3$ (m/z): $[\text{M}+1]^+$ 388.15829, found: 388.16513.

5-Amino-3-(2,4-dichlorophenethyl)-8-ethoxy-1*H*-chromeno[3,4-*c*]pyridine-2,4(3*H*,10*bH*)-dione (18)



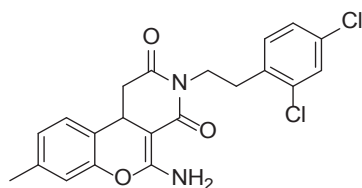
Brown solid; ^1H NMR (600 MHz, $\text{DMSO-}d_6$) δ [ppm] 7.56 (d, $J = 2.4$ Hz, 1H), 7.36 (dd, $J = 8.4, 1.8$ Hz, 1H), 7.32 (d, $J = 8.4$ Hz, 1H), 7.30 (d, $J = 8.4$ Hz, 1H), 6.74 (dd, $J = 9.0, 3.0$ Hz, 1H), 6.53 (d, $J = 2.4$ Hz, 1H), 4.00-4.09 (m, 3H), 3.89 (dd, $J = 13.8, 7.2$ Hz, 1H), 3.85 (dd, $J = 13.8, 4.2$ Hz, 1H), 3.17 (dd, $J = 15.6, 4.2$ Hz, 1H), 2.87-2.94 (m, 2H), 2.47 (t, $J = 15.6$ Hz, 1H). MS (ESI): Calcd for $\text{C}_{22}\text{H}_{20}\text{Cl}_2\text{N}_2\text{O}_4$ (m/z): 446.0801, found: 446.0807.

5-Amino-3-(2,4-dichlorophenethyl)-9-methyl-1*H*-chromeno[3,4-*c*]pyridine-2,4(3*H*,10*bH*)-dione (19)



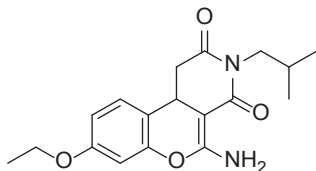
Yellow solid; $^1\text{H NMR}$ (600 MHz, $\text{DMSO-}d_6$) δ [ppm] 8.20 (brs, 2H), 7.56 (d, $J = 2.4$ Hz, 1H), 7.36 (dd, $J = 7.8, 1.8$ Hz, 1H), 7.30 (d, $J = 8.4$ Hz, 1H), 7.24 (s, 1H), 7.09 (d, $J = 7.8$ Hz, 1H), 6.92 (d, $J = 8.4$ Hz, 1H), 4.00-4.08 (m, 1H), 3.87-3.94 (m, 2H), 3.19 (dd, $J = 15.6, 4.2$ Hz, 1H), 2.88-2.94 (m, 2H), 2.52 (t, $J = 15.0$ Hz, 1H), 2.28 (s, 3H). MS (ESI): Calcd for $\text{C}_{21}\text{H}_{18}\text{Cl}_2\text{N}_2\text{O}_3$ (m/z): 416.0694, found: 416.0688.

5-Amino-3-(2,4-dichlorophenethyl)-8-methyl-1*H*-chromeno[3,4-*c*]pyridine-2,4(3*H*,10*bH*)-dione (20)



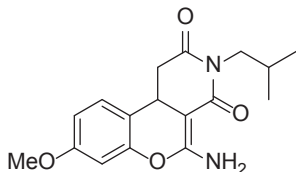
Brown solid; $^1\text{H NMR}$ (600 MHz, $\text{DMSO-}d_6$) δ [ppm] 8.15 (s, 2H), 7.56 (s, 1H), 7.36 (d, $J = 8.4$ Hz, 1H), 7.30 (d, $J = 8.4$ Hz, 2H), 6.98 (d, $J = 7.2$ Hz, 1H), 6.85 (s, 1H), 3.98-4.05 (m, 1H), 3.85-3.92 (m, 2H), 3.18 (d, $J = 15.6$ Hz, 1H), 2.87-2.93 (m, 2H), 2.30 (s, 3H). MS (ESI): Calcd for $\text{C}_{21}\text{H}_{18}\text{Cl}_2\text{N}_2\text{O}_3$ (m/z): 416.0694, found: 416.0698.

5-Amino-8-ethoxy-3-isobutyl-1*H*-chromeno[3,4-*c*]pyridine-2,4(3*H*,10*bH*)-dione (21)



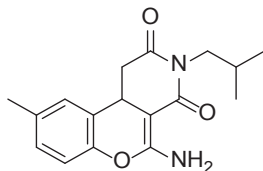
Light brown solid; ^1H NMR (600 MHz, $\text{DMSO-}d_6$) δ [ppm] 7.32 (d, $J = 9.0$ Hz, 1H), 6.73 (dd, $J = 9.0, 2.4$ Hz, 1H), 6.53 (d, $J = 2.4$ Hz, 1H), 4.03 (q, $J = 7.2$ Hz, 2H), 3.90 (dd, $J = 13.8, 4.2$ Hz, 1H), 3.64 (dd, $J = 13.2, 7.8$ Hz, 1H), 3.50 (dd, $J = 13.2, 7.8$ Hz, 1H), 3.21 (dd, $J = 15.6, 4.2$ Hz, 1H), 2.52 (t, $J = 15.0$ Hz, 1H), 1.88-1.94 (m, 1H), 1.31 (t, $J = 7.2$ Hz, 3H), 0.86 (d, $J = 7.2$ Hz, 3H), 0.82 (d, $J = 7.2$ Hz, 3H). MS (ESI): Calcd for $\text{C}_{18}\text{H}_{22}\text{N}_2\text{O}_4$ (m/z): 330.158, found: 330.1571.

5-Amino-3-isobutyl-8-methoxy-1*H*-chromeno[3,4-*c*]pyridine-2,4(3*H*,10*bH*)-dione (22)



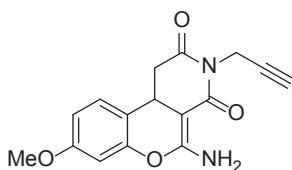
Light brown solid; ^1H NMR (500 MHz, $\text{DMSO-}d_6$) δ [ppm] 7.35 (d, $J = 9.0$ Hz, 1H), 6.80 (dd, $J = 9.0, 2.4$ Hz, 1H), 6.56 (d, $J = 2.4$ Hz, 1H), 3.97 (dd, $J = 13.8, 4.2$ Hz, 1H), 3.83 (s, 3H), 3.75 (dd, $J = 13.2, 7.8$ Hz, 1H), 3.59 (dd, $J = 13.2, 7.8$ Hz, 1H), 3.22 (dd, $J = 15.6, 4.2$ Hz, 1H), 2.53 (t, $J = 15.0$ Hz, 1H), 1.98-2.06 (m, 1H), 0.90 (d, $J = 7.2$ Hz, 3H), 0.86 (d, $J = 7.2$ Hz, 3H). MS (ESI): Calcd for $\text{C}_{17}\text{H}_{20}\text{N}_2\text{O}_4$ (m/z): 316.1423, found: 316.1418.

5-Amino-3-isobutyl-9-methyl-1*H*-chromeno[3,4-*c*]pyridine-2,4(3*H*,10*bH*)-dione (23)



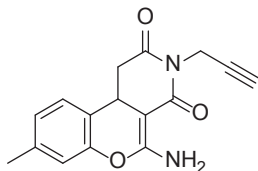
Brown solid; ¹H NMR (600 MHz, DMSO-*d*₆) δ [ppm] 8.20 (brs, 1H), 7.24 (s, 1H), 7.08 (d, $J = 8.4$ Hz, 1H), 6.92 (d, $J = 8.4$ Hz, 1H), 3.96 (dd, $J = 13.8, 4.2$ Hz, 1H), 3.65 (dd, $J = 12.6, 7.2$ Hz, 1H), 3.50 (dd, $J = 13.2, 7.8$ Hz, 1H), 3.23 (dd, $J = 15.6, 4.2$ Hz, 1H), 2.58 (t, $J = 14.4$ Hz, 1H), 2.28 (s, 3H), 1.88-1.94 (m, 1H), 0.83 (t, $J = 7.2$ Hz, 3H), 0.80 (t, $J = 7.2$ Hz, 3H). MS (ESI): Calcd for C₁₇H₂₀N₂O₃ (m/z): 300.1474, found: 300.1469.

5-Amino-8-methoxy-3-(prop-2-ynyl)-1*H*-chromeno[3,4-*c*]pyridine-2,4(3*H*,10*bH*)-dione (24)



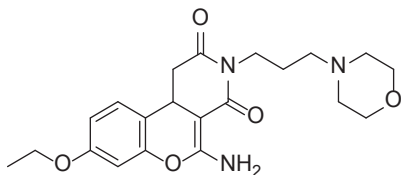
Brown solid; ¹H NMR (500 MHz, DMSO-*d*₆) δ [ppm] 7.29 (d, $J = 5.0$ Hz, 1H), 6.73 (dd, $J = 10.0, 5.0$ Hz, 1H), 6.52 (d, $J = 0.5$ Hz, 1H), 4.40 (ddd, $J = 15.0, 10.0, 5.0$ Hz, 2H), 3.87 (dd, $J = 10.0, 5.0$ Hz, 1H), 3.72 (s, 3H), 3.22 (dd, $J = 10.0, 5.0$ Hz, 1H), 3.60 (s, 1H). MS (ESI): Calcd for C₁₆H₁₄N₂O₄ (m/z): 298.0954, found: 298.0949.

5-Amino-8-methyl-3-(prop-2-ynyl)-1*H*-chromeno[3,4-*c*]pyridine-2,4(3*H*,10*bH*)-dione (25)



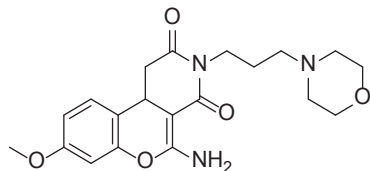
Brown solid; $^1\text{H NMR}$ (600 MHz, $\text{DMSO-}d_6$) δ [ppm] 8.20 (brs, 2H), 7.30 (d, $J = 7.8$ Hz, 1H), 6.99 (d, $J = 7.8$ Hz, 1H), 6.85 (s, 1H), 4.47 (dd, $J = 14.4, 2.4$ Hz, 1H), 4.37 (dd, $J = 14.4, 2.4$ Hz, 1H), 3.95 (dd, $J = 14.4, 4.8$ Hz, 1H), 3.27 (dd, $J = 15.6, 4.2$ Hz, 1H), 3.01 (t, $J = 2.4$ Hz, 1H), 2.55 (dd, $J = 15.0, 13.8$ Hz, 1H), 2.30 (s, 3H). MS (ESI): Calcd for $\text{C}_{16}\text{H}_{14}\text{N}_2\text{O}_3$ (m/z): 282.1004, found: 282.1011.

5-Amino-8-ethoxy-3-(3-morpholinopropyl)-1*H*-chromeno[3,4-*c*]pyridine-2,4(3*H*,10*bH*)-dione (26)



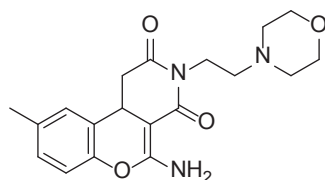
Brown solid; $^1\text{H NMR}$ (600 MHz, $\text{DMSO-}d_6$) δ [ppm] 8.20 (s, 2H), 7.31 (d, $J = 9.0$ Hz, 1H), 6.74 (dd, $J = 8.4, 2.4$ Hz, 1H), 6.53 (d, $J = 2.4$ Hz, 1H), 4.03 (q, $J = 6.6$ Hz, 2H), 3.88 (dd, $J = 13.8, 4.2$ Hz, 1H), 3.75-3.82 (m, 1H), 3.62-3.68 (m, 1H), 3.51-3.58 (m, 4H), 3.18 (dd, $J = 15.6, 4.2$ Hz, 1H), 2.32 (s, 4H), 2.27 (t, $J = 7.2$ Hz, 4H), 1.58-1.64 (m, 2H), 1.32 (t, $J = 7.2$ Hz, 3H). MS (ESI): Calcd for $\text{C}_{21}\text{H}_{27}\text{N}_3\text{O}_5$ (m/z): 401.1951, found: 401.1944.

5-Amino-8-methoxy-3-(3-morpholinopropyl)-1*H*-chromeno[3,4-*c*]pyridine-2,4(3*H*,10*bH*)-dione (27)



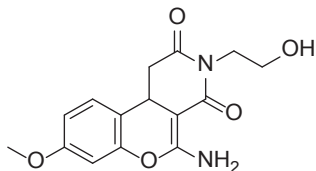
Light brown solid; ^1H NMR (600 MHz, DMSO-*d*₆) δ [ppm] 7.34 (d, $J = 9.0$ Hz, 1H), 6.79 (dd, $J = 9.0, 3.0$ Hz, 1H), 6.56 (d, $J = 8.4$ Hz, 1H), 3.96 (dd, $J = 14.4, 4.2$ Hz, 1H), 3.92 (ddd, $J = 15.0, 8.4, 6.6$ Hz, 1H), 3.83 (s, 3H), 3.78 (ddd, $J = 15.0, 8.4, 6.6$ Hz, 1H), 3.61 (t, $J = 4.8$ Hz, 4H), 3.21 (dd, $J = 15.6, 4.2$ Hz, 1H), 2.84 (m, 4H), 2.52 (t, $J = 8.4$ Hz, 1H), 2.38 (s, 4H), 2.35 (t, $J = 6.6$ Hz, 2H), 1.68-1.78 (m, 2H). MS (ESI): Calcd for C₂₀H₂₅N₃O₅ (m/z): 387.1794, found: 387.1799.

5-Amino-9-methyl-3-(2-morpholinoethyl)-1*H*-chromeno[3,4-*c*]pyridine-2,4(3*H*,10*bH*)-dione (28)



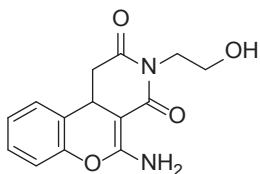
Brown solid; ^1H NMR (600 MHz, DMSO-*d*₆) δ [ppm] 8.20 (brs, 1H), 7.24 (s, 1H), 7.08 (d, $J = 7.2$ Hz, 1H), 6.91 (d, $J = 7.8$ Hz, 1H), 3.93 (dd, $J = 13.8, 4.2$ Hz, 1H), 3.88-3.92 (m, 1H), 3.72-3.78 (m, 1H), 3.50-3.60 (m, 4H), 2.55 (t, $J = 13.8$ Hz, 1H), 2.35-2.45 (m, 5H), 2.32 (s, 3H). MS (ESI): Calcd for C₁₉H₂₃N₃O₄ (m/z): 357.1689, found: 357.1697.

5-Amino-3-(2-hydroxyethyl)-8-methoxy-1*H*-chromeno[3,4-*c*]pyridine-2,4(3*H*,10*bH*)-dione (29)



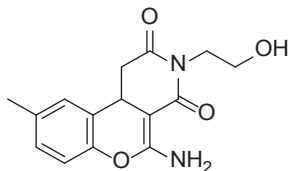
Brown solid; $^1\text{H NMR}$ (600 MHz, $\text{DMSO-}d_6$) δ [ppm] 7.33 (d, $J = 8.4$ Hz, 1H), 6.76 (dd, $J = 8.4, 2.4$ Hz, 1H), 6.56 (d, $J = 2.4$ Hz, 1H), 4.70 (s, 1H), 3.84-3.92 (m, 3H), 3.77 (s, 3H), 3.65-3.73 (m, 2H), 3.19 (dd, $J = 15.6, 4.2$ Hz, 1H), 2.50 (t, $J = 15.6$ Hz, 1H). MS (ESI): Calcd for $\text{C}_{15}\text{H}_{16}\text{N}_2\text{O}_5$ (m/z): 304.1059, found: 304.1051.

5-Amino-3-(2-hydroxyethyl)-1*H*-chromeno[3,4-*c*]pyridine-2,4(3*H*,10*bH*)-dione (30)



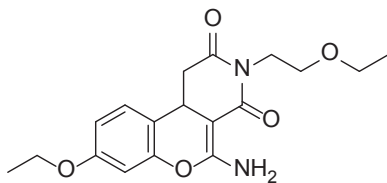
Yellow solid; $^1\text{H NMR}$ (600 MHz, $\text{DMSO-}d_6$) δ [ppm] 8.20 (s, 2H), 7.44 (d, $J = 7.8$ Hz, 1H), 7.31 (t, $J = 7.8$ Hz, 1H), 7.21 (t, $J = 7.8$ Hz, 1H), 7.03 (d, $J = 7.8$ Hz, 1H), 4.04-4.10 (m, 2H), 3.82-3.90 (m, 2H), 3.60-3.65 (m, 2H), 3.26 (dd, $J = 15.6, 4.8$ Hz, 1H), 2.60 (t, $J = 14.4$ Hz, 1H). MS (ESI): Calcd for $\text{C}_{14}\text{H}_{14}\text{N}_2\text{O}_4$ (m/z): 274.0954, found: 274.0955.

5-Amino-3-(2-hydroxyethyl)-9-methyl-1*H*-chromeno[3,4-*c*]pyridine-2,4(3*H*,10*bH*)-dione (31)



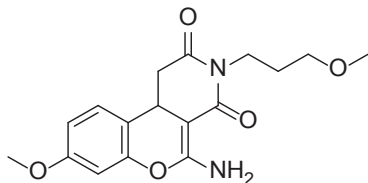
Brown solid; ¹H NMR (600 MHz, DMSO-*d*₆) δ [ppm] 8.10 (brs, 1H), 7.23 (s, 1H), 7.08 (d, $J = 8.4$ Hz, 1H), 6.92 (d, $J = 7.8$ Hz, 1H), 4.70 (s, 1H), 3.95 (dd, $J = 14.4, 4.2$ Hz, 1H), 3.85-3.91 (m, 1H), 3.67-3.73 (m, 1H), 3.33-3.49 (m, 2H), 3.22 (dd, $J = 15.6, 4.2$ Hz, 1H), 2.55 (t, $J = 14.4$ Hz, 1H), 2.28 (s, 3H). MS (ESI): Calcd for C₁₅H₁₆N₂O₄ (m/z): 288.1110, found: 288.1117.

5-Amino-8-ethoxy-3-(2-ethoxyethyl)-1*H*-chromeno[3,4-*c*]pyridine-2,4(3*H*,10*bH*)-dione (32)



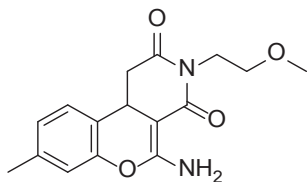
Brown solid; ¹H NMR (600 MHz, DMSO-*d*₆) δ [ppm] 8.20 (brs, 1H), 7.32 (d, $J = 8.4$ Hz, 1H), 6.75 (dd, $J = 8.4, 2.4$ Hz, 1H), 6.53 (d, $J = 2.4$ Hz, 1H), 4.03 (q, $J = 6.6$ Hz, 2H), 3.94-3.98 (m, 1H), 3.87 (dd, $J = 13.8, 4.2$ Hz, 1H), 3.76-3.81 (m, 1H), 3.42 (q, $J = 7.2$ Hz, 2H), 3.21 (dd, $J = 15.6, 4.2$ Hz, 1H), 1.32 (t, $J = 6.6$ Hz, 3H), 1.08 (t, $J = 7.2$ Hz, 3H). MS (ESI): Calcd for C₁₈H₂₂N₂O₅ (m/z): 346.1529, found: 346.1521.

5-Amino-8-methoxy-3-(3-methoxypropyl)-1H-chromeno[3,4-c]pyridine-2,4(3H,10bH)-dione (33)



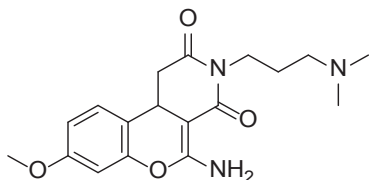
Light brown solid; ^1H NMR (600 MHz, DMSO-*d*6) δ [ppm] 7.33 (d, $J = 9.0$ Hz, 1H), 6.80 (dd, $J = 9.0, 2.4$ Hz, 1H), 6.56 (d, $J = 2.4$ Hz, 1H), 3.92-3.98 (m, 2H), 3.83 (s, 3H), 3.79 (dd, $J = 12.6, 6.6$ Hz, 1H), 3.39 (t, $J = 6.6$ Hz, 2H), 3.27 (s, 3H), 3.20 (dd, $J = 15.6, 4.2$ Hz, 1H), 2.52 (t, $J = 15.0$ Hz, 1H), 1.78-1.84 (m, 2H). MS (ESI): Calcd for $\text{C}_{17}\text{H}_{20}\text{N}_2\text{O}_5$ (m/z): 332.1372, found: 332.1368.

5-Amino-3-(2-methoxyethyl)-8-methyl-1H-chromeno[3,4-c]pyridine-2,4(3H,10bH)-dione (34)



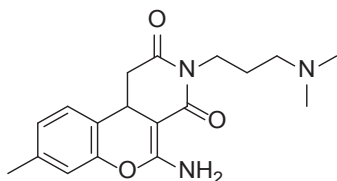
Yellow solid; ^1H NMR (600 MHz, DMSO-*d*6) δ [ppm] 6.94 (d, $J = 7.8$ Hz, 1H), 6.55 (s, 1H), 6.48 (d, $J = 7.8$ Hz, 1H), 3.83 (dt, $J = 12.6, 7.2$ Hz, 1H), 3.68 (dd, $J = 6.6, 3.0$ Hz, 1H), 3.61 (dt, $J = 12.0, 7.2$ Hz, 1H), 3.19-3.24 (m, 2H), 3.21 (s, 3H), 2.64 (dd, $J = 15.0, 7.2$ Hz, 1H), 2.37 (dd, $J = 15.0, 2.4$ Hz, 1H), 2.16 (s, 3H). MS (ESI): Calcd for $\text{C}_{16}\text{H}_{18}\text{N}_2\text{O}_4$ (m/z): 302.1267, found: 302.1261.

5-Amino-3-(3-(dimethylamino)propyl)-8-methoxy-1*H*-chromeno[3,4-*c*]pyridine-2,4(3*H*,10*bH*)-dione (35)



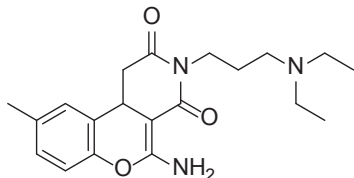
Brown solid; $^1\text{H NMR}$ (600 MHz, $\text{DMSO-}d_6$) δ [ppm] 8.10 (brs, 2H), 7.33 (d, $J = 8.4$ Hz, 1H), 6.76 (dd, $J = 8.4, 1.8$ Hz, 1H), 6.55 (d, $J = 1.8$ Hz, 1H), 3.89 (dd, $J = 13.8, 4.2$ Hz, 1H), 3.76 (s, 3H), 3.62-3.68 (m, 2H), 3.19 (dd, $J = 15.6, 4.2$ Hz, 1H), 2.51 (t, $J = 15.6$ Hz, 1H), 2.16 (t, $J = 7.2$ Hz, 2H), 2.10 (s, 6H), 1.55-1.60 (m, 2H). MS (ESI): Calcd for $\text{C}_{18}\text{H}_{23}\text{N}_3\text{O}_4$ (m/z): 345.1689, found: 345.3929.

5-Amino-3-(3-(dimethylamino)propyl)-8-methyl-1*H*-chromeno[3,4-*c*]pyridine-2,4(3*H*,10*bH*)-dione (36)



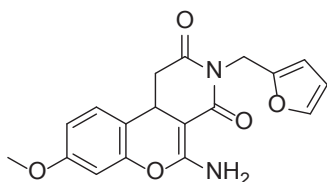
Yellow solid; $^1\text{H NMR}$ (600 MHz, $\text{DMSO-}d_6$) δ [ppm] 8.20 (brs, 2H), 7.29 (d, $J = 7.8$ Hz, 1H), 6.98 (d, $J = 7.8$ Hz, 1H), 6.84 (s, 1H), 3.92 (dd, $J = 13.8, 4.2$ Hz, 1H), 3.74-3.80 (m, 1H), 3.60-3.65 (m, 1H), 3.20 (dd, $J = 15.6, 4.2$ Hz, 1H), 2.29 (s, 3H), 2.20 (t, $J = 7.2$ Hz, 2H), 2.11 (s, 6H), 1.56-1.62 (m, 2H). MS (ESI): Calcd for $\text{C}_{18}\text{H}_{23}\text{N}_3\text{O}$ (m/z): 329.1739, found: 329.1732.

5-Amino-3-(3-(diethylamino)propyl)-9-methyl-1H-chromeno[3,4-c]pyridine-2,4(3H,10bH)-dione (37)



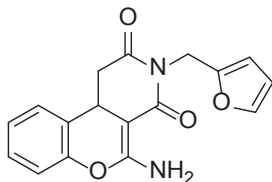
Yellow solid; $^1\text{H NMR}$ (600 MHz, $\text{DMSO-}d_6$) δ [ppm] 8.10 (brs, 2H), 7.23 (s, 1H), 7.08 (d, $J = 7.8$ Hz, 1H), 6.91 (d, $J = 7.8$ Hz, 1H), 3.93 (dd, $J = 13.8, 4.2$ Hz, 1H), 3.73-3.79 (m, 1H), 3.59-3.65 (m, 1H), 3.20 (dd, $J = 15.6, 4.2$ Hz, 1H), 2.57 (t, $J = 15.6$ Hz, 1H), 2.45 (q, $J = 7.2$ Hz, 4H), 2.37 (t, $J = 7.2$ Hz, 2H), 2.28 (s, 3H), 1.50-1.65 (m, 2H), 0.93 (t, $J = 7.2$ Hz, 6H). MS (ESI): Calcd for $\text{C}_{20}\text{H}_{27}\text{N}_3\text{O}_3$ (m/z): 357.2052, found: 357.2059.

5-Amino-3-(furan-2-ylmethyl)-8-methoxy-1H-chromeno[3,4-c]pyridine-2,4(3H,10bH)-dione (38)



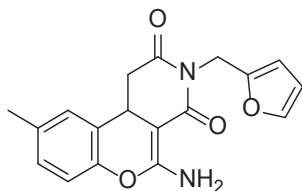
Yellow solid; $^1\text{H NMR}$ (600 MHz, $\text{DMSO-}d_6$) δ [ppm] 8.20 (brs, 2H), 7.52 (s, 1H), 7.35 (d, $J = 8.4$ Hz, 1H), 6.77 (dd, $J = 9.0, 2.4$ Hz, 1H), 6.56 (d, $J = 2.4$ Hz, 1H), 6.36 (s, 1H), 6.19 (d, $J = 3.0$ Hz, 1H), 4.96 (d, $J = 15.0$ Hz, 1H), 4.84 (d, $J = 15.0$ Hz, 1H), 3.92 (dd, $J = 13.8, 4.2$ Hz, 1H), 3.77 (s, 3H), 3.26 (dd, $J = 15.6, 4.2$ Hz, 1H), 2.57 (t, $J = 15.0$ Hz, 1H). MS (ESI): Calcd for $\text{C}_{18}\text{H}_{16}\text{N}_2\text{O}_5$ (m/z): 340.1059, found: 340.1050.

5-Amino-3-(furan-2-ylmethyl)-1*H*-chromeno[3,4-*c*]pyridine-2,4(3*H*,10*bH*)-dione (39)



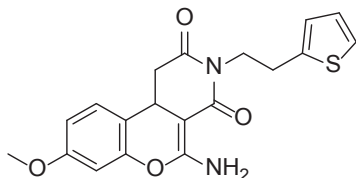
Brown solid; $^1\text{H NMR}$ (600 MHz, $\text{DMSO-}d_6$) δ [ppm] 8.20 (s, 2H), 7.52 (s, 1H), 7.44 (d, $J = 7.8$ Hz, 1H), 7.30 (t, $J = 7.2$ Hz, 1H), 7.18 (t, $J = 7.8$ Hz, 1H), 7.04 (d, $J = 8.4$ Hz, 1H), 6.36 (s, 1H), 6.20 (d, $J = 4.2$ Hz, 1H), 4.97 (d, $J = 15.0$ Hz, 1H), 4.83 (d, $J = 15.0$ Hz, 1H), 4.02 (dd, $J = 13.8, 4.2$ Hz, 1H), 3.30 (dd, $J = 15.6, 4.8$ Hz, 1H), 2.64 (t, $J = 14.4$ Hz). MS (ESI): Calcd for $\text{C}_{17}\text{H}_{14}\text{N}_2\text{O}_4$ (m/z): 310.0954, found: 310.0950.

5-Amino-9-methyl-3-(pyridin-3-ylmethyl)-1*H*-chromeno[3,4-*c*]pyridine-2,4(3*H*,10*bH*)-dione (40)



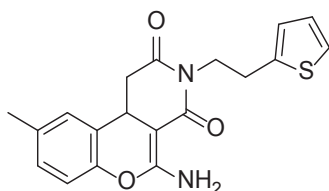
Brown solid; $^1\text{H NMR}$ (600 MHz, $\text{DMSO-}d_6$) δ [ppm] 8.20 (brs, 1H), 7.52 (s, 1H), 7.25 (s, 1H), 7.09 (d, $J = 8.4$ Hz, 1H), 6.92 (d, $J = 8.4$ Hz, 1H), 6.36 (s, 1H), 6.20 (d, $J = 2.4$ Hz, 1H), 4.96 (d, $J = 15.6$ Hz, 1H), 4.83 (d, $J = 15.6$ Hz, 1H), 3.98 (dd, $J = 15.6, 4.2$ Hz, 1H), 3.28 (dd, $J = 15.6, 4.2$ Hz, 1H), 2.61 (t, $J = 14.4$ Hz, 1H), 2.29 (s, 3H). MS (ESI): Calcd for $\text{C}_{18}\text{H}_{16}\text{N}_2\text{O}_4$ (m/z): 324.1110, found: 324.1118.

5-Amino-8-methoxy-3-(2-(thiophen-2-yl)ethyl)-1*H*-chromeno[3,4-*c*]pyridine-2,4(3*H*,10*bH*)-dione (41)



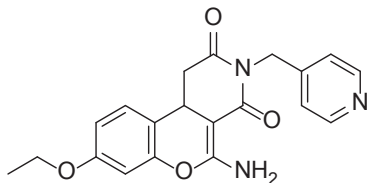
Brown solid; $^1\text{H NMR}$ (600 MHz, $\text{DMSO-}d_6$) δ [ppm] 7.24 (d, $J = 9.0$ Hz, 1H), 7.21 (d, $J = 5.4$ Hz, 1H), 6.94 (t, $J = 3.0$ Hz, 1H), 6.89 (s, 1H), 6.78 (dd, $J = 8.4, 2.4$ Hz, 1H), 6.62 (d, $J = 2.4$ Hz, 1H), 4.14 (ddd, $J = 15.6, 9.0, 6.6$ Hz, 1H), 4.00 (ddd, $J = 15.6, 9.0, 6.6$ Hz, 1H), 3.91 (dd, $J = 13.8, 4.2$ Hz, 1H), 3.80 (s, 3H), 3.24 (dd, $J = 15.6, 3.6$ Hz, 1H), 3.07-3.14 (m, 2H), 2.52 (t, $J = 15.6$ Hz, 1H). MS (ESI): Calcd for $\text{C}_{19}\text{H}_{18}\text{N}_2\text{O}_4\text{S}$ (m/z): 370.0987, found: 370.0980.

5-Amino-9-methyl-3-(2-(thiophen-2-yl)ethyl)-1*H*-chromeno[3,4-*c*]pyridine-2,4(3*H*,10*bH*)-dione (42)



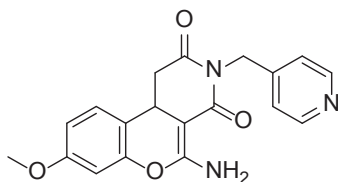
Brown solid; $^1\text{H NMR}$ (600 MHz, $\text{DMSO-}d_6$) δ [ppm] 8.20 (brs, 2H), 7.35 (d, $J = 7.2$ Hz, 1H), 7.25 (d, 1H), 7.09 (d, $J = 8.4$ Hz, 1H), 6.96 (dd, $J = 4.8, 3.0$ Hz, 1H), 6.92 (d, $J = 7.8$ Hz, 1H), 6.89 (d, $J = 3.0$ Hz, 1H), 3.99 (ddd, $J = 15.0, 9.0, 6.0$ Hz, 1H), 3.84 (dd, $J = 14.4, 4.2$ Hz, 1H), 3.86 (ddd, $J = 15.6, 9.0, 6.0$ Hz, 1H), 3.23 (dd, $J = 15.6, 4.2$ Hz, 1H), 2.94-3.04 (m, 2H), 2.57 (t, $J = 14.4$ Hz, 1H), 2.28 (s, 3H). MS (ESI): Calcd for $\text{C}_{19}\text{H}_{18}\text{N}_2\text{O}_3\text{S}$ (m/z): 354.1038, found: 354.1044.

5-Amino-8-ethoxy-3-(pyridin-4-ylmethyl)-1*H*-chromeno[3,4-*c*]pyridine-2,4(3*H*,10*bH*)-dione (43)



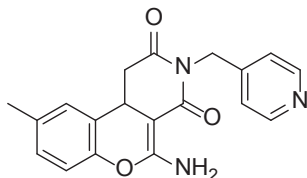
Light brown solid; ^1H NMR (600 MHz, $\text{DMSO-}d_6$) δ [ppm] 8.47 (d, $J = 6.0$ Hz, 2H), 8.20 (br s, 2H), 7.35 (d, $J = 9.0$ Hz, 1H), 7.21 (d, $J = 5.4$ Hz, 2H), 6.77 (dd, $J = 8.4, 2.4$ Hz, 1H), 6.55 (d, $J = 2.4$ Hz, 1H), 4.99 (d, $J = 15.6$ Hz, 1H), 4.87 (d, $J = 15.6$ Hz, 1H), 4.00-4.10 (m, 2H), 3.29 (dd, $J = 15.6, 4.2$ Hz, 1H), 2.69 (t, $J = 15.6$ Hz, 1H), 1.33 (t, $J = 7.2$ Hz, 3H). MS (ESI): Calcd for $\text{C}_{20}\text{H}_{19}\text{N}_3\text{O}_4$ (m/z): 365.1376, found: 365.1371.

5-Amino-8-methoxy-3-(pyridin-4-ylmethyl)-1*H*-chromeno[3,4-*c*]pyridine-2,4(3*H*,10*bH*)-dione (44)



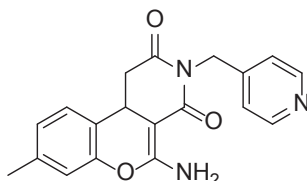
Brown solid; ^1H NMR (600 MHz, $\text{DMSO-}d_6$) δ [ppm] 8.47 (d, $J = 4.8$ Hz, 2H), 8.20 (brs, 2H), 7.37 (d, $J = 8.4$ Hz, 1H), 7.21 (d, $J = 10.8$ Hz, 1H), 6.78 (dd, $J = 8.4, 2.4$ Hz, 1H), 6.57 (d, $J = 2.4$ Hz, 1H), 4.99 (d, $J = 14.4$ Hz, 1H), 4.86 (d, $J = 14.4$ Hz, 1H), 4.05 (dd, $J = 13.8, 4.2$ Hz, 1H), 3.76 (s, 3H), 3.29 (dd, $J = 15.6, 4.2$ Hz, 1H), 2.69 (t, $J = 14.4$ Hz, 1H). MS (ESI): Calcd for $\text{C}_{19}\text{H}_{17}\text{N}_3\text{O}_4$ (m/z): 351.1219, found: 351.1211.

5-Amino-9-methyl-3-(pyridin-4-ylmethyl)-1*H*-chromeno[3,4-*c*]pyridine-2,4(3*H*,10*bH*)-dione (45)



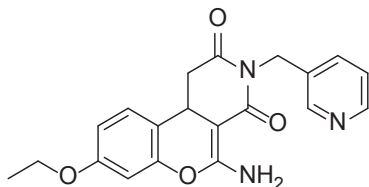
Brown solid; ^1H NMR (600 MHz, $\text{DMSO-}d_6$) δ [ppm] 8.47 (d, $J = 5.4$ Hz, 2H), 7.27 (s, 1H), 7.21 (d, $J = 5.4$ Hz, 2H), 7.10 (d, $J = 7.8$ Hz, 1H), 6.94 (d, $J = 7.8$ Hz, 1H), 4.98 (d, $J = 15.6$ Hz, 1H), 4.86 (d, $J = 15.6$ Hz, 1H), 4.11 (dd, $J = 13.8, 4.2$ Hz, 1H), 2.74 (t, $J = 14.4$ Hz, 1H), 2.29 (s, 3H). MS (ESI): Calcd for $\text{C}_{19}\text{H}_{17}\text{N}_3\text{O}_3$ (m/z): 335.127, found: 335.1278.

5-Amino-8-methyl-3-(pyridin-4-ylmethyl)-1*H*-chromeno[3,4-*c*]pyridine-2,4(3*H*,10*bH*)-dione (46)



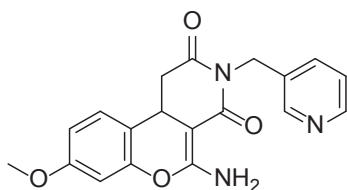
Yellow solid; ^1H NMR (600 MHz, $\text{DMSO-}d_6$) δ [ppm] 8.53 (d, $J = 6.0$ Hz, 2H), 8.20 (brs, 2H), 7.39 (d, $J = 7.8$ Hz, 1H), 7.27 (d, $J = 8.4$ Hz, 2H), 7.07 (d, $J = 7.8$ Hz, 1H), 6.93 (s, 1H), 5.04 (d, $J = 15.0$ Hz, 1H), 4.93 (d, $J = 15.0$ Hz, 1H), 4.13 (dd, $J = 15.0, 4.2$ Hz, 1H), 3.26 (dd, $J = 15.6, 4.2$ Hz, 1H), 2.78 (t, $J = 15.0$ Hz, 1H), 2.28 (s, 3H). MS (ESI): Calcd for $\text{C}_{19}\text{H}_{17}\text{N}_3\text{O}_3$ (m/z): 335.1272, found: 335.1267.

5-Amino-8-ethoxy-3-(pyridin-3-ylmethyl)-1*H*-chromeno[3,4-*c*]pyridine-2,4(3*H*,10*bH*)-dione (47)



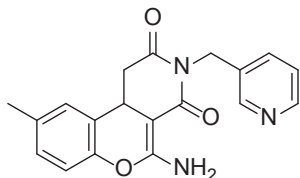
Brown solid; ¹H NMR (600 MHz, DMSO-*d*₆) δ [ppm] 8.50 (s, 1H), 8.43 (d, *J* = 4.8 Hz, 1H), 8.20 (brs, 2H), 7.64 (d, *J* = 6.0 Hz, 1H), 7.30-7.35 (m, 2H), 6.76 (dd, *J* = 8.4, 2.4 Hz, 1H), 6.54 (d, *J* = 2.4 Hz, 1H), 4.98 (d, *J* = 14.4 Hz, 1H), 4.88 (d, *J* = 14.4 Hz, 1H), 4.03 (q, *J* = 7.2 Hz, 2H), 3.98 (dd, *J* = 13.8, 4.2 Hz, 1H), 3.26 (dd, *J* = 15.6, 4.2 Hz, 1H), 2.64 (t, *J* = 14.4 Hz, 1H), 1.32 (t, *J* = 6.6 Hz, 3H). MS (ESI): Calcd for C₂₀H₁₉N₃O₄ (m/z): 365.1376, found: 365.1377.

5-Amino-8-methoxy-3-(pyridin-3-ylmethyl)-1*H*-chromeno[3,4-*c*]pyridine-2,4(3*H*,10*bH*)-dione (48)



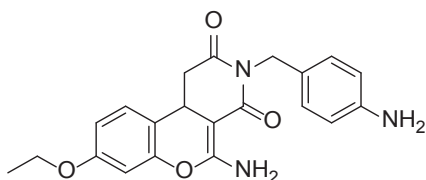
Brown solid; ¹H NMR (600 MHz, DMSO-*d*₆) δ [ppm] 8.50 (s, 1H), 8.43 (d, *J* = 4.8 Hz, 1H), 8.20 (brs, 2H), 7.65 (d, *J* = 7.8 Hz, 1H), 7.35 (d, *J* = 8.4 Hz, 1H), 7.32 (dd, *J* = 7.8, 4.8 Hz, 1H), 6.77 (d, *J* = 9.0 Hz, 1H), 6.56 (s, 1H), 4.98 (d, *J* = 14.4 Hz, 1H), 4.88 (d, *J* = 14.4 Hz, 1H), 4.00 (dd, *J* = 13.8, 4.2 Hz, 1H), 3.76 (s, 3H), 3.27 (dd, *J* = 15.6, 4.2 Hz, 1H), 2.64 (t, *J* = 14.4 Hz, 1H). MS (ESI): Calcd for C₁₉H₁₇N₃O₄ (m/z): 351.1219, found: 351.1210.

5-Amino-9-methyl-3-(pyridin-3-ylmethyl)-1*H*-chromeno[3,4-*c*]pyridine-2,4(3*H*,10*bH*)-dione (49)



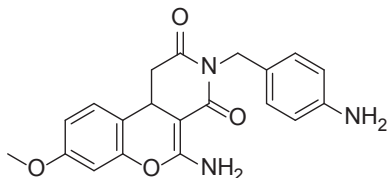
Brown solid; $^1\text{H NMR}$ (600 MHz, $\text{DMSO-}d_6$) δ [ppm] 8.50 (s, 1H), 8.43 (d, $J = 4.8$ Hz, 1H), 7.65 (d, $J = 7.8$ Hz, 1H), 7.32 (dd, $J = 7.8, 4.8$ Hz, 1H), 7.25 (s, 1H), 7.09 (d, $J = 7.8$ Hz, 1H), 6.93 (d, $J = 8.4$ Hz, 1H), 4.98 (d, $J = 14.4$ Hz, 1H), 4.88 (d, $J = 14.4$ Hz, 1H), 4.04 (dd, $J = 13.8, 4.2$ Hz, 1H), 3.28 (dd, $J = 15.6, 4.2$ Hz, 1H), 2.68 (t, $J = 8.4$ Hz, 1H), 2.28 (s, 3H). MS (ESI): Calcd for $\text{C}_{19}\text{H}_{17}\text{N}_3\text{O}_3$ (m/z): 335.1270, found: 335.1262.

5-Amino-3-(4-aminobenzyl)-8-ethoxy-1*H*-chromeno[3,4-*c*]pyridine-2,4(3*H*,10*bH*)-dione (50)



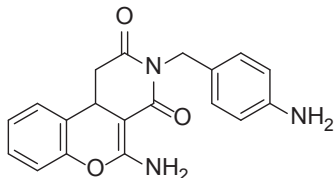
Brown solid; $^1\text{H NMR}$ (600 MHz, $\text{DMSO-}d_6$) δ [ppm] 8.20 (s, 1H), 7.32 (d, $J = 7.8$ Hz, 1H), 6.94 (d, $J = 8.4$ Hz, 2H), 6.74 (s, 1H), 6.46 (d, $J = 8.4$ Hz, 2H), 4.93 (s, 2H), 4.77 (d, $J = 13.8$ Hz, 1H), 4.69 (d, $J = 13.8$ Hz, 1H), 4.03 (q, $J = 7.2$ Hz, 2H), 3.93 (dd, $J = 13.8, 3.6$ Hz, 1H), 3.23 (dd, $J = 15.6, 4.2$ Hz, 1H), 2.56 (t, $J = 14.4$ Hz, 1H), 1.32 (t, $J = 7.2$ Hz, 3H). MS (ESI): Calcd for $\text{C}_{21}\text{H}_{21}\text{N}_3\text{O}_4$ (m/z): 379.1532, found: 379.4084.

5-Amino-3-(4-aminobenzyl)-8-methoxy-1*H*-chromeno[3,4-*c*]pyridine-2,4(3*H*,10*bH*)-dione (51)



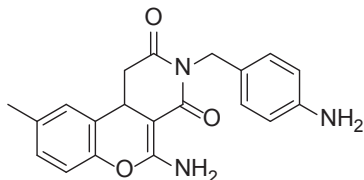
Brown solid; $^1\text{H NMR}$ (600 MHz, $\text{DMSO-}d_6$) δ [ppm] 7.34 (d, $J = 8.4$ Hz, 1H), 6.94 (d, $J = 8.4$ Hz, 2H), 6.76 (dd, $J = 8.4, 2.4$ Hz, 1H), 6.55 (d, $J = 2.4$ Hz, 1H), 6.46 (d, $J = 8.4$ Hz, 2H), 4.93 (s, 2H), 4.77 (d, $J = 13.8$ Hz, 1H), 4.70 (d, $J = 13.8$ Hz, 1H), 3.90 (dd, $J = 13.8, 4.2$ Hz, 1H), 3.78 (s, 3H), 3.23 (dd, $J = 15.6, 4.2$ Hz, 1H), 2.54 (t, $J = 13.8$ Hz, 1H). MS (ESI): Calcd for $\text{C}_{20}\text{H}_{19}\text{N}_3\text{O}_4$ (m/z): 365.1376, found: 365.1382.

5-Amino-3-(4-aminobenzyl)-1*H*-chromeno[3,4-*c*]pyridine-2,4(3*H*,10*bH*)-dione (52)



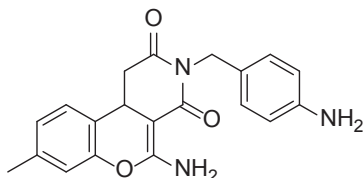
Yellow solid; $^1\text{H NMR}$ (600 MHz, $\text{DMSO-}d_6$) δ [ppm] 8.20 (brs, 2H), 7.43 (d, $J = 7.8$ Hz, 1H), 7.29 (t, $J = 7.8$ Hz, 1H), 7.17 (t, $J = 7.2$ Hz, 1H), 7.03 (d, $J = 8.4$ Hz, 1H), 6.95 (d, $J = 7.8$ Hz, 2H), 6.46 (d, $J = 8.4$ Hz, 2H), 4.93 (s, 2H), 4.77 (d, $J = 14.4$ Hz, 1H), 4.70 (d, $J = 14.4$ Hz, 1H), 3.99 (dd, $J = 13.8, 2.8$ Hz, 1H), 3.26 (dd, $J = 16.8, 4.8$ Hz, 1H), 2.61 (t, $J = 15.0$ Hz, 1H). MS (ESI): Calcd for $\text{C}_{19}\text{H}_{17}\text{N}_3\text{O}_3$ (m/z): 335.1270, found: 335.1277.

5-Amino-3-(4-aminobenzyl)-9-methyl-1*H*-chromeno[3,4-*c*]pyridine-2,4(3*H*,10*bH*)-dione (53)



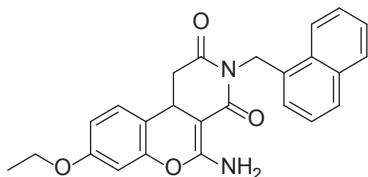
Yellow solid; $^1\text{H NMR}$ (600 MHz, $\text{DMSO-}d_6$) δ [ppm] 8.20 (brs, 2H), 7.24 (s, 1H), 7.08 (t, $J = 7.8$ Hz, 1H), 6.95 (d, $J = 7.8$ Hz, 2H), 6.91 (d, $J = 8.4$ Hz, 1H), 6.46 (d, $J = 8.4$ Hz, 2H), 4.93 (s, 2H), 4.77 (d, $J = 14.4$ Hz, 1H), 4.70 (d, $J = 14.4$ Hz, 1H), 3.99 (dd, $J = 13.8, 2.8$ Hz, 1H), 3.26 (dd, $J = 16.8, 4.8$ Hz, 1H), 2.61 (t, $J = 15.0$ Hz, 1H), 2.28 (s, 3H). MS (ESI): Calcd for $\text{C}_{20}\text{H}_{19}\text{N}_3\text{O}_3$ (m/z): 349.1426, found: 349.1434.

5-Amino-3-(4-aminobenzyl)-8-methyl-1*H*-chromeno[3,4-*c*]pyridine-2,4(3*H*,10*bH*)-dione (54)



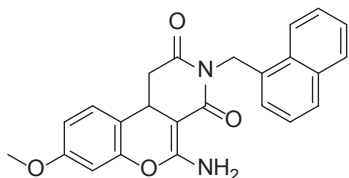
Brown solid; $^1\text{H NMR}$ (600 MHz, $\text{DMSO-}d_6$) δ [ppm] 8.20 (s, 1H), 7.29 (d, $J = 7.8$ Hz, 1H), 6.98 (d, $J = 7.8$ Hz, 1H), 6.94 (d, $J = 8.4$ Hz, 2H), 6.84 (s, 1H), 6.46 (d, $J = 8.4$ Hz, 2H), 4.93 (s, 2H), 4.77 (d, $J = 13.8$ Hz, 1H), 4.69 (d, $J = 13.8$ Hz, 1H), 3.93 (dd, $J = 13.8, 3.6$ Hz, 1H), 3.23 (dd, $J = 15.6, 4.2$ Hz, 1H), 2.56 (t, $J = 14.4$ Hz, 1H), 2.29 (s, 3H). MS (ESI): Calcd for $\text{C}_{20}\text{H}_{19}\text{N}_3\text{O}_3$ (m/z): 349.1426, found: 349.1419.

5-Amino-8-ethoxy-3-(naphthalen-1-ylmethyl)-1*H*-chromeno[3,4-*c*]pyridine-2,4(3*H*,10*bH*)-dione (55)



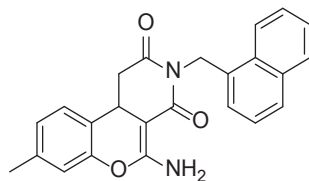
Brown solid; $^1\text{H NMR}$ (600 MHz, $\text{DMSO-}d_6$) δ [ppm] $^1\text{H NMR}$ ($\text{DMSO-}d_6$, 600 MHz): 8.30 (brs, 2H), 8.20 (d, $J = 8.4$ Hz, 1H), 7.98 (d, $J = 7.8$ Hz, 1H), 7.80 (d, $J = 8.4$ Hz, 1H), 7.61 (t, $J = 7.2$ Hz, 1H), 7.57 (t, $J = 7.2$ Hz, 1H), 7.42 (t, $J = 7.2$ Hz, 1H), 7.38 (d, $J = 7.2$ Hz, 1H), 7.12 (d, $J = 7.2$ Hz, 1H), 6.77 (d, $J = 7.2$ Hz, 1H), 6.56 (s, 1H), 5.47 (d, $J = 16.2$ Hz, 1H), 5.32 (d, $J = 16.2$ Hz, 1H), 4.12 (dd, $J = 13.8, 4.2$ Hz, 1H), 4.05 (q, $J = 7.2$ Hz, 2H), 3.46 (dd, $J = 13.8, 4.2$ Hz, 1H), 2.76 (t, $J = 13.8$ Hz, 1H), 1.33 (t, $J = 7.8$ Hz, 3H). MS (ESI): Calcd for $\text{C}_{25}\text{H}_{22}\text{N}_2\text{O}_4$ (m/z): 414.158, found: 414.1584.

5-Amino-8-methoxy-3-(naphthalen-1-ylmethyl)-1*H*-chromeno[3,4-*c*]pyridine-2,4(3*H*,10*bH*)-dione (56)



Brown solid; $^1\text{H NMR}$ (600 MHz, $\text{DMSO-}d_6$) δ [ppm] 8.18 (d, $J = 8.4$ Hz, 1H), 7.96 (d, $J = 8.4$ Hz, 1H), 7.81 (d, $J = 7.8$ Hz, 1H), 7.61 (t, $J = 8.4$ Hz, 1H), 7.56 (t, $J = 8.4$ Hz, 1H), 7.41 (t, $J = 8.4$ Hz, 2H), 7.13 (d, $J = 7.2$ Hz, 1H), 6.80 (dd, $J = 8.4, 2.4$ Hz, 1H), 6.59 (d, $J = 2.4$ Hz, 1H), 5.48 (d, $J = 15.6$ Hz, 1H), 5.33 (d, $J = 15.6$ Hz, 1H), 4.12 (dd, $J = 13.8, 3.6$ Hz, 1H), 3.77 (s, 3H), 2.76 (t, $J = 14.4$ Hz, 1H). MS (ESI): Calcd for $\text{C}_{24}\text{H}_{20}\text{N}_2\text{O}_4$ (m/z): 400.1423, found: 400.1429.

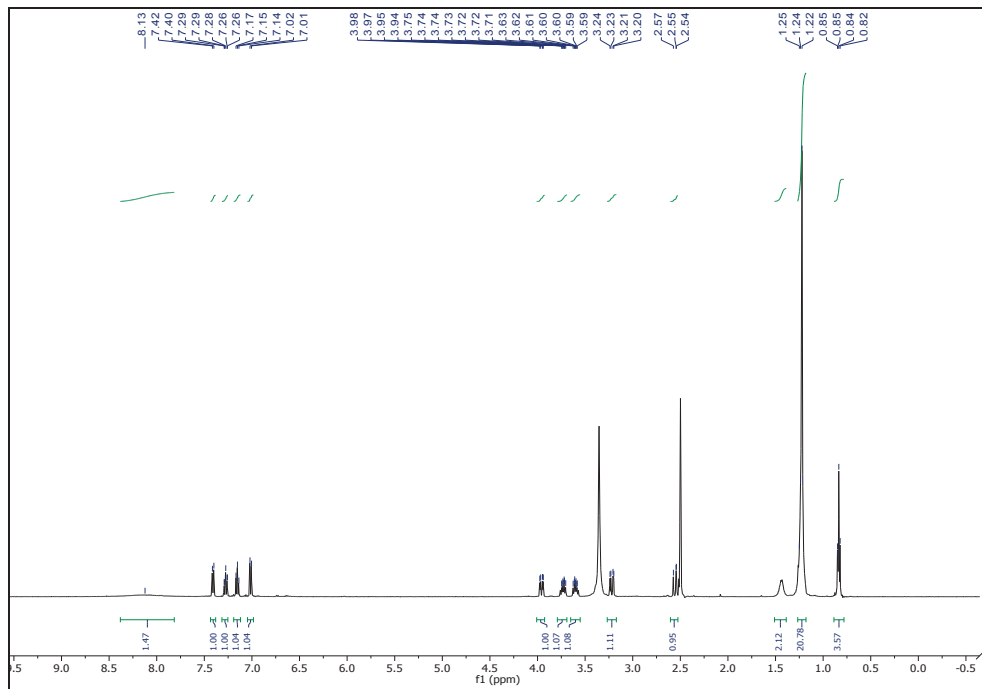
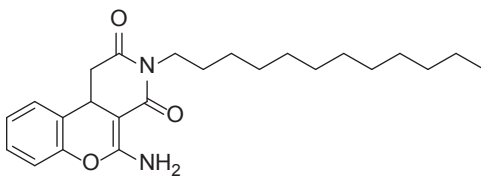
5-Amino-8-methyl-3-(naphthalen-1-ylmethyl)-1*H*-chromeno[3,4-*c*]pyridine-2,4(3*H*,10*bH*)-dione (57)

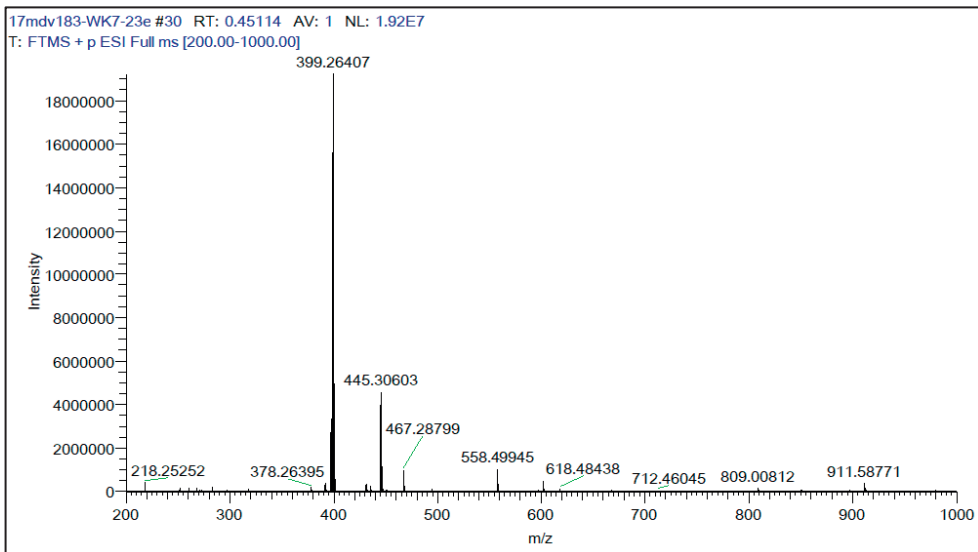
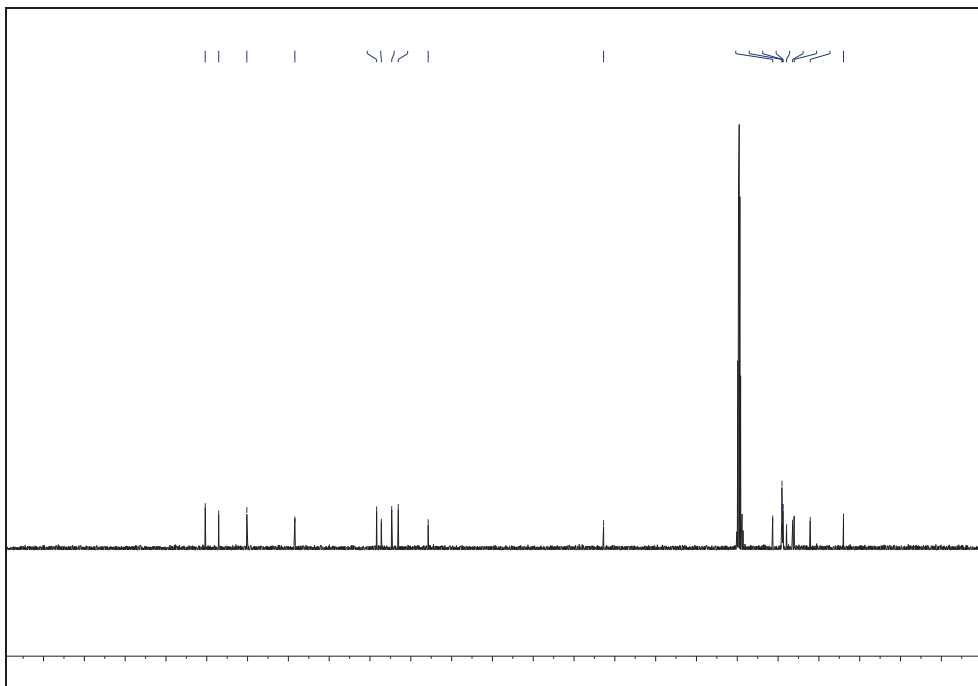


Brown solid; $^1\text{H NMR}$ (600 MHz, $\text{DMSO-}d_6$) δ [ppm] 8.30 (brs, 2H), 8.18 (d, $J = 8.4$ Hz, 1H), 7.96 (d, $J = 7.8$ Hz, 1H), 7.80 (d, $J = 8.4$ Hz, 1H), 7.61 (t, $J = 7.2$ Hz, 1H), 7.57 (t, $J = 7.2$ Hz, 1H), 7.41 (t, $J = 7.2$ Hz, 1H), 7.36 (d, $J = 7.2$ Hz, 1H), 7.12 (d, $J = 7.2$ Hz, 1H), 7.02 (d, $J = 7.2$ Hz, 1H), 6.88 (s, 1H), 5.47 (d, $J = 16.2$ Hz, 1H), 5.32 (d, $J = 16.2$ Hz, 1H), 4.14 (dd, $J = 13.8, 4.2$ Hz, 1H), 3.46 (dd, $J = 13.8, 4.2$ Hz, 1H), 2.78 (t, $J = 13.8$ Hz, 1H), 2.32 (s, 3H). MS (ESI): Calcd for $\text{C}_{24}\text{H}_{20}\text{N}_2\text{O}_3$ (m/z): 384.1474, found: 384.1481.

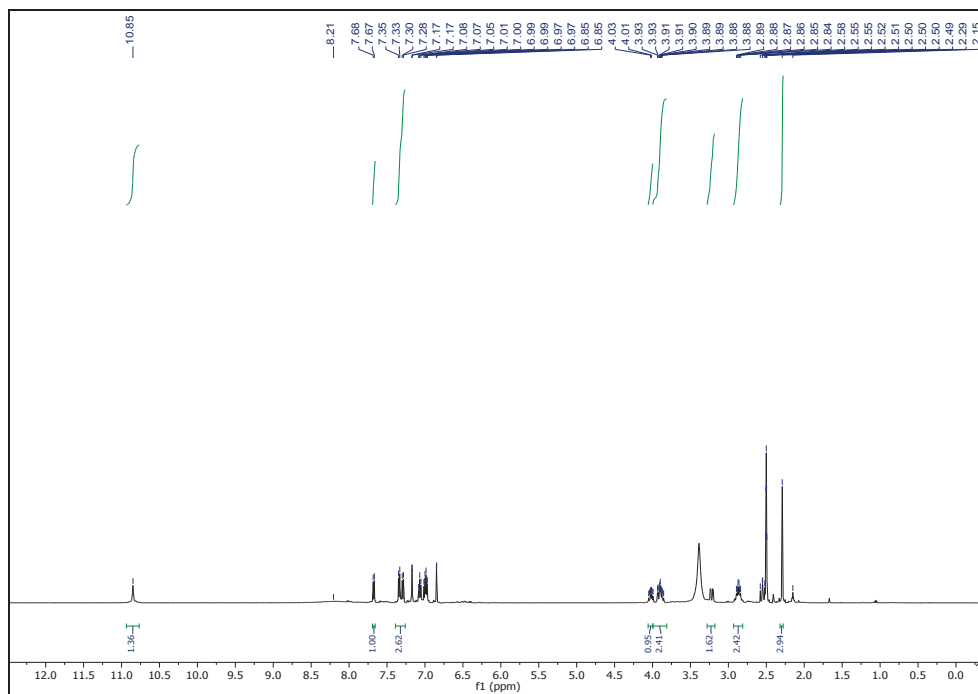
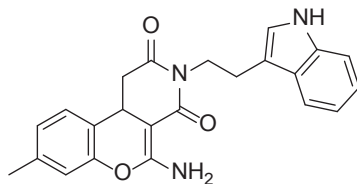
Exemplary copies of NMR and MS data of final compounds

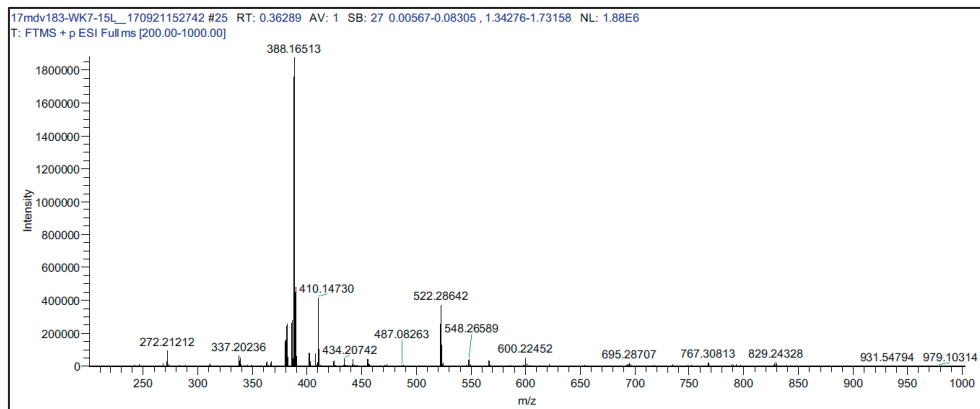
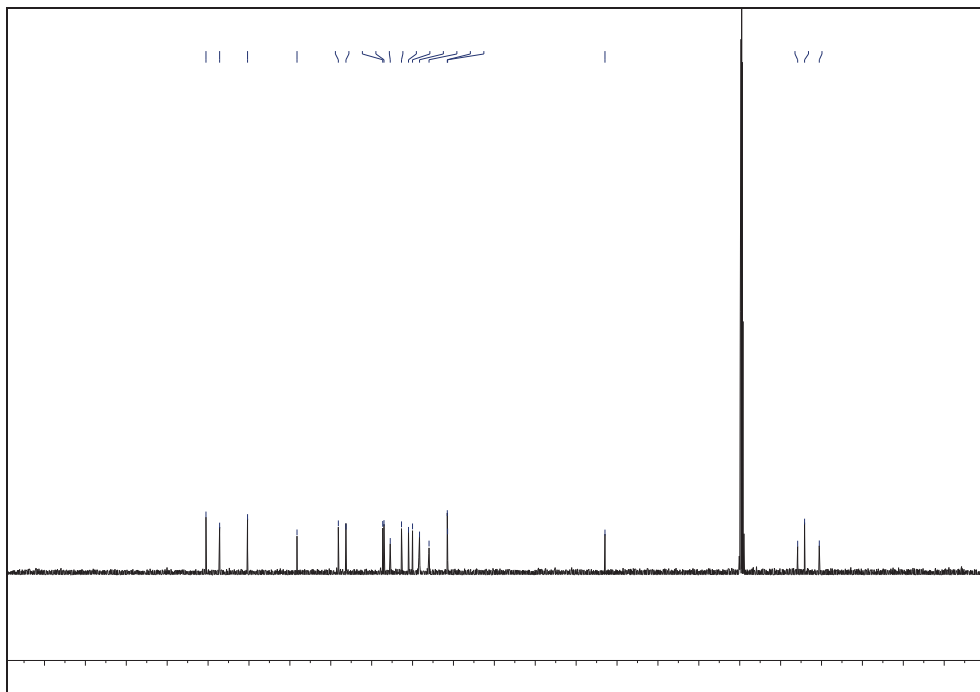
5-Amino-3-dodecyl-1*H*-chromeno[3,4-*c*]pyridine-2,4(3*H*,10*bH*)-dione (10)





3-(2-(1*H*-Indol-3-yl)ethyl)-5-amino-8-methyl-1*H*-chromeno[3,4-*c*]pyridine-2,4(3*H*,10*bH*)-dione (17)



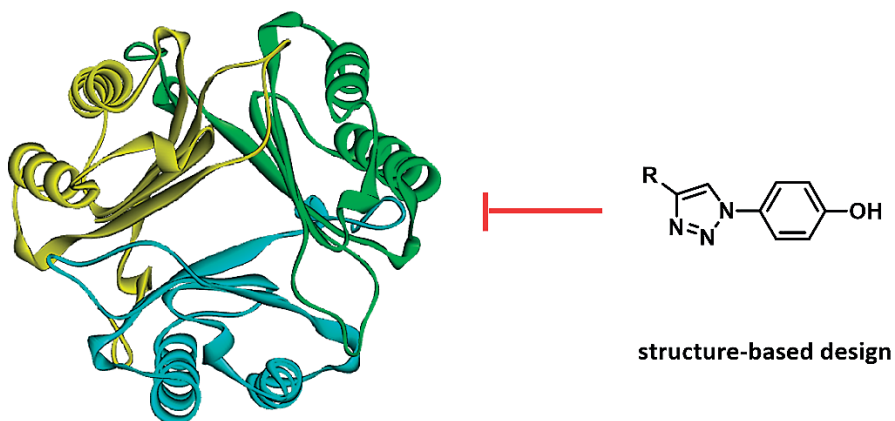


References

- [S1] Rigaku-Oxford Diffraction; CrysAlisPro Oxford Diffraction Ltd, Abingdon, England V 1. 171. 36. 2. (release 27-06-2012 CN (2006))
- [S2] Maria C. Burla, Rocco Caliandro, Mercedes Camalli, Benedetta Carrozzini, Giovanni L. Cascarano, Liberato De Caro, Carmelo Giacovazzo, Giampiero Polidori and Riccardo Spagna J. Appl. Cryst. 2005 Vol. 38, Issue 2, pages 381–388.
- [S3] Sheldrick, G. M. Acta Cryst. 2008, A64, 112-122.
- [S4] Farrugia, L., J. J. Appl. Cryst. 1999, 32, 837-838.
- [S5] Macrae C. F., Edgington P.R., McCabe P., Pidcock E., Shields G.P., Taylor R., Towler M., & van de Streek J., J. Appl. Cryst. 2006, 39, 453-457.

Chapter 5

Synthesis of a focused compound collection of isoxazole, benzoxazole and triazole-phenol scaffolds to explore the structure-activity relationship for MIF tautomerase activity inhibition



Kok T, Xiao ZP, Fokkens M, Wapenaar H, Proietti G, Poelarends GJ, Dekker FJ. Synthesis of a focused compound collection of isoxazole, benzoxazole and triazole-phenol scaffolds to explore the structure-activity relationship for MIF tautomerase activity inhibition – ongoing work.

Abstract

Macrophage migration inhibitory factor (MIF) is a cytokine that plays a key role in immune responses as well as in the progression of inflammatory diseases and cancer. MIF exerts its activity through the binding to its molecular receptors such as the CD74 receptor. Due to its important role, significant efforts have been taken to discover small-molecules having potential to inhibit the cytokine activity of MIF. To this end, MIF tautomerase activity has been used in high-throughput screening to identify small-molecule MIF binders. Based on the previously identified class of biaryl-triazole MIF tautomerase inhibitors, we designed and synthesized a focused collection of compounds with isoxazole, benzoxazole and triazole scaffolds and evaluated their inhibition of MIF tautomerase activity. Thus, we were able to derive structure-activity relationship for inhibition of MIF tautomerase activity. This sets the stage for further exploration of the structure-activity relationship for this class of compounds in order to identify more potent binders that have the potential to be developed further into therapeutic agents against diseases in which MIF is involved.

Keywords: MIF, isoxazole, benzoxazole, triazole-phenol scaffold, tautomerase activity

Introduction

MIF is a well known cytokine that plays a key role in the regulation of the immune system and is therefore connected to the progression of multiple diseases with an immunological component [1]. MIF is known to bind to several receptors such as the CD74 receptor [2], and the hemokine receptors CXCR2, CXCR4 and CXCR7 [3][4]. Due to its key role in the immune system MIF binding molecules have been recognized as potential therapeutics in various inflammatory diseases and cancer [5].

A crystal structure of MIF in complex with 4-hydroxyphenylpyruvate (PDB 1CA7) demonstrated that three MIF monomers associate to form a symmetrical trimer [6]. MIF belongs to the tautomerase superfamily of enzymes [7]. It catalyses the interconversion of keto substrates, such as D-dopachrome, phenylpyruvate and 4-hydroxyphenylpyruvate, into their corresponding enol forms [8][9]. The tautomerase activity can be used for efficient screening of a compound collection for MIF binding. Interference with MIF cytokine activities should be evaluated in cell-based assay and eventually animal models [10].

Recent findings show that binding of CD74 to MIF occurs in the vicinity of the MIF enzymatic pocket [11]. This supports the idea that rationally designed MIF tautomerase inhibitors with substituents protruding to the solvent interface of MIF enzymatic pocket (“caps”) may have potential to interfere with MIF cytokine activity.

The effects of MIF inhibitors in various cell-based or animal models have been explored with ISO-1 as a common reference inhibitor [10]. A crystal structure of ISO-1 bound to MIF showed that the inhibitor binds to the MIF enzymatic pocket, which is positioned at the interface between two MIF monomers. The phenol group of ISO-1 makes a hydrogen-bonding interaction with residue Asp-97 and the isoxazoline ring interact with residues Lys-32, Ile-64 and Pro-1 of MIF [12]. Based on the ISO-1 structure, several other MIF inhibitors have been developed, among which are Alam-4b, ISO-66, CPSI-2705, CPSI-1306 and inhibitors with a triazole scaffold [10]. These triazole inhibitors contain the same phenol group as ISO-1 that interacts with residue Asp-97 and the triazole ring that interacts with residues Lys-32, Ile-64 and Pro-1 in the MIF enzymatic pocket [10].

Furthermore, using a structure-based virtual screening method, Orita-13 containing a chromen-4-one scaffold was identified as a MIF tautomerase activity inhibitor, and inspired by its structure, T-614 [13] and substituted-chromene compounds including Kok-10 and Kok-17 [14], were developed as MIF inhibitors. Taken together, rational design to provide a compound collection of small-

molecule inhibitors of MIF tautomerase activity is required to discover potent compounds that are targeted to interfere with MIF cytokine activity.

Here, we describe the synthesis of a focused compound collection of isoxazole, benzoxazole and triazole-phenol scaffolds and the evaluation of their inhibition on MIF tautomerase activity. Our effort yielded MIF inhibitors with a triazole-phenol scaffold with IC₅₀'s in the micromolar range. These inhibitors expand the number of compounds with triazole-phenol scaffold available for further development of therapeutic agents against MIF cytokine-related diseases.

Materials and methods

Chemistry general

Chemicals were purchased from commercial suppliers. Reactions in the microwave were carried out in a Biotage Initiator™ Microwave Synthesizer. The reactions were monitored by thin layer chromatography (TLC) using Silica Gel 60 F254 aluminium sheets. TLC's were visualized using UV light or KMnO₄ solution. The stationary phase used in column chromatography was MP Ecochrom Silica Gel 32-63, 60 Å. Products were analyzed by proton (¹H) and carbon (¹³C) nuclear magnetic resonance (NMR), recorded on the Bruker Advance 500 MHz. Chemical shifts were reported as part per million (ppm) relative to residual solvent peaks (CDCl₃, ¹H δ = 7.26, ¹³C δ = 77.16; CD₃OD, ¹H δ = 3.31, ¹³C δ = 49.00). Intermediate products were analysed by electrospray ionization mass spectra (ESI-MS) using an Applied Biosystems/SCIEX API3000-triple quadrupole mass spectrometer. Final products were analysed by high resolution mass spectrometry (HRMS) on a LTQ-Orbitrap XL mass spectrometer with a resolution of 60,000 at m/z 400 at a scan rate of 1Hz.

Isoxazole compound **1** was synthesized using a one-pot three-step reaction as described by Koufaki *et al.* [15]. In this reaction, anisaldehyde was firstly converted to the corresponding oxime, which was subsequently reacted with chloramine-T to produce nitrile oxide. The nitrile oxide was then rapidly coupled with phenylacetylene to produce compound **1**. Demethylation of compound **1** with boron trichloride in the presence of tetra-N-butylammonium resulted in compound **2** [16]. Compounds **1** and **2** were then purified by column chromatography.

Benzoxazole compounds **3** and **4** were prepared from the corresponding 2-aminophenols and p-toluenesulphonic acid in dimethylmalonate [17], and selective demethylation of compound **4** under the same condition as the synthesis of compound **2** produced compound **5** [16]. Compound **6** was synthesized similarly to compound **3** and **4** through reaction of 2-aminophenol and 4-hydroxybenzoic acid

in the presence of boric acid [17]. Compound **7** was prepared from 2-aminophenol, 3-methylbenzoic acid and Lawessons's reagent (C₁₄H₁₄O₂P₂S₄) as described by Seijas *et al.* [18]. Compounds **3-7** were purified using column chromatography.

Triazole compounds **8-12** were synthesized through a conversion of 4-aminophenol by concentrated hydrochloric acid and NaNO₂ to the diazonium ion that was substituted with sodium azide to provide the corresponding azide [19]. The azide was then reacted with substituted alkynes using the copper-catalyzed alkyne to azide cycloaddition (CuAAC) method to produce diversely substituted triazole-phenol compounds [20].

MIF tautomerase activity assay

MIF used in this assay was recombinantly expressed and purified as His-tagged MIF [21]. The assay was conducted based on the previous procedure of Kok *et al.* [14]. 4-hydroxyphenyl pyruvate (4-HPP) was used as a substrate. A stock solution of 4-HPP 10 mM was provided in ammonium acetate 50 mM pH 6.0 and incubated overnight at room temperature to allow equilibration between the keto and enol form. The same ammonium acetate buffer was used for further dilutions of this substrate. Stock solutions of inhibitors with a concentration of 50 mM were made in DMSO. For screening, inhibitor solutions with a final concentration of 250 μM were made by further dilution of the mixture with MIF in boric acid 0.4 M pH 6.2. And for IC₅₀ determinations, inhibitors with a final concentrations of 125 – 0 μM in DMSO 5% (1.6 fold dilution series) were prepared. This DMSO dilution with a final concentration of 5% was used as a vehicle control. At this concentration, DMSO has already been known to give no significant influence on MIF tautomerase activity.

In the assays, mixtures of 45 μL MIF (solution in boric acid 0.4 M pH 6.2, to give a final concentration of 340 nM) and 5 μL of the synthesized compounds were put in a UV-star F bottom 96-well plate. The reaction was started by the introduction of 50 μL 4-HPP in ammonium acetate buffer (to give a final concentration of 0.5 mM), and the increase of absorbance at 306 nm over the time was monitored by Spectrostar Omega BMG Labtech plate reader. Mixtures of all the components in DMSO 5% (final concentration) excluding the inhibitor were used as positive control. The negative control was the positive control excluding MIF. The analysis of data was done by initially taking the slopes of the linear part of the increase in absorbance over the time (i.e. the rate of reaction), then normalizing them to the slope of the positive and negative controls to obtain the

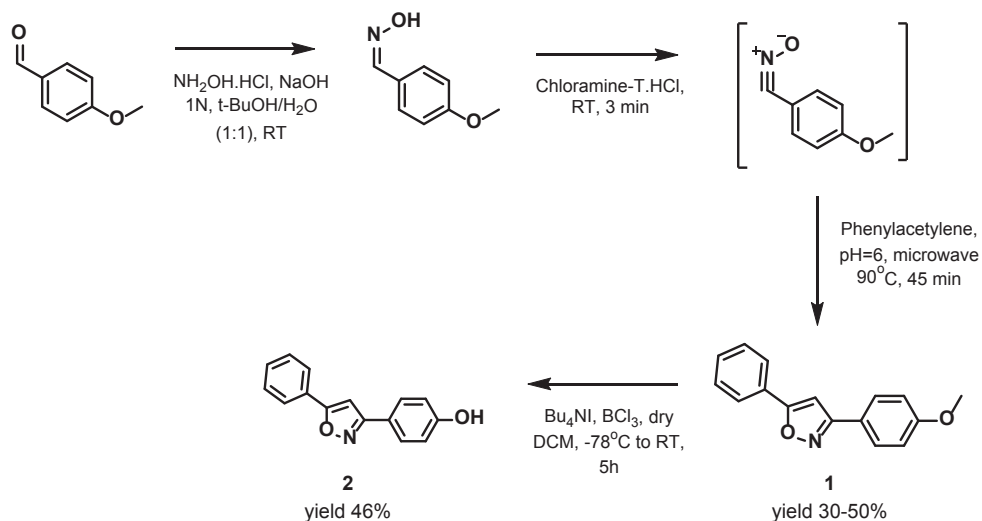
percentage of residual enzyme activity. This percentage of residual enzyme activity was plotted against the logarithm of the inhibitor concentration.

Results and discussion

2.1 Chemistry

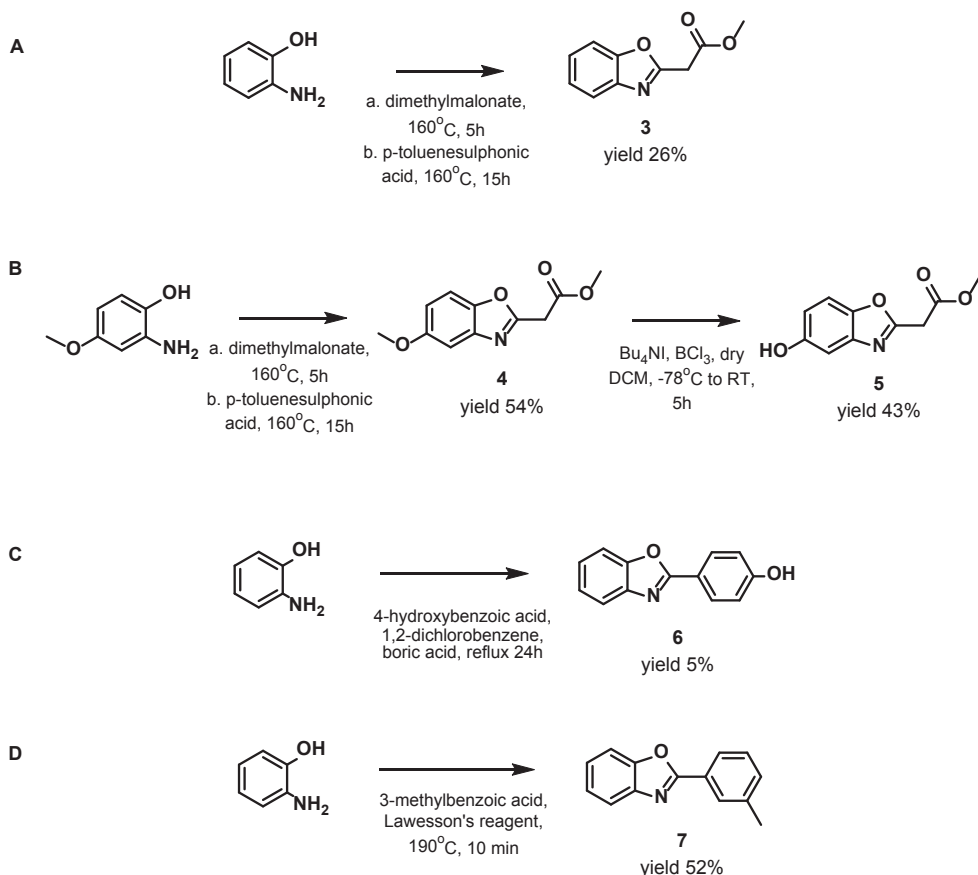
Based on the known inhibitor ISO-1, we synthesized a focus collection of compounds with isoxazole or benzoxazole scaffolds. For compounds **1** and **2**, we replaced the isoxazoline ring by an isoxazole ring and for compounds **3-7**, we combined the isoxazoline ring and phenyl ring to a benzoxazole ring. Based on the known biaryltriazole compounds, we synthesized diversely-substituted triazole-phenol compounds **8-12**.

We successfully synthesized the isoxazole compound **1** using a one-pot three-step reaction as described by Koufaki *et al.* [15] with a yield of 30-50% (**Scheme 1**). Interestingly, the oxime is stable up to 48 hours in this reaction system. This property would allow for making a parallel set up in preparing other compounds with isoxazole scaffold. Subsequently, we demethylated the methoxy group on the phenyl ring of compound **1** with boron trichloride in the presence of tetra-N-butylammonium iodide to produce compound **2**. The yield was 46% (**Scheme 1**).



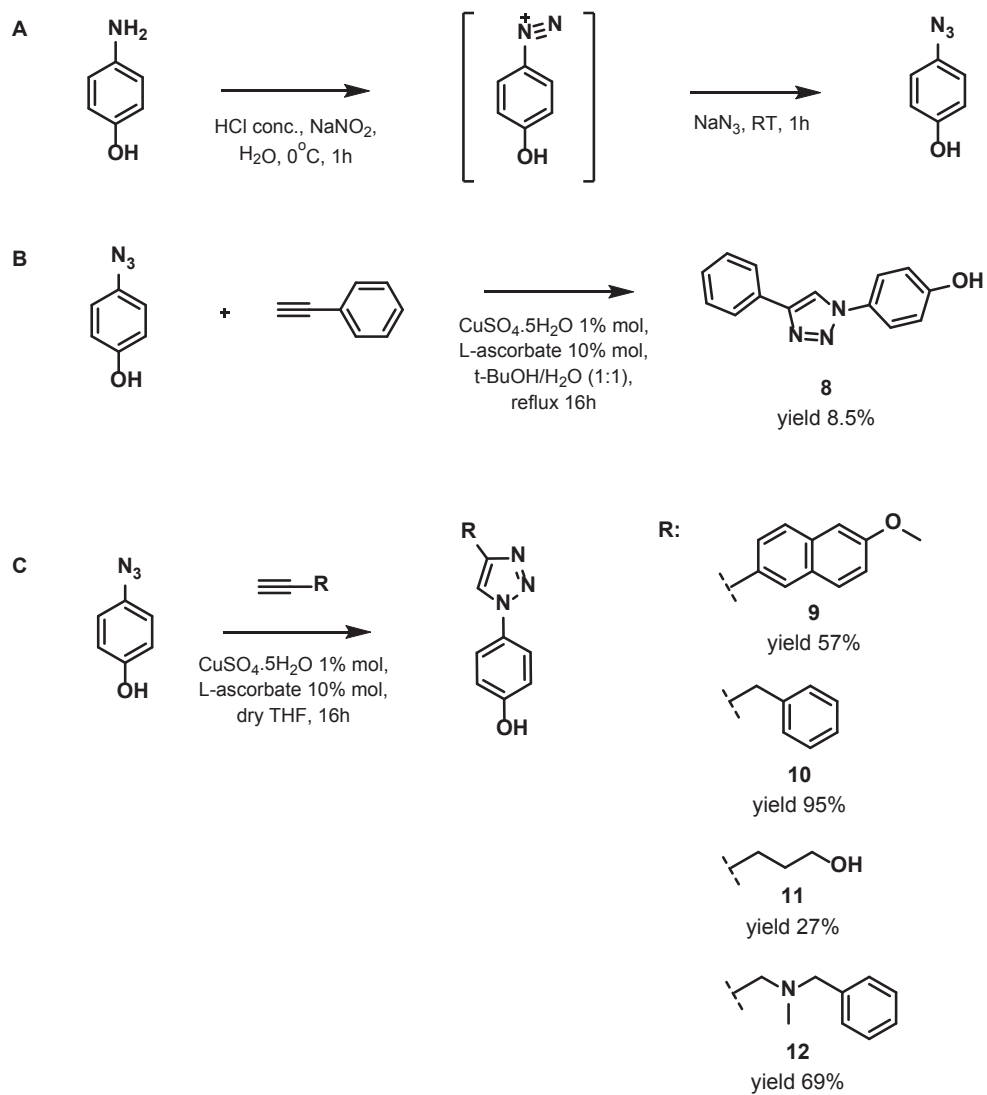
Scheme 1. Synthesis routes of isoxazoles **1** and **2**.

We prepared benzoxazole compounds **3** and **4** from the corresponding 2-aminophenols and p-toluenesulphonic acid in dimethylmalonate, giving a yield of 26% and 54%, respectively (**Scheme 2A** and **2B**). Subsequently, we selectively demethylated the methoxy group on the benzoxazole ring of compound **4** under the same condition as the synthesis of isoxazole compound **2** to obtain compound **5**, with a yield of 43% (**Scheme 2B**). Compound **6** was synthesized similarly to compound **3** and **4** through a reaction of 2-aminophenol and 4-hydroxybenzoic acid in 1,2-dichlorobenzene in the presence of boric acid; its yield was only 5% (**Scheme 2C**). And compound **7** was prepared by a reaction of 2-aminophenol with 3-methylbenzoic acid and Lawesson's reagent, with a yield of 52% (**Scheme 2D**). We found that the solvent-free reaction using Lawesson's reagent as described by Seijas *et al.* that was used for synthesis of compound **7** is more efficient method than the method used for the synthesis of compound **6**.



Scheme 2. Synthesis routes of benzoxazoles **3-7**.

Finally, we prepared triazole-phenol compounds **8-12** from 4-aminophenol through a conversion of the amine to azide (**Scheme 3A**). The azide was subsequently reacted with diversely substituted alkynes using the copper-catalyzed alkyne to azide cycloaddition (CuAAC) method (via 1,3-dipolar cycloaddition mechanism) to produce compounds **8**, **9**, **10**, **11** and **12** with a yield of 8.5%, 57%, 95%, 27% and 69%, respectively (**Scheme 3B** and **3C**). We found that dry tetrahydrofuran (used for the synthesis of compound **9-12**) is a better solvent than t-butyl alcohol/H₂O (1:1) (used for the synthesis of compounds **8**), because of the limited solubility of the alkynes in water. Therefore, the yield of compounds **9-12** was much greater than that of compound **8**.



Scheme 3. Synthesis routes of triazole-phenol compounds **8-12**.

2.2 Structure-activity relationship of MIF tautomerase inhibitors

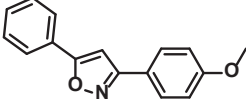
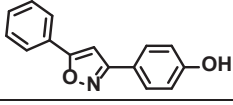
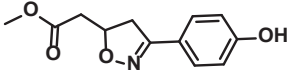
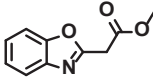
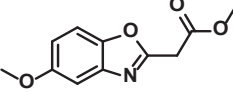
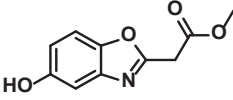
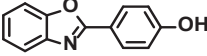
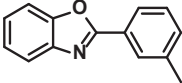
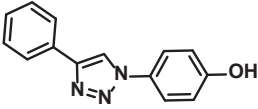
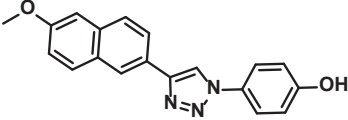
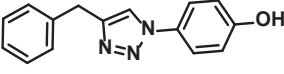
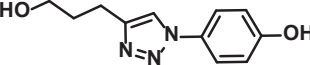
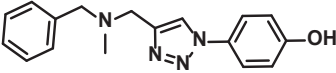
We used the previous assay as described by Kok *et al.* [14] to evaluate the inhibition on MIF tautomerase activity by the synthesized compounds (**Table 1**). In this assay, the measurement was based on the absorbance detection of the enol form of 4-HPP, as the product of the tautomerase reaction, in complex with boric acid.

We screened compounds **1-7** at a concentration of 250 μM and the compound(s) giving inhibition greater than 50% would be tested further for IC_{50} determination. Compounds **8-12** were not screened at a single point concentration of 250 μM , but directly tested for IC_{50} determination.

In the screening at a concentration of 250 μM , compounds **1-7** gave no inhibition. No inhibition on MIF tautomerase activity by the isoxazole compounds **1** and **2** could be due to the more rigidity of the isoxazole ring (planar shape – sp^2 hybridisation) compared to the isoxazoline ring (tetrahedral shape – sp^3 hybridisation), influencing the binding orientation of these compounds in MIF enzymatic pocket. No inhibition given by the benzoxazole compounds **3-7** might be due to no interaction between the benzoxazole ring of these compounds with amino acid residues in MIF enzymatic pocket. These findings indicate that the isoxazoline ring possesses a property needed for the binding of such compounds with amino acid residues in MIF enzymatic pocket.

All the triazole-phenol compounds, except compound **9**, showed inhibition with similar IC_{50} (**Table 1** and **Figure 1**), suggesting that the phenol group binds in a similar way as was demonstrated in the crystal structure of MIF-biaryltriazole (making a hydrogen-bonding interaction with residue Asp-97) [22], but the substituents on the triazole ring positioned almost outside of MIF enzymatic pocket give no big difference in the inhibition of the compounds on MIF tautomerase activity. In compound **9** the naphthalene ring substituent on its triazole ring might be too bulky and rigid, resulting in the loss of interaction between the triazole ring and amino acid residues in the MIF enzymatic pocket. In comparison, a similar compound from literature with a quinoline ring instead of a naphthalene ring inhibits MIF tautomerase activity presumably due to hydrogen-bonding of the quinoline ring with residue Lys-32 of MIF (PDB 5HVS) [22]. Taken together, the triazole-phenol group is a promising scaffold for MIF binding compounds that can be employed as an anchor to identify structure-activity-relationships of MIF binding compounds. Ultimately, this will provide a comprehensive insight in the structural requirements for MIF binding and the development of potent and drug-like inhibitors.

Table 1. IC₅₀ values of compounds 1-12 and ISO-1 as the inhibitor of reference. IC₅₀ values were given as mean and standard error of mean from at least 3 independent experiments. ND = not determined due to no inhibition in the single point screening at 250 μM.

| Scaffold | Compound | Structure | IC ₅₀ |
|-----------------|----------|---|------------------|
| Isoxazole | 1 |  | ND |
| | 2 |  | ND |
| Isoxazoline | ISO-1 |  | 79 ± 1.0 |
| Benzoxazole | 3 |  | ND |
| | 4 |  | ND |
| | 5 |  | ND |
| | 6 |  | ND |
| | 7 |  | ND |
| Triazole-phenol | 8 |  | 52 ± 4.0 |
| | 9 |  | ND |
| | 10 |  | 34 ± 2.3 |
| | 11 |  | 37 ± 2.1 |
| | 12 |  | 34 ± 2.6 |

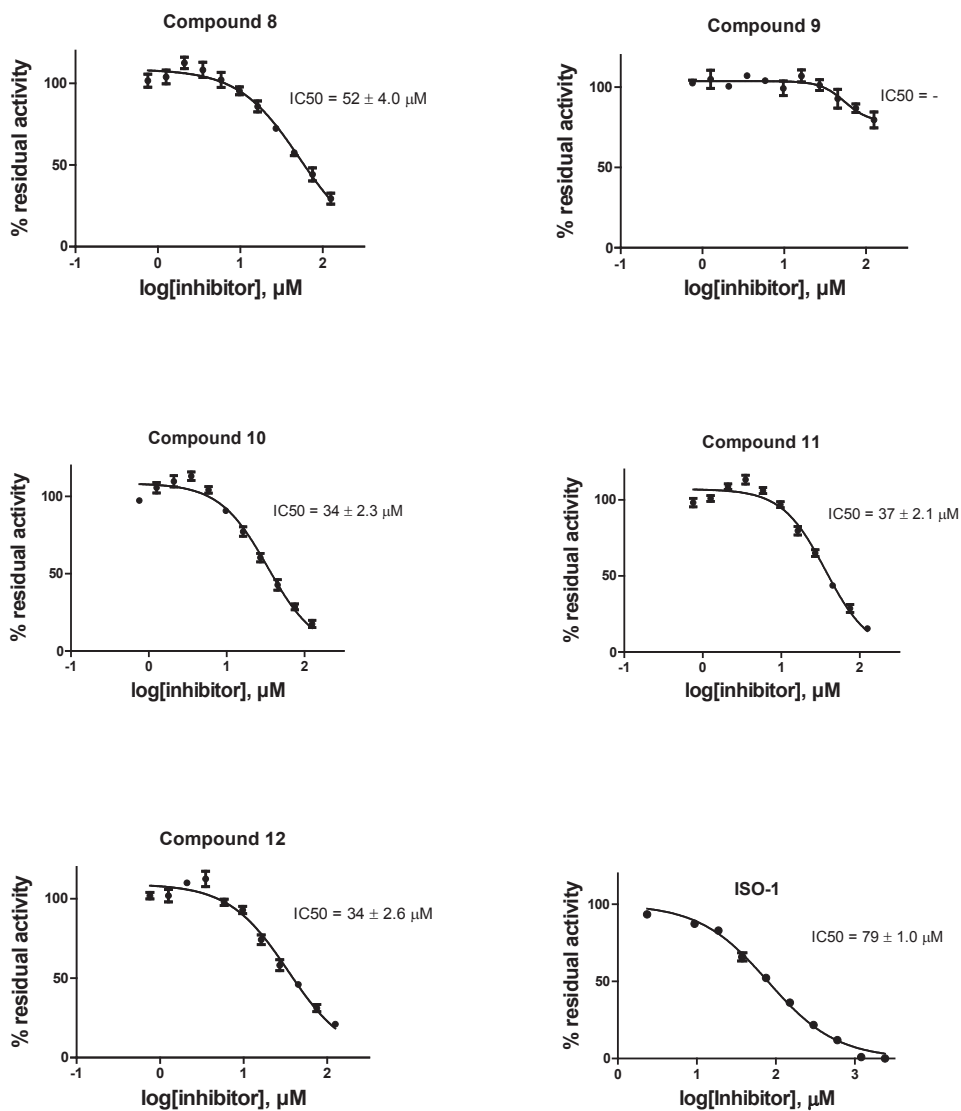


Figure 1. IC_{50} curves at 125 – 0 μM (with 1.6 fold dilution series) of triazole-phenol compounds and of ISO-1 as the inhibitor of reference; final concentration of MIF and 4-HPP were 340 nM and 0.5 mM, respectively.

Conclusions and future perspectives

Because binding of MIF to its cellular receptors such as the CD74 receptor, plays a key role in inflammatory processes and cancer, MIF inhibitors are considered to be potential therapeutics for diseases related to MIF cytokine activity. In this study, we employed the MIF tautomerase activity assay to discover small-molecule inhibitors that could potentially interfere with MIF cytokine activity. Using known synthesis routes, we synthesized a focus compound collection of isoxazole and benzoxazole scaffolds; and we used copper-catalyzed alkyne to azide cycloaddition (CuAAC) for the synthesis of compounds with a triazole-phenol scaffold. We subsequently evaluated the inhibition by the synthesized compounds on MIF tautomerase activity. This successfully provided diversely-substituted triazole-phenol compounds as MIF tautomerase inhibitors with IC_{50} 's in the micromolar range. In addition, we suggest that the triazole-phenol scaffold is one of the promising cores for further development of potent inhibitors targeting MIF-CD74 interaction. The reversibility and kinetics of binding of the inhibitors need to be evaluated to gain insight on the mode of inhibition. Once the inhibition is confirmed to be reversible and competitive, we expect that MIF enzymatic pocket can be employed to anchor small-molecule inhibitors with substituents that protrude into the solvent interface of the pocket ("caps"). This would enable interfering with the MIF-CD74 interaction in order to develop therapeutic agents against MIF cytokine-related diseases.

References

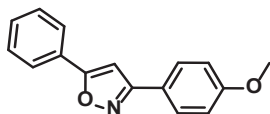
- [1] Bloom J, Sun S, Al-Abed Y. MIF, a controversial cytokine: a review of structural features, challenges, and opportunities for drug development. *Expert Opin Ther Targets* 2016;20:1463–75. doi:10.1080/14728222.2016.1251582.
- [2] Leng L, Metz CN, Fang Y, Xu J, Donnelly S, Baugh J, et al. MIF Signal Transduction Initiated by Binding to CD74. *J Exp Med* 2003;197:1467–76. doi:10.1084/jem.20030286.
- [3] Weber C, Kraemer S, Drechsler M, Lue H, Koenen RR, Kapurniotu A, et al. Structural determinants of MIF functions in CXCR2-mediated inflammatory and atherogenic leukocyte recruitment. *Proc Natl Acad Sci U S A* 2008;105:16278–83. doi:10.1073/pnas.0804017105.
- [4] Bernhagen J, Krohn R, Lue H, Gregory JL, Zernecke A, Koenen RR, et al. MIF is a noncognate ligand of CXC chemokine receptors in inflammatory and atherogenic cell recruitment. *Nat Med* 2007;13:587–96. doi:10.1038/nm1567.
- [5] Calandra T, Roger T. Macrophage migration inhibitory factor: a regulator of innate immunity. *Nat Rev Immunol* 2003;3:791–800. doi:10.1038/nri1200.
- [6] Lubetsky JB, Swope M, Dealwis C, Blake P, Lolis E. Pro-1 of macrophage migration inhibitory factor functions as a catalytic base in the phenylpyruvate tautomerase activity. *Biochemistry* 1999;38:7346–54. doi:10.1021/bi990306m.
- [7] Poelarends GJ, Veetil VP, Whitman CP. The chemical versatility of the beta-alpha-beta fold: catalytic promiscuity and divergent evolution in the tautomerase superfamily. *Cell Mol Life Sci* 2008;65:3606–18. doi:10.1007/s00018-008-8285-x.
- [8] Rosengren E, Åman P, Thelin S, Hansson C, Ahlfors S, Björk P, et al. The macrophage migration inhibitory factor MIF is a phenylpyruvate tautomerase. *FEBS Lett* 1997;417:85–8. doi:10.1016/S0014-5793(97)01261-1.
- [9] Donnelly SC, Bucala R. Macrophage migration inhibitory factor: a regulator of glucocorticoid activity with a critical role in inflammatory disease. *Mol Med Today* 1997;3:502–7. doi:10.1016/S1357-4310(97)01133-7.
- [10] Kok T, Wasiel AA, Cool RH, Melgert BN, Poelarends GJ, Dekker FJ. Small-molecule inhibitors of macrophage migration inhibitory factor (MIF) as an emerging class of therapeutics for immune disorders. *Drug Discov Today* 2018. doi:10.1016/j.drudis.2018.06.017.
- [11] Pantouris G, Syed MA, Fan C, Rajasekaran D, Cho TY, Rosenberg EM, et al. An Analysis of MIF Structural Features that Control Functional Activation of CD74. *Chem Biol* 2015;22:1197–205. doi:10.1016/j.chembiol.2015.08.006.
- [12] Lubetsky JB, Dios A, Han J, Aljabari B, Ruzsicska B, Mitchell R, et al. The Tautomerase Active Site of Macrophage Migration Inhibitory Factor Is a Potential Target for Discovery of Novel Anti-inflammatory Agents. *J Biol Chem* 2002;277:24976–82. doi:10.1074/jbc.M203220200.
- [13] Bloom J, Metz C, Nalawade S, Casabar J, Cheng KF, He M, et al. Identification of Iguratimod as an Inhibitor of Macrophage Migration Inhibitory Factor (MIF) with Steroid-sparing Potential. *J Biol Chem* 2016;291:26502–14. doi:10.1074/jbc.M116.743328.
- [14] Kok T, Wapenaar H, Wang K, Neochoritis CG, Zarganes-Tzitzikas T, Proietti G, et al. Discovery of chromenes as inhibitors of macrophage migration inhibitory factor. *Bioorg Med Chem* 2018;26:999–1005. doi:10.1016/J.BMC.2017.12.032.
- [15] Koufaki M, Fotopoulou T, Kapetanou M, Heropoulos GA, Gonos ES, Chondrogianni N. Microwave-assisted synthesis of 3,5-disubstituted isoxazoles and evaluation of their anti-ageing activity. *Eur J Med Chem* 2014;83:508–15. doi:10.1016/j.ejmech.2014.06.046.
- [16] Brooks PR, Wirtz MC, Vetelino MG, Rescek DM, Woodworth GF, Morgan BP, et al. Boron Trichloride/Tetra-n-Butylammonium Iodide: A Mild, Selective Combination Reagent for the Cleavage of Primary Alkyl Aryl Ethers. *J Org Chem* 1999;64:9719–21. doi:10.1021/jo9910740.
- [17] Waetzig S, Tunge J. Regio- and Diastereoselective Decarboxylative Coupling of Heteroaromatic Alkanes. *J Am Chem Soc* 2007;129:4138–4139. doi:10.1021/JA070116W.
- [18] Seijas J, Vázquez-Tato M, Carballido-Reboredo M, Crecente-Campo J, Romar-López L. Lawesson's Reagent and Microwaves: A New Efficient Access to Benzoxazoles and Benzothiazoles from Carboxylic Acids under Solvent-Free Conditions. *Synlett* 2007;2007:0313–7. doi:10.1055/s-2007-967994.
- [19] Patil SS, Tawade B V., Wadgaonkar PP. A convenient synthesis of α,α' - homo- and α,α' -hetero-bifunctionalized poly(ϵ -caprolactone)s by ring opening polymerization: The potentially valuable precursors for mikroarm star copolymers. *J Polym Sci Part A Polym Chem* 2016;54:844–60. doi:10.1002/pola.27924.
- [20] Himó F, Lovell T, Hilgraf R, Rostovtsev V V., Noodleman L, K. Barry Sharpless A, et al. Copper(I)-Catalyzed Synthesis of Azoles. DFT Study Predicts Unprecedented Reactivity and Intermediates. *J Am Chem Soc* 2005;127:210–216. doi:10.1021/JA0471525.

- [21] Wasiel AA, Rozeboom HJ, Hauke D, Baas BJ, Zandvoort E, Quax WJ, et al. Structural and functional characterization of a macrophage migration inhibitory factor homologue from the marine cyanobacterium *Prochlorococcus marinus*. *Biochemistry* 2010;49:7572–81. doi:10.1021/bi1008276.
- [22] Dziedzic P, Cisneros JA, Robertson MJ, Hare AA, Danford NE, Baxter RHG, et al. Design, Synthesis, and Protein Crystallography of Biaryltriazoles as Potent Tautomerase Inhibitors of Macrophage Migration Inhibitory Factor. *J Am Chem Soc* 2015;137:2996–3003. doi:10.1021/ja512112j.
- [23] Munagala G, Yempalla KR, Singh S, Sharma S, Kalia NP, Rajput VS, et al. Synthesis of new generation triazolyl- and isoxazolyl-containing 6-nitro-2,3-dihydroimidazooxazoles as anti-TB agents: in vitro, structure-activity relationship, pharmacokinetics and in vivo evaluation. *Org Biomol Chem* 2015;13:3610–24. doi:10.1039/c5ob00054h.
- [24] Zhang G, Wang P, Yang F, Wu Y. Copper-catalyzed synthesis of 2-arylbenzoxazoles from o-aminophenol derivatives with arylmethyl chlorides. *Tetrahedron* 2015;71:57–63. doi:10.1016/J.TET.2014.11.040.
- [25] Mohammed S, Padala AK, Dar BA, Singh B, Sreedhar B, Vishwakarma RA, et al. Recyclable clay supported Cu (II) catalyzed tandem one-pot synthesis of 1-aryl-1,2,3-triazoles. *Tetrahedron* 2012;68:8156–62. doi:10.1016/J.TET.2012.07.080.

Supplementary information

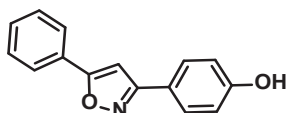
Synthesis and characterization of compounds 1-12

3-(4-methoxyphenyl)-5-phenylisoxazole (1)



Hydroxylamine hydrochloride (1.5 mmol) was added to a solution of p-methoxy benzaldehyde (1.5 mmol) in water:t-BuOH (1:1 ratio, 7 mL) in a MW tube. Subsequently, NaOH (1.5 mmol, 1 M solution in water) was added. The reaction mixture was left stirring at RT until the p-methoxy benzaldehyde was consumed. Then Chloramine-T hydrochloride (1.5 mmol) was added. After 3 minutes, phenyl acetylene (1.5 mmol) was added and the pH of the reaction was adjusted to 6. The reaction was then MW irradiated for 45 minutes at 90°C. The product was extracted with ethyl acetate (3 x 25 mL), was with water (3 x 25 mL), dried over MgSO₄, filtered and concentrated under reduced pressure. The crude product was purified using column chromatography (20:1 petroleum ether:ethyl acetate), affording the product as a colorless solid. Yield: 31 %, R_f = 0.77 (2:1 petroleum ether:ethyl acetate). ¹H NMR (500 MHz, CDCl₃) δ 7.85- 7.80 (m, 4H), 7.50-7.45 (m, 3H), 7.00 (d, *J* = 8.8 Hz, 2H), 6.78 (s, 1H), 3.87 (s, 3H). ¹³C NMR (126 MHz, CDCl₃) δ 170.04, 162.47, 160.91, 130.02, 128.87 (2x), 128.09 (2x), 127.46, 125.71 (2x), 121.55, 114.22 (2x), 97.15, 55.26. Spectroscopic data are in line with literature [15].

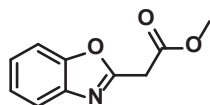
4-(5-phenylisoxazol-3-yl)phenol (2)



Tetra-N-butylammonium iodide (0.25 mmol) was added to a solution of 3-(4-methoxyphenyl)-5-phenylisoxazole (0.19 mmol) in dry CH₂Cl₂ (10 ml) under nitrogen atmosphere. Subsequently the reaction was cooled down to -78°C using a mixture of acetone and liquid N₂. Then boron trichloride (0.3 mmol, 1M solution in DCM) was added dropwise and stirred for 5 minutes. The reaction was allowed to heat to RT and stirred for 5 hours. The mixture was quenched in ice-water, the product was extracted with DCM (3 x 20 ml), dried over MgSO₄, filtered and

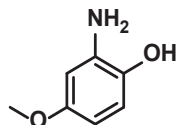
concentrated under reduced pressure. The crude product was purified on column chromatography (5:1 petroleum ether:ethyl acetate), to yield a white powder. Yield: 46 %, $R_f = 0.16$ (2:1 petroleum ether:ethyl acetate). $^1\text{H NMR}$ (500 MHz, Methanol- d_4) δ 7.92 (d, $J = 7.5$ Hz, 2H), 7.78 (d, $J = 8.6$ Hz, 2H), 7.54 (m, 3H), 7.19 (s, 1H), 6.93 (d, $J = 8.6$ Hz, 2H). $^{13}\text{C NMR}$ (126 MHz, Methanol- d_4) δ 171.44, 164.44, 160.76, 136.96, 131.40, 130.18 (2x), 129.36, 128.81, 126.79 (2x), 121.30, 116.80 (2x), 98.63. Spectroscopic data are in line with literature [23].

Methyl 2-(benzo[d]oxazol-2-yl)acetate (3)



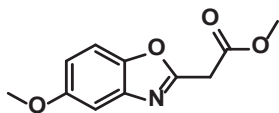
2-aminophenol (2 mmol) was added to dimethylmalonate (10 mmol, 1.1 mL) under nitrogen. The mixture was heated to 160 °C for 5 hours until 2-aminophenol was consumed. Then p-toluenesulphonic acid (0.2 mmol) was added and the mixture was stirred at 160 °C for 15 hours. The mixture was directly purified by column chromatography (1:20 ethyl acetate:petroleum ether) to yield the product as a yellow solid. Yield 26 %, $R_f = 0.6$ (1:1 ethyl acetate:petroleum ether). $^1\text{H NMR}$ (500 MHz, CDCl_3) δ 7.79 – 7.69 (m, 1H), 7.58 – 7.48 (m, 1H), 7.35 (dd, $J = 6.5$, 2.8 Hz, 2H), 4.05 (s, 2H), 3.79 (s, 3H). $^{13}\text{C NMR}$ (126 MHz, CDCl_3) δ 167.50, 159.49, 151.20, 141.20, 125.29, 124.55, 120.17, 110.72, 52.90, 35.17. MS (ESI): m/z [M+H], calculated $\text{C}_{10}\text{H}_{10}\text{O}_3\text{N}$ 191.1, found 192.1.

2-amino-4-methoxyphenol



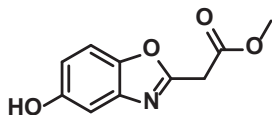
To a solution of 4-methoxy-2-nitrophenol (5 mmol) in MeOH (10 mL) was added palladium on carbon (10% w/w, 10% Pd on carbon) under hydrogen atmosphere. The mixture was stirred for 3 hours at RT, filtered over celite and concentrated under reduced pressure. The product was used in the following reaction without further purification. $^1\text{H NMR}$ (500 MHz, CDCl_3) δ 6.47 (dd, $J = 8.5$, 2.9 Hz, 1H), 6.18 (d, $J = 2.9$ Hz, 1H), 6.02 (dd, $J = 8.5$, 3.0 Hz, 1H), 3.53 (s, 3H). $^{13}\text{C NMR}$ (126 MHz, CDCl_3) δ 153.75, 139.10, 135.79, 115.43, 103.60, 103.04, 55.69.

Methyl 2-(5-methoxybenzo[d]oxazol-2-yl)acetate (4)



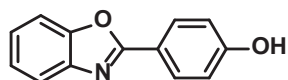
2-amino-4-methoxyphenol (3.6 mmol) was added to dimethylmalonate (18 mmol, 2.4 mL) under nitrogen atmosphere. The mixture was heated to 160 °C for 2 hours until 2-aminophenol was consumed. Then p-toluenesulphonic acid (0.4 mmol) was added and the mixture was stirred at 160 °C for 15 hours. The mixture was directly purified by column chromatography (1:10 ethyl acetate:petroleum ether) to yield the product as a yellow solid. Yield 54 %, $R_f = 0.63$ (1:2 ethyl acetate:petroleum ether). ^1H NMR (500 MHz, CDCl_3) δ 7.39 (d, $J = 8.9$ Hz, 1H), 7.18 (d, $J = 2.5$ Hz, 1H), 6.93 (dd, $J = 8.9, 2.5$ Hz, 1H), 3.99 (s, 2H), 3.84 (s, 3H), 3.77 (s, 3H). ^{13}C NMR (126 MHz, CDCl_3) δ 167.46, 160.13, 157.27, 145.77, 141.95, 113.79, 110.79, 103.00, 55.96, 52.82, 35.17. MS (ESI): m/z $[\text{M}+\text{H}]$, calculated $\text{C}_{11}\text{H}_{12}\text{O}_4\text{N}$ 221.1, found 222.1.

Methyl 2-(5-hydroxybenzo[d]oxazol-2-yl)acetate (5)



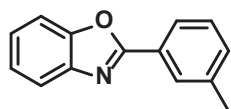
To a solution of Methyl 2-(5-methoxybenzo[d]oxazol-2-yl)acetate (**4**, 0.5 mmol) in dry DCM was added t-butylammonium iodide (0.65 mmol) under nitrogen atmosphere. The mixture was cooled down to -78 °C and boron trichloride (2.5 mL, 1M in DCM) was added dropwise. The mixture was allowed to warm to room temperature and stirred for 1 hour turning bright orange. The reaction was quenched with ice-water and saturated NaHCO_3 . The product was extracted with DCM and purified by column chromatography (1:2 ethyl acetate:petroleum ether) yielding the product as a light yellow solid. Yield 43 %, $R_f = 0.3$ (1:1 ethyl acetate:petroleum ether). ^1H NMR (500 MHz, MeOD) δ 7.39 (d, $J = 8.8$ Hz, 1H), 7.02 (d, $J = 2.3$ Hz, 1H), 6.86 (dd, $J = 8.8, 2.4$ Hz, 1H), 4.06 (s, 2H), 3.76 (s, 3H). ^{13}C NMR (126 MHz, DMSO) δ 168.27, 160.93, 155.18, 144.63, 142.05, 113.90, 111.13, 105.05, 52.90, 35.01. MS (ESI): m/z $[\text{M}+\text{H}]$, calculated $\text{C}_{10}\text{H}_{10}\text{O}_4\text{N}$ 207.1, found 208.1.

4-(benzo[d]oxazol-2-yl)phenol (6)



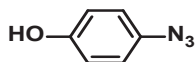
4-hydroxybenzoic acid (1.8 mmol) was added to a solution of 2-aminophenol (1.8 mmol) in 1,2-dichlorobenzene (10 mL) under nitrogen atmosphere. The flask was equipped with a condenser and boric acid (0.2 mmol) was added. The suspension was refluxed for 24 hours, after which it was cooled down. The product was precipitated using petroleum ether, filtered and directly purified by column chromatography (4:1 petroleum ether:ethyl acetate) to yield the product as a red solid. Yield: 5.2 %. $R_f = 0.43$ (2:1 petroleum ether:ethyl acetate). ^1H NMR (500 MHz, chloroform/MeOH) δ 7.87 (d, $J = 8.7$ Hz, 2H), 7.49-7.45 (m, 1H), 7.38-7.34 (m, 1H), 7.15-7.10 (m, 2H), 6.75 (d, $J = 8.7$ Hz, 2H). ^{13}C NMR (126 MHz, Methanol- d_4) δ 163.81, 161.32, 150.41, 141.46, 129.22 (2x), 124.64, 124.45, 118.55, 117.45, 115.62 (2x), 110.12. MS (ESI): m/z [M+H], calculated $\text{C}_{11}\text{H}_{14}\text{O}_2\text{N}_3$ 211.06, found 212.07.

2-(m-tolyl)benzo[d]oxazole (7)



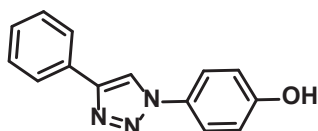
3-methylbenzoic acid (4.6 mmol) was added to a mixture of 2-aminophenol (4.6 mmol) and Lawesson's reagent (1.6 mmol). The solid mixture was heated at 190°C for 10 minutes, turning into a thick dark solution. The mixture was directly purified by column chromatography (60:1 petroleum ether:ethyl acetate), to yield the product as a light pink solid. Yield: 52 %, $R_f = 0.85$ (2:1 petroleum ether:ethyl acetate). ^1H NMR (500 MHz, CDCl_3) δ 8.11(s, 1H), 8.05 (s, 1H), 7.79- 7.76 (m, 1H), 7.61-7.57 (m, 1H), 7.44-7.39 (m, 1H), 7.37- 7.34 (m, 3H), 2.46 (s, 3H). ^{13}C NMR (126 MHz, CDCl_3) δ 163.22, 150.74, 142.11, 138.76, 132.38, 128.83, 128.20, 127.02, 125.04, 124.77, 124.55, 119.97, 110.57, 77.48, 21.37. Spectroscopic data are in line with the literature [24].

4-azidophenol



To a suspension of p-aminophenol (14 mmol) in water (20 mL), concentrated hydrochloric acid (3.5 mL) was added dropwise over a period of 5 min. The resulting solution was cooled down to 0°C and then NaNO₂ (27 mmol) was added portion wise. The reaction was then left stirring for 1h, after which a freshly made solution of NaN₃ (16 mmol) in water, was added dropwise. The reaction was left stirring for another hour at room temperature. The product was then extracted with ethyl acetate (3x50ml), dried over MgSO₄, filtered and concentrated under reduced pressure to yield the product as a dark red oil. The product was used in other reactions without further purification. Yield: 96 %, R_f = 0.63 (2:1 petroleum ether:ethyl acetate). ¹H NMR (500 MHz, CDCl₃) δ 6.83-6.81 (m, 2H), 6.77- 6.75 (m, 2H). ¹³C NMR (126 MHz, CDCl₃) δ 154.18, 131.12, 119.93 (2x), 116.41 (2x). Spectroscopic data are in line with the literature [19].

4-(4-phenyl-1H-1,2,3-triazol-1-yl)phenol (8)

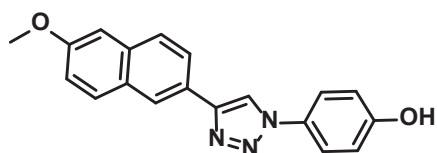


Phenylacetylene (1.5 mmol) was added to a solution of 4-azidophenol (1.5 mmol) in water:t-BuOH (1:1 ratio, 7 mL). To the vigorously stirred solution, were added in sequence, a freshly made solution of CuSO₄·5H₂O (0.015 mmol) in water (100 μL) and a freshly made solution of L-ascorbate (0.15 mmol) water (100 μL). The reaction was refluxed for 15 hours. The resulting mixture was then extracted with ethyl acetate (3 x 20ml), washed with water (5 x 20 mL) dried over MgSO₄, filtered and concentrate. The product was recrystallized in DCM, which yielded a brown solid. Yield: 8.5 %, R_f = 0.23 (2:1 petroleum ether:ethyl acetate). ¹H NMR (500 MHz, Methanol-*d*₄) δ 8.74 (s, 1H), 7.91 (d, *J* = 7.2 Hz, 2H), 7.67 (d, *J* = 6.2 Hz, 2H), 7.46 (t, *J* = 7.2 Hz, 2H), 7.38 (t, *J* = 6.2 Hz, 1H), 6.96 (m, 2H). ¹³C NMR (126 MHz, Methanol-*d*₄) δ 158.25, 147.90, 130.14, 129.31, 128.61 (2x), 128.09, 125.35 (2x), 121.94 (2x), 119.02, 115.75 (2x). Spectroscopic data are in line with the literature [25].

General procedure for the synthesis of compounds 9-12

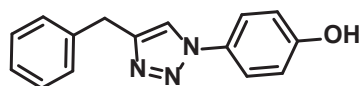
The appropriate alkyne (0.5 mmol) was added to a solution of 4-azidophenol (0.5 mmol) in dry THF (2 mL). To the vigorously stirred solution were added in sequence a freshly made solution of $\text{CuSO}_4 \cdot 5\text{H}_2\text{O}$ (0.01 mmol) in water (50 μL) and a freshly made solution of L-ascorbate (0.05 mmol) in water (50 μL). The reaction was stirred for 15 hours and quenched by pouring into ice-water. The product was extracted with ethyl acetate (2 x 20 mL), washed with water (5 x 20 mL), dried over MgSO_4 , filtered and concentrated under reduced pressure to afford the products as a brown solid.

4-(4-(6-methoxynaphthalen-2-yl)-1H-1,2,3-triazol-1-yl)phenol (9)



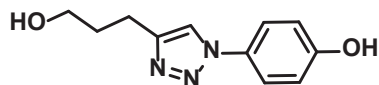
Yield: 57 %, R_f = 0.68 (2:1 ethyl acetate:petroleum ether). ^1H NMR (500 MHz, DMSO) δ 10.02 (s, broad, 1H), 9.20 (s, 1H), 8.41 (s, 1H), 8.02 (d, J = 8.5 Hz, 1H), 7.96-7.88 (m, 2H), 7.75 (d, J = 8.8 Hz, 2H), 7.37 (s, 1H), 7.22 (d, J = 8.9 Hz, 1H), 6.99 (d, J = 8.8 Hz, 2H). ^{13}C NMR (126 MHz, DMSO) δ 158.24, 157.99, 147.66, 134.47, 130.06-129.98 (1x), 129.31, 128.98, 127.94-127.89 (1x), 126.14, 124.62, 124.07-124.02 (1x), 122.37, 122.27, 119.89, 119.69, 116.55 (2x), 106.52-106.50 (1x), 55.67. MS (ESI): m/z [$\text{M}+\text{H}$], calculated $\text{C}_{19}\text{H}_{16}\text{O}_2\text{N}_3$ 317.35, found 318.12.

4-(4-benzyl-1H-1,2,3-triazol-1-yl)phenol (10)



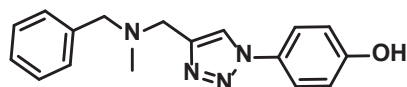
Yield: 95 %, R_f = 0.66 (2:1 ethyl acetate:petroleum ether). ^1H NMR (500 MHz, DMSO) δ 9.92 (s, 1H), 8.42 (s, 1H), 7.64 (d, J = 8.9 Hz, 2H), 7.35-7.29 (m, 4H), 7.26-7.15 (m, 1H), 6.92 (d, J = 8.9 Hz, 2H), 4.07 (s, 2H). ^{13}C NMR (126 MHz, DMSO) δ 157.98, 147.21, 139.89, 129.37, 128.99 (2x), 128.91 (2x), 126.67, 122.19, 121.13, 121.09, 116.42 (2x), 31.69. MS (ESI): m/z [$\text{M}+\text{H}$], calculated $\text{C}_{11}\text{H}_{14}\text{O}_2\text{N}_3$ 251.11, found 252.11.

4-(4-(3-hydroxypropyl)-1H-1,2,3-triazol-1-yl)phenol (11)



Yield: 27 %, $R_f = 0.7$ (2:1 ethyl acetate:petroleum ether). ^1H NMR (500 MHz, Methanol- d_4) δ 8.18 (s, 1H), 7.62 (d, $J = 6.0$ Hz, 2H), 6.96 (d, $J = 5.9$ Hz, 2H), 3.67 (t, $J = 5.8$ Hz, 2H), 2.87 (d, $J = 5.8$ Hz, 2H), 1.97 (t, $J = 5.8$ Hz, 2H). ^{13}C NMR (126 MHz, Methanol- d_4) δ 158.06, 147.99, 129.43, 121.89, 120.24, 115.71, 60.61, 31.86, 21.35. MS (ESI): m/z $[M+H]$, calculated $\text{C}_{11}\text{H}_{14}\text{O}_2\text{N}_3$ 219.24, found 220.10.

4-(4-((benzyl(methyl)amino)methyl)-1H-1,2,3-triazol-1-yl)phenol (12)



Yield: 69 %, $R_f = 0.26$ (2:1 ethyl acetate:petroleum ether). ^1H NMR (500 MHz, MeOD) δ 8.28 (s, 1H), 7.61 (d, $J = 8.5$ Hz, 2H), 7.32 (m, 6H), 6.94 (d, $J = 8.5$ Hz, 2H), 3.77 (s, 2H), 3.61 (s, 2H), 2.25 (s, 3H). ^{13}C NMR (126 MHz, DMSO) δ 158.02, 144.97, 139.24, 129.40 (2x), 129.25 (2x), 128.62, 127.37, 122.23 (2x), 122.19, 116.43 (2x), 60.86, 51.84, 41.91. MS (ESI): m/z $[M+H]$, calculated $\text{C}_{17}\text{H}_{19}\text{ON}_4$ 294.36, found 295.15.

Chapter 6

Summary and future perspectives

Summary

MIF is a cytokine that plays a key role in innate and adaptive immune responses. Its activity has been associated with the development of multiple inflammatory diseases and cancer. MIF exerts its biological functions through the interaction with its cellular receptors such as CD74. Hence, MIF-CD74 binding is considered to be a promising target in the development of therapeutics for MIF cytokine-related diseases. We aim to improve the production of the purified CD74 protein in bacteria in order to provide a suitable MIF-CD74 binding assay. Furthermore, we aim to develop novel MIF inhibitors.

Chapter 1 provides the introduction and scope of the thesis. In **Chapter 2**, we provide an overview on the described role of MIF in the pathogenesis of inflammatory diseases and cancer, and on the emerging classes and types of small-molecule inhibitors targeting MIF activity as potential therapeutics for immune disorders. MIF was reported to be associated with acute and chronic inflammatory diseases such as asthma, chronic obstructive pulmonary disease (COPD), rheumatoid arthritis, sepsis, diabetes, atherosclerosis and cardiovascular diseases. In addition, many studies described MIF as a biomarker for multiple diseases with an inflammatory component, such as systemic infections and sepsis, cancer, autoimmune diseases and different metabolic disorders. Taken together, these studies demonstrate the essential role of MIF in immune-related diseases. Consequently, many efforts have been taken over the past few years to discover MIF-directed therapeutics. One line of the efforts is the development of biologicals, for instance anti-MIF antibodies. The other line is the development of small-molecule MIF inhibitors aiming at interfering with MIF cytokine activity. This interference can be due to the binding-induced conformational changes of MIF and/or disruption of MIF-CD74 interaction. Compared with biologicals, small-molecule MIF inhibitors offer advantages such as lower manufacturing costs, non-immunogenicity and the possibility of oral administration. Hence, this route of exploration gained tremendous interest.

Targeting MIF tautomerase activity remains a convenient and efficient approach to develop small-molecule MIF inhibitors. In this chapter, we present the

currently identified classes and types of MIF small-molecule inhibitors in two tables. In Table 1 on page 27, the inhibitors with a phenol functionality as the key structural group that presumably interacts with the active site residue Asn-97 of MIF are shown. In Table 2 on page 28, the covalent inhibitors and inhibitors with other structures are presented. We also discuss their structure-activity relationships and new lines of development. In this perspective, we note that the evaluation of the functional consequences on MIF cytokine activity upon treatment with MIF inhibitors is highly important.

This chapter also describes D-DT (MIF2) as a protein that is suggested to have an overlapping functional spectrum with MIF due to its marked homology. Therefore, D-DT should be taken into consideration in the evaluation of MIF cytokine activities and in the development of small molecule MIF inhibitors. Moreover, post-translational modification of MIF that can affect its biological functions has also been reported. MIF has a CXXC motif that can be oxidized to an intramolecular disulfide-bond. Although this redox behavior could interfere with the binding of small molecules, the structural and functional implications for MIF binding remain to be elucidated.

Taken together, Chapter 2 provides an overview on the pivotal role of MIF in inflammatory diseases and cancer, and on the increasing efforts to develop MIF-directed therapeutics from small-molecule inhibitors.

Chapter 3 reports high-yield production and purification of the functional extracellular CD74 proteins using two solubility enhancing peptides. The MIF-CD74 binding was shown *in vitro* to be located in the extracellular moiety of CD74, but the unstable and protease-prone character of this moiety has hampered further characterisation. Attempts to produce the moiety in bacteria provided low yields of soluble protein. We tackled this problem by fusing it to MBP and Fh8 peptides. We put a factor Xa cleavage site on the MBP-CD74 fusion protein and a 3C cleavage site on the Fh8-CD74 fusion protein. After expression, the MBP and Fh8 peptides were removed from the fusion proteins by cleavage with factor Xa and 3C proteases. Following the cleavage, we purified the CD74 cleavage products. However, this effort did not give its full fruits, because the expected CD74 cleavage products were accompanied by further degradation products and the subsequent purification was problematic.

MIF-binding assays showed that all the CD74 fusion proteins and CD74 cleavage products, except sssCD74 that lacks amino acids 77-125, are functional. Due to the purity issue of the functional CD74 cleavage products, the MBP-sCD74 and Fh8-ssCD74 fusion proteins were used in further binding assays for the determination of EC_{50} and/or K_D . The dose-dependent ELISA showed an EC_{50} -

value of around 110 nM for MBP-sCD74 and 280 nM for Fh8-ssCD74. The ITC binding assay demonstrated a K_D -value of around 1.3 μ M for MBP-sCD74. We did not measure the K_D -value of Fh8-ssCD74, because the reaction enthalpy in ITC experimentation was low. This made obtaining solid binding data via ITC difficult. Size exclusion chromatography indicated that all the purified CD74 proteins are mostly present in their homotrimeric form, which is the native form of CD74 proteins.

Furthermore, the ELISA binding experimentation with different CD74 constructs showed that removal of amino acids 77-112 from CD74 (in Fh8-ssCD74 construct) is influencing but not destructing the MIF-binding. This suggests that the amino acids 113-125 of CD74 are involved in the interaction with MIF. In addition, the deletion of amino acids 77-125 (in sssCD74 construct) resulted in the lack of MIF-binding. This implies that the extracellular CD74 trimerisation domain is not or only slightly involved in the binding to MIF, and hence it does not give sufficient response in the binding assays.

In **Chapter 4**, we investigate a diversely-substituted collection of compounds with a chromene scaffold that was synthesized using versatile cyanoacetamide chemistry. The substitution-oriented screening (SOS) for inhibition on MIF tautomerase activity resulted in several hit compounds with IC_{50} 's in the low micromolar range. Preincubation and dilution assays indicated that the inhibitors bind to MIF reversibly. Enzyme kinetic analysis of the most potent inhibitor showed that the inhibitor does not bind in direct competition with the substrate 4-HPP.

Chapter 5 describes the synthesis of a structure-based-designed compounds with isoxazole, benzoxazole and triazole-phenol scaffolds using known synthesis routes. Various substituents were put at specific positions on the scaffolds. The compounds were then assessed for their inhibition on MIF tautomerase activity and their structure-activity relationships was evaluated. This effort has successfully provided several MIF inhibitors with triazole-phenol scaffold with IC_{50} 's in the micromolar range. In addition, we suggest that the triazole-phenol is a promising scaffold for systematic cycles of design and synthesis to elucidate the structure-activity relationship in MIF binding and, ultimately, for the development of potent inhibitors targeting MIF-CD74 binding.

Future perspectives

MIF has been reported as a cytokine that plays a key role in the progression of inflammatory diseases and cancer. Small-molecule inhibitors have been developed and applied to study the role of MIF in immune-related diseases. In addition to ISO-1, that is widely used as a reference compound, other small-molecule inhibitors that were identified in a MIF tautomerase assay also showed positive effects in various disease models. The isoxazolines and 1,2,3-triazoles are two important classes of compounds from which potent MIF inhibitors have been developed. Taken together, these signify the potential of MIF inhibitors in the development of novel therapeutics for inflammatory diseases and cancer.

Concerning the development of MIF inhibitors, it should be noted that the sigmoidal enzyme kinetics and covalent or slow-tight binding behavior can result in overestimation of the inhibitor potency in the MIF tautomerase assay. These issues complicate the analysis of MIF binding. In this perspective, we propose to anticipate on these issues by conducting preincubation and dilution experiments as well as enzyme kinetic studies. The identification of potent MIF inhibitors with favorable properties will enable the development of novel therapeutics for MIF cytokine-related diseases.

Attention should be given toward the MIF homolog D-DT, which has been suggested to have an overlapping functional spectrum with MIF. This implies that a combined therapeutic targeting of MIF and D-DT could bring a synergistic effect. However, further details need to be elucidated.

Also, MIF post-translational modifications including modifications related to redox behavior could interfere with binding of small-molecule inhibitors. This represents an interesting novel line of investigation.

The MIF-CD74 binding assays showed that the CD74 region comprising at least amino acids 113-125 appears to be essential for the interaction with MIF (as described in Chapter 3). This provides useful insight for future work on the construction of functional and stable extracellular CD74 proteins and on the further investigation of a MIF-CD74 binding map.

The identified chromene MIF inhibitors (in Chapter 4) need to be evaluated for their interference with MIF-CD74 interaction in PPI binding assays. Furthermore, their functional consequences to interfere with MIF cytokine-activity need to be investigated in cell-based assays and in relevant disease models.

The identified triazole-phenol MIF inhibitors (Chapter 5) need to be evaluated for their reversibility and kinetic of binding to gain insight in the mode of inhibition. Once the inhibition is confirmed to be reversible and competitive, we can employ the MIF enzymatic pocket to anchor small-molecule inhibitors with

assembled substituents on the triazole ring protruding out of the active site. We anticipate that this construction will interfere with the MIF-CD74 interaction that is described to occur close to the active site. Thus, structure-based design would enable the discovery of inhibitors that can disrupt the MIF-CD74 interaction and potentially provide therapeutics with favorable properties. Further work continuing from Chapter 5 aims at exploring this possibility.

Nederlandse samenvatting

Het eiwit Macrophage Inhibitory Factor (MIF) is een cytokine dat een sleutelrol speelt in signalen van zowel het aangeboren als het verworven immuunsysteem. Zijn activiteit is geassocieerd met tal van ontstekingsziekten en kanker. MIF oefent zijn biologische functie uit door interacties met cellulaire receptoren zoals CD74. Daarom is de binding tussen MIF en CD74 een veelbelovend doelwit voor het ontwikkelen van geneesmiddelen voor MIF-gerelateerde ziekten. Het is ons doel om de productie van gezuiverd CD74 eiwit te verbeteren voor het gebruik in een geschikte bindingstest met MIF. Daarnaast proberen we nieuwe MIF-remmers te ontwikkelen.

Hoofdstuk 1 beschrijft het doel en de reikwijdte van dit proefschrift. In **Hoofdstuk 2** geven we een overzicht van de reeds beschreven rol van MIF in de pathogenese van ontstekingsziekten en kanker, en van het gebruik van de verschillende opkomende klassen van kleine remmers van MIF als medicijn voor immuunziekten. In eerdere studies is reeds gerapporteerd dat MIF geassocieerd is met acute en chronische ontstekingsziekten zoals astma, chronische obstructieve longziekte (COPD), reumatoïde artritis, bloedvergiftiging, kanker, auto-immuunziekten en verschillende stofwisselingsziekten. Samenvattend laten deze studies de essentiële rol zien van MIF in immuun gerelateerde ziekten. Daarom zijn er de laatste jaren veel inspanningen geleverd in het ontdekken van MIF-gerichte medicijnen. Een van de onderzoekslijnen is gericht op het ontwikkelen van biologicals, zoals anti-MIF antilichamen. Een andere onderzoekslijn is gericht op het ontwikkelen van kleine moleculen als remmers die de cytokine activiteit van MIF remmen. Deze remming van cytokine activiteit kan veroorzaakt worden doordat binding van de remmer aan MIF leidt tot een conformationele verandering van MIF en/of doordat de interactie van MIF met CD74 wordt verstoord. In vergelijking met biologicals hebben kleine remmers een aantal voordelen zoals lagere productiekosten, niet-immunogeniciteit en de mogelijkheid van orale toediening. Daarom heeft het ontdekken van kleine remmers grote belangstelling gekregen.

Het richten op de tautomerase activiteit van MIF is nog steeds een gemakkelijke en efficiënte strategie voor het ontwikkelen van kleine MIF remmers. In dit hoofdstuk beschrijven we de bekende klassen en typen van kleine MIF remmers in twee tabellen. In tabel 1, op pagina 27, worden de remmers met een fenol-groep als belangrijkste structurele groep weergegeven, waarvan wordt aangenomen dat deze groep een interactie aangaat met asparagine-97 van MIF. In tabel 2, op pagina 28, worden de covalente remmers en remmers met andere

structurele groepen weergegeven. We bediscussiëren ook de structuur-activiteitsrelatie en nieuwe ontwikkelingen. In dit kader, merken we op dat het erg belangrijk is om het effect van MIF remmers op de cytokine activiteit van MIF te bepalen.

Dit hoofdstuk beschrijft ook D-DT (MIF2) als een eiwit waarvan gesuggereerd is dat het een overlappende functie met MIF heeft vanwege de opvallende homologie met MIF. Daarom zou, bij het bepalen van de cytokine activiteit van MIF en bij het ontwikkelen van kleine remmers van MIF, ook de activiteit van D-DT in overweging moeten worden genomen. Verder zijn er post-translationele modificaties van MIF beschreven die ook een effect kunnen hebben op de biologische functie. MIF heeft een CXXC-motief, dat geoxideerd kan worden tot een intramoleculaire zwavelbrug. Hoewel dit redox gedrag zou kunnen interfereren met de binding van een klein molecuul, moeten de structurele en functionele implicaties daarvan nog worden opgehelderd.

Samenvattend, geeft **hoofdstuk 2** een overzicht van de centrale rol van MIF in ontstekingsziekten en kanker, en de toenemende pogingen om MIF-gerichte medicijnen te ontwikkelen.

Hoofdstuk 3 beschrijft de productie met hoge opbrengst en de zuivering van functioneel extracellulair CD74 eiwit door gebruik te maken van twee oplosbaarheid-verhogende peptiden. In een *in vitro* experiment werd aangetoond dat de binding van MIF met CD74 plaatsvindt op een extracellulair deel van CD74, maar het onstabiele karakter en de vatbaarheid voor proteasen van CD74 heeft verdere karakterisering verhinderd. Pogingen om het extracellulaire deel in bacteriën te produceren resulteerde in lage opbrengsten van oplosbaar eiwit. We losten dit probleem op door CD74 te fuseren met MBP en Fh8 peptiden. We introduceerden een factor Xa knipsequentie op het MBP-CD74 fusie eiwit en een 3C knipsequentie op het Fh8-CD74 fusie eiwit. Na expressie werd het MBP en de Fh8 peptide verwijderd van het fusie-eiwit door te knippen met factor Xa en 3C proteasen. Na het knippen zuiverden we het CD74 knipproduct. Dit gaf echter niet helemaal het gewenste resultaat omdat het gewenste CD74 knipproduct vergezeld werd door andere CD74 degradatie producten en verdere zuivering erg problematisch bleek.

MIF-bindingsstudies lieten zien dat alle CD74 fusie-eiwitten en knipproducten, behalve sssCD74 die de aminozuren 77-125 mist, functioneel waren. Vanwege de zuiveringsproblemen van de functionele CD74 knipproducten werden de MBP-sCD74 en de Fh8-ssCD74 fusie-eiwitten gebruikt in verdere bindingsstudies voor het bepalen van de EC_{50} en/of de K_D . De dosis-afhankelijke ELISA liet een EC_{50} -waarde van ongeveer 110 nM voor MBP-sCD74 en 280 nM

voor Fh8-ssCD74 zien. De ITC bindingsstudie liet een K_D -waarde van ongeveer 1.3 μM zien voor MBP-sCD74. We hebben niet de K_D -waarde van Fh8-ssCD74 gemeten omdat de reactie enthalpie in het ITC experiment laag was. Hierdoor was het lastig om solide bindingsdata via ITC te verkrijgen. Gelchromatographie experimenten lieten zien dat al de gezuiverde CD74 eiwitten zich voornamelijk in hun trimere vorm bevonden, hetgeen de natuurlijke vorm is van CD74 eiwitten.

Verder lieten de ELISA-bindingsexperimenten met verschillende CD74 constructen zien dat het verwijderen van de aminozuren 77-112 van CD74 (in het Fh8-ssCD74 construct) de binding met MIF beïnvloed, maar niet volledig verwoest. Dit suggereert dat de aminozuren 113-125 van CD74 betrokken zijn bij de interactie met MIF. Verder leidde de deletie van de aminozuren 77-125 (in het sssCD74 construct) tot een totaal gebrek aan binding met MIF. Dit impliceert dat het extracellulaire trimerisatie domein van CD74 niet of slechts beperkt betrokken is in het binden van MIF, waardoor het niet genoeg respons geeft in de bindingsstudies.

In **hoofdstuk 4** onderzoeken we een divers-gesubstitueerde collectie van stoffen met een chroomen-groep die gesynthetiseerd is door middel van veelzijdige cyano-acetamide chemie. De SOS voor de remming op MIF tautomerase activiteit resulteerde in een aantal hits met een IC_{50} in de lage micromolair range. Preincubatie en verdunningsexperimenten lieten zien dat de remmers reversibel aan MIF binden. Enzym kinetiek analyse van de meest potente remmer liet zien dat deze remmer niet direct competitief met het substraat 4-HPP bindt.

Hoofdstuk 5 beschrijft de synthese van structuur-gebaseerde-ontwerp stoffen van stoffen met een isoxazool, benzoxazool of triazool-fenolgroep door gebruik te maken van bekende synthese routes. Verschillende substituenten werden op specifieke plekken in de stoffen aangebracht. De stoffen werden vervolgens getest voor hun effect op de remming van MIF tautomerase activiteit en de structuur-functie relatie werd geanalyseerd. Dit resulteerde in een aantal MIF remmers met een triazool-fenolgroep met IC_{50} 's in de micromolair range. Verder suggereren we dat triazool-fenol een veelbelovende klasse van stoffen is voor systematische rondes van ontwerp en synthese om de structuur-activiteit relatie van MIF binding op te helderen en, uiteindelijk, voor het ontwikkelen van krachtige remmers van de MIF-CD74 binding.

Toekomstperspectieven

MIF is een cytokine die een sleutelrol speelt in de progressie van ontstekingsziekten en kanker. Kleine remmers zijn ontwikkeld en toegepast om de rol van MIF in immuun gerelateerde ziekten te onderzoeken. Naast ISO-1, een remmer die veelvuldig wordt gebruikt als referentiestof, lieten ook andere kleine remmers die ontdekt waren in MIF tautomerase activiteitstesten een positief effect zien op tal van ziektemodellen. De isoxazolen en de 1,2,3-triazolen zijn twee belangrijke klassen van stoffen waarvan krachtige MIF remmers zijn ontwikkeld. Samenvattend laat dit de potentie van MIF remmers zien op de ontwikkeling van nieuwe medicijnen voor ontstekingsziekten en kanker.

Als het gaat om de ontwikkeling van MIF remmers, moet opgemerkt worden dat sigmoïdale enzym kinetiek, covalent- of slow-tight bindingsgedrag ertoe kan leiden dat het remmingspotentieel wordt overschat in een MIF tautomerase activiteitstest. Deze problemen maken de analyse van MIF binding complex. Vanwege deze problemen stellen we voor om naast de enzym kinetiek experimenten ook preincubatie en verdunningsexperimenten uit te voeren. Het vinden van krachtige MIF remmers met de gewenste eigenschappen zal de ontwikkeling van nieuwe medicijnen voor ontstekingsziekten en kanker mogelijk te maken.

Er zou ook aandacht gegeven moeten worden aan de MIF homoloog D-DT, waarvan gesuggereerd is dat het een overlappend functioneel spectrum heeft met MIF. Dit impliceert dat een medicijn dat zowel gericht is op MIF als op D-DT synergistische effecten teweeg kan brengen. Verdere details moeten echter nog worden opgehelderd.

Post-translationele modificaties van MIF, zoals modificaties gerelateerd aan redox gedrag, zouden de binding van kleine remmers kunnen verstoren. Dit is een interessante en nieuwe onderzoekslijn.

De bindingstesten van MIF aan CD74 laten zien dat de CD74 regio bestaande uit, op zijn minst, de aminozuren 113-125 essentieel lijken te zijn voor de interactie met MIF (zoals beschreven in **hoofdstuk 3**). Dit levert bruikbare inzichten op voor toekomstige onderzoeken aangaande de constructie van functionele en stabiele extracellulaire CD74 eiwitten en voor verder onderzoek van de MIF-CD74 bindingskaart.

De gevonden chromeen MIF remmers (in **hoofdstuk 4**) moeten verder onderzocht worden met betrekking tot de interferentie van de MIF-CD74 interactie in PPI bindingsstudies. Verder moeten de functionele consequenties van de verstoring van de MIF cytokine activiteit in kaart worden gebracht in cel-studies en in relevante ziektemodellen.

De gevonden triazool-fenol MIF remmers (**hoofdstuk 5**) moet verder worden onderzocht voor hun reversibiliteit en hun kinetische eigenschappen, om verder inzicht te krijgen in hun type van inhibitie. Wanneer wordt bepaald dat de inhibitie reversibel en competitief is, kunnen we de MIF enzymatische active site gebruiken om de kleine remmers in te verankeren, terwijl we andere substituenten op de triazoolring plaatsen die uit de active site steken. We verwachten dat een dergelijk construct de interactie tussen MIF en CD74 verstoord, aangezien bekend is dat de interactie tussen MIF en CD74 dicht bij de active site plaats vindt. Structuur-gebaseerd ontwerp zou het daarom mogelijk moeten maken om nieuwe remmers te vinden die de MIF-CD74 interactie kunnen verstoren en mogelijk kunnen leiden tot nieuwe medicijnen met betere eigenschappen. Vervolgonderzoek van **hoofdstuk 5** richt zich op deze mogelijkheid.

Appendix

Acknowledgements

List of publications

About the author

Acknowledgements

Thanks to God, Jesus Christ, who has opened the way for me to start my PhD journey in Groningen. My first two weeks living in Groningen was the most shocking time, due to completely different circumstances (environment, climate, culture, etc.) between Groningen and my hometown.

The aim of my project can be achieved by normal effort. That was my first impression in several months working on MIF-CD74 project. However, time has given an evidence that greater effort than usual was needed to accomplish the project. Indeed, the unstable nature of the extracellular CD74 and the irregularities of MIF enzyme activity have arisen both challenge and opportunity.

Sometimes desperation came. Two years elapsed for an effort of producing stable and functional CD74 fusion proteins, specifically the CD74 cleavage products of which the purification proved to be problematic. Fortunately, the subsequent steps went faster than the expectation and the end of the project is at hand. After all, the more I was engaged in the project, the more interesting it was. I found myself eventually become more excited to continue the project and see further good results to come. The work has been attracting me a lot!

Time is flying. My interesting PhD journey in Groningen has finally come to an end. Accordingly, I would like to express my gratitude to all the companions in my PhD trip.

Firstly, I would like to express my gratitude to my first supervisor Prof. dr. F.J. Dekker. Frank, thank you for providing me a place to start my PhD journey in the Department of Chemical and Pharmaceutical Biology, University of Groningen. It is honorable for me to be a part of this research group. Thank you for your supervision, your patience and your encouragement that enabled me to cope with all the problems I encountered during my work. You are a great supervisor. You often encouraged me to stay focused and keep a close eye on the schedule already made, that maintained me to be on track for the final destination (even though sometimes I felt under pressure). Thank you for all those matters.

Secondly, I would like to thank Prof. dr. G.J. Poelarends, my second supervisor. Gerrit, you are a good supervisor with great achievements. I am happy to be counted as a member of your research group. I really enjoyed the way you share your valuable knowledge comprehensibly. Thank you for your encouragement, valuable input and remarks, as well as your willingness to provide further financial support when needed during my PhD journey.

Thirdly, I would thank Dr. R.H. Cool. Robbert, it is a pleasure working with you. You are very cool, indeed! You always try to allocate your time to give others a hand in time of need, even during your busy days! You have many

experiences in cloning, protein expression and purification, and are willing to share them with your colleagues. Thank you for your kindness and assistance.

My next gratitude is to all the faculty members in our department. Prof. dr. W.J. Quax, Dr. Y.L. Boersma and Prof. dr. H.J. Haisma, thank you for all your cooperation during my work in this department and your eagerness to share with us your broad knowledges. Your passion to achieve the best in your respective research field is highly appreciated. You all have given us good academic atmosphere.

Special thanks to all our technicians. Ronald, Pieter, Rita and Petra, you are all so helpful in my PhD work. Your willingness to assist us in providing the stuffs needed for our research and to help us with technical problems in laboratory is highly respected. Thanks to all secretaries, too. Yvonne, Janita and Janine, your willingness to help all the students with administration matters is excellent. I do appreciate it.

I would further thank my previous roommates in room 905. Zainal, Jielin, Lieuwe, Saravanan, Saif, Haigan, Guangcai, Andreas, Chao and Michele, thanks for your togetherness. It was so enjoyable to dwell among you, sharing ideas, knowledges, experiences and food. In the moment when full concentration was really needed, frankly I sometimes got disturbed with a noisy environment you made. However, it represented a rigorous academic and daily life in this room. So, it is not bad.

Also, I would thank my other labmates. Jan, Joko, Xinyu, Putri, Christel, Hegar, Linda, Ingy, Yafeng, Magda, Yizhou, Abel, Brenda, Marie, Eleonora, Laura, Roberta, Shanshan, Binliu, Olivia, Ali, Siwei, Zhangping, Fangyuan, Hao, Martijn and Hannah, thank you for being my good colleagues and for your cooperation.

(Special thanks to Joko and Lieuwe for your willingness to be my paranymphs for PhD ceremony).

Next, I want to thank the assessment committee and the opponents. Thank you for spending your valuable time in giving assessment for my thesis. I also thank all other parties that are involved in my PhD ceremony.

I would further thank my Indonesian colleagues in Groningen. Ira, Nur, Ima, Dina, Adji, Tri, Ronny, Adhyat, Ury, Erna and Angela (Planetenlaan group), thanks for all your cooperation and gatherings for sharing and eating. Also, Indonesian student association Groningen (PPIG) and all the diaspora in Groningen, thanks for togetherness in our various Indonesian events. I really enjoyed and appreciated our relationship.

My “close family”, congregation in Jemaat di Surabaya (JdS) and GBI De Rank, thanks for your support through prayers. It really strengthened me to handle all difficult circumstances in my PhD life. May God bless you all.

Then, I would express my gratitude to all my family. My older and younger brothers, my sisters-in-law, all my nieces and nephew, thanks for your constructive support during my PhD journey.

Finally, I give a lot of appreciation to DIKTI in collaboration with Ubaya and RuG for giving me financial support until the end of my PhD study.

List of publications

1. Kok T, Wapenaar H, Wang K, Neochoritis CG, Zarganes-Tzitzikas T, Proietti G, et al. Discovery of chromenes as inhibitors of macrophage migration inhibitory factor. *Bioorg Med Chem* 2018;26:999–1005. doi:10.1016/J.BMC.2017.12.032.
2. Kok T, Wasiel AA, Dekker FJ, Poelarends GJ, Cool RH. High yield production of human invariant chain CD74 constructs fused to solubility-enhancing peptides and characterization of their MIF-binding capacities. *Protein Expr Purif* 2018;148:46–53. doi:10.1016/j.pep.2018.03.008.
3. Kok T, Wasiel AA, Cool RH, Melgert BN, Poelarends GJ, Dekker FJ. Small-molecule inhibitors of macrophage migration inhibitory factor (MIF) as an emerging class of therapeutics for immune disorders. *Drug Discov Today* 2018. doi:10.1016/j.drudis.2018.06.017.
4. Kok T, Xiao ZP, Fokkens M, Wapenaar H, Proietti G, Poelarends GJ, Dekker FJ. Synthesis of a focused compound collection of isoxazole, benzoxazole and triazole-phenol scaffolds to explore the structure-activity relationship for MIF tautomerase activity inhibition – ongoing work.

About the author



Tjie Kok was born in Surabaya, Indonesia on 20 August 1969. He received his bachelor and master degree from Airlangga University (Unair), Surabaya, Indonesia and has been doing his career as a lecturer/researcher in University of Surabaya (Ubaya), Surabaya, Indonesia since 1994. In 2005-2010 he became a member of American Chemical Society (ACS). Tjie was appointed head of several departments in University of Surabaya before holding his office as the vice dean of Faculty of Biotechnology, Ubaya in 2011-2014. He was then pursuing his PhD degree at Groningen Research Institute of Pharmacy (GRIP) University of Groningen (RuG), The Netherlands in 2014-2018 under supervision of Prof. dr. F.J. Dekker and Prof. dr. G.J. Poelarends. He worked on the project: Towards novel anti-inflammatory therapies aimed at the cytokine macrophage migration inhibitory factor, with financial support from Directorate General of Higher Education Indonesia (DIKTI) in collaboration with Ubaya and RuG. Tjie has published more than 25 papers in national and international journals/proceedings, including 3 papers recently in reputed international journals. He has become speaker in many national and several international conferences/seminars/symposiums. He has also become a reviewer for some international journals.

